Università degli studi di Napoli "Federico II"

Dipartimento di Fisica "Ettore Pancini"

DOTTORATO IN RISCHIO SISMICO

CICLO XXVIII

"Feasibility study for the implementation and the integration of earthquake early warning systems to national scale and for specific site"

Presentata da: Piero Brondi

Coordinatore del Dottorato:
Prof. Aldo Zollo

Supervisor:
Dr. Matteo Picozzi

Contents

Introduction

Earthquakes are physical phenomena that can cause huge losses in terms of economic activities and human lives. As an example in 2011, after the 9.0 M_W Tohoku-Oki earthquake, Japan was hit by severe civil structures damage, collapses, explosions, fires, landslides, a huge tsunami and more than 15000 persons died.

The Earthquake Early Warning Systems (EEWS) are modern and technological frameworks able to mitigate the seismic risk, providing useful real-time warnings for schools, power plants, industrial structures, transportation systems and gas pipelines. In fact, even only a few seconds can be sufficient for trained users to undertake safety operations able to reduce their exposure to seismic risk, initiate industrial shutdown process and start stopping procedure for trains.

Due to the dramatic increase in vulnerability to earthquakes for metropolitan areas over the last decades and to the unfeasibility of earthquake forecasting, EEWS are considered an effective means to the real-time reduction of vulnerability and societal exposure to seismic hazard.

EEWS are systems that integrate seismic networks and software capable of performing real-time data telemetry and analysis of faster early P-wave signals in order to detect an occurring earthquake, predict the maximum ground shaking at target sites, and provide an alert to these targets before the arrival of the potential damaging S-waves. The time interval between the alert issuing instant and the arrival time of the S-wave is called “lead time” and it represents a crucial parameter for undertaking protective operations before the occurrence of the most intense ground motion. It depends on the source-to-site distance and it can be equal to a few seconds, tens of seconds or even minutes for sites very far from the epicenter. Another key concept of P-wave based EEWS is the blind zone, that is the area where the S-waves reach the target site before the alert is issued, and hence no lead time is available.

P-wave based EEWS typically follow two types of approaches: the “regional”(or “network based”), and the “on-site”(or “site-specific”). Regional EEWS are based on a seismic network located near

an expected epicentral area and through the early P-wave signal recorded at their stations they are able to detect and locate an event, estimating its magnitude. In this approach the "lead time" is defined as the difference between the arrival of the first S waves at the target site and the alert issuing instant, which depends also on the analysis, computation and data transmission times.

On-Site EEWS are designed to cope with the condition of target sites within a seismogenic area, where the Regional EEW provide a lead time too small to issuing an effective earthquake warning. These systems use the information carried by the early first seconds of P-wave to directly predict the strong ground shaking related to the incoming S and surface waves at the same site through empirical relationships. In this case the "lead time" can be considered as the difference between the arrival times of the S-wave and the P-wave, accounting the necessary computation time. Respect to the Regional EEW, the on-site systems can provide faster warning for target located near the epicenter. On the other hand, they are not supported by robust algorithms capable of providing information concerning the earthquake location and the dimension.

Modern technology and methodological advances in real-time data analyses pushed the implementation of the EEWS in many active seismic regions of the world. Earthquake Early Warning Systems are currently operative in Japan, Mexico, California and Romania, while their development and testing is currently conducted in Southern Italy, Turkey, China, Switzerland and South Korea. Feasibility studies are finally carried out for Greece, South Iberia region, Israel, and Eastern Caribbean Islands.

This thesis focuses on EEW, and in particular, it explored two novel approaches for which recent methods have been tested and new methodologies have been built in order to potentiate the on-site and regional EW in Italy. The thesis is divided into three main parts.

The first part focused on a feasibility study for a nation-wide EEWS in Italy obtained by the integration of the Italian Accelerometric Network, RAN, and the software PRobabilistic and Evolutionary early warning SysTem (hereinafter, PRESTo). The performance of the RAN-PRESTo EEWS has been assessed by testing it on real strong motion recordings of 40 largest earthquakes (M_L>4) occurred during the last ten years on the Italian territory. In particular great attention has been paid to ability of PRESTo to retrieve the epicentral location and the magnitude of the selected earthquakes, available from ITACA 2.0 Portal. Furthermore the analysis has been extended to regions that didn't experience earthquakes by considering a nation-wide grid of synthetic sources capable of generating Gutenberg-Richter sequences corresponding to the one adopted by the seismic hazard map of the Italian territory.

Taking into account the non-homogeneous distribution of the RAN stations, the considered key parameters for evaluating the RAN-PRESTo performance with both real and synthetic data have been the first alert time and the blind zone.

The Second part of thesis is centered on a new EEW on-site methodology for Italy, aimed to obtain real time estimation of the Macroseismic Intensity (hereinafter IM) for a target site during an ongoing earthquake. In particular, this study is based on two seismic parameters: the squared velocity integral (hereinafter IV2) and the Housner Intensity. The first quantity, measured on P-wave, is considered as a proxy of the early radiated energy during an earthquake, while the second one is a ground motion parameter that, according to recent studies, is better related to the structural damage than PGA, PGV and Arias Intensity. Analyzing the correlation between these two parameters, and exploiting the data set of Housner and Macroseismic Intensities over the Italian territory collected by Chiauzzi et al. (2011), a direct relation between IM and IV2 has been derived.
The method has been calibrated on the same data used on the first part of thesis, and it has been tested on the strong motion recordings of the largest events occurred in Italy during the last 6 years recorded by the Osservatorio Sismico delle Strutture (OSS) and the Istituto Nazionale di Geofisica e Vulcanologia (INGV) networks. On these last data, the performance of the new method has been assessed with respect to the commonly used on-site methodology that exploits the relations between the P-wave peak displacement (Pd) and the S-wave peak ground velocity (PGV).

In the third part of the thesis, the possibility to extract in EEW timeframe information on the seismic energy irradiated during an earthquake is explored. The importance of being able to estimate the seismic energy in real time is that this source parameter is able to better characterize, with respect to the moment magnitude (i.e. seismic moment), the damage potential of the ground motion in the frequency range of interest for most of the civil infrastructures.
In particular, in this last part of the thesis, a novel procedure for the estimation of the Energy Magnitude in real time operations by means of the IV2 is presented. The analysis has been carried out considering 29 events occurred in Italy between 2009 and 2012 having local magnitude higher than 4.

PART I – The feasibility study of a Regional Early Warning approach for Italy

The Italian Accelerometric Network, RAN, which consists of about five hundred stations installed over all the active seismic zones, as well as many cities and strategic infrastructures in Italy, has the potential to serve as a nation-wide early warning system.

In the first chapter we introduce the main concepts of the regional approach of the PRESTo (PRobabilistic and Evolutionary early warning SysTem) and we describe the main characteristics of the RAN Network. In the following two chapters the potential of RAN-PRESTo EEWS at national scale is evaluated by testing it on real-data using forty of the largest earthquakes that have occurred during last ten years in Italy and recorded by RAN (freely available by the Italian ACcelerometric Archive, ITACA 2.0). Moreover, a novel approach for the assessment of the RAN performance is proposed and tested with synthetic data, extending the feasibility analysis to the whole Italian territory and considering the regions that did not experience earthquakes during the last ten years.

1. The Regional Early Warning approach in Italy

1.1 The Early Warning Systems Regional approach

A regional EEWS is based on a dense sensor network covering an area that is affected by earthquakes. In this approach the relevant source parameters, such as event location and magnitude, are estimated from the early portion of recorded signals and are used to predict a ground motions intensity measure at distant target sites.

The main advantage of a network-based EEWS is that they provide a continuously updated and accurate estimation of source parameters in real time, as new data are acquired by the network (Zollo et al, 2010). The accuracy on peak ground motion prediction at distant sites is mainly determinated by the uncertainty of the adopted ground motion prediction equation (GMPE).

The lead-time at a target site is defined as the time interval between the arrival of the alert notification and damaging waves. For regional EEWS, the lead-time is defined as the travel-time

difference between the arrival of the first S-waves at the target site and the early P-wave recorded at source, after accounting for the necessary computation and data transmission times.

An optimal performing EEWS can be defined as the system providing at the same time the largest 'lead-time' and minimum prediction error on peak ground motion (e.g. difference between observed and predicted logarithmic peak motion amplitude) (Zollo *et al.* 2009a,b).

Several regional EEWS algorithms are being tested in different countries, and the most known are the Virtual Seismologist (Cua & Heaton, 2007; Behr et al., 2015), ElarmS (Allen, 2007; Kuyuk et al.,2014), and PRESTo (Iannacone at al., 2010; Satriano et al., 2011; Zollo et al., 2011). In particular, the main algorithms and their principles of the PRESTo system are described in the next section.

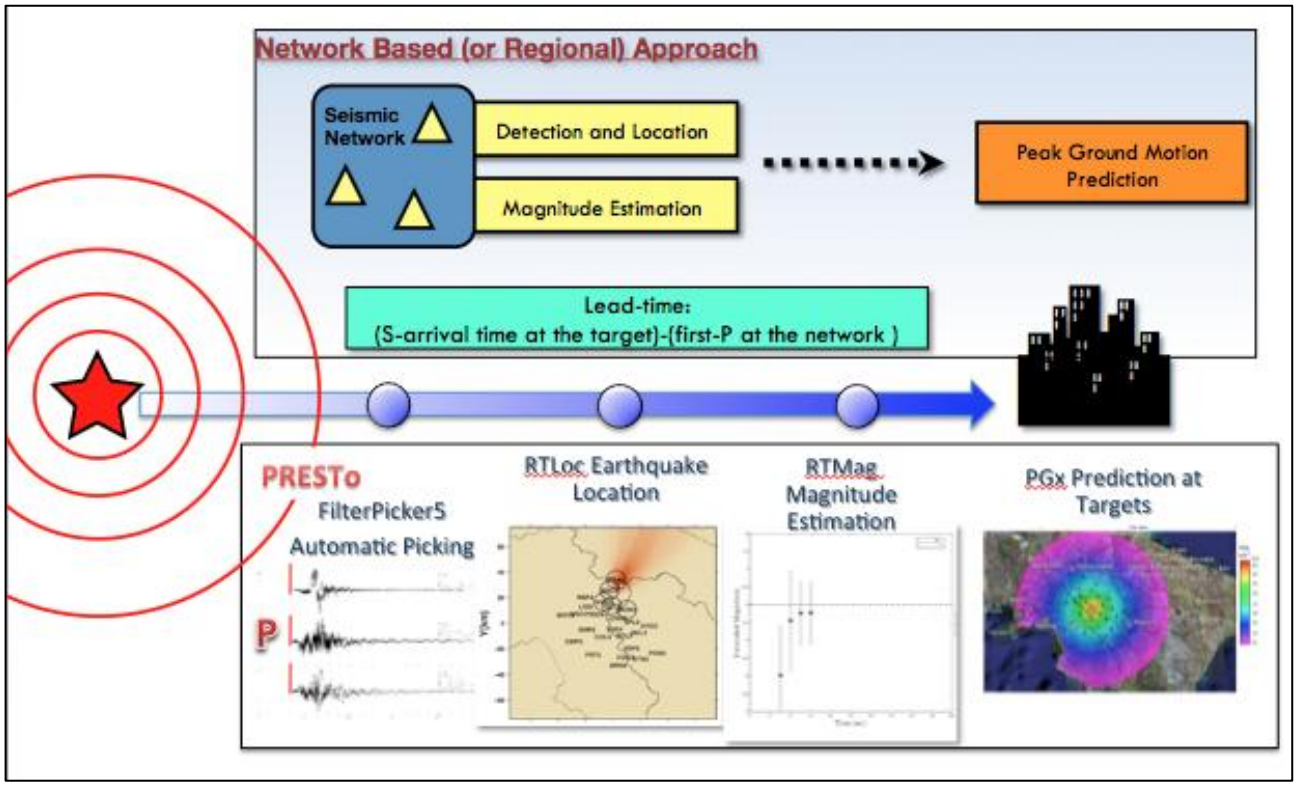

Figure 1.1: Schematic representation of the Regional approach for EW (modified from Satriano et al., 2011), and an overview of the analyses carried out by the PRESTo software system for the real-time event characterization and prediction of the level of ground motion at target sites.

1.2 The PRobabilistic and Evolutionary early warning SysTem PRESTo

PRESTo is a free, open source, highly configurable and easily portable platform for EEW (Iannacone et al., 2010; Satriano et al. 2011). Figure (1.1) shows an outline of the system, which is based on the data streams coming from a seismic network located in the epicentral area, aimed to

rapidly estimate the source parameters of a potentially destructive earthquake and to predict the ground motion at distant target sites (Satriano et al, 2011). During the occurrence of an earthquake, PRESTo is able to provide alert messages containing source parameters information to target sites before the arrival of the S and Surface waves, in order to allow safety procedures (Picozzi et al, 2015a).

The PRESTo's main modules are described in the following sections.

1.2.1 Data acquisition and event detection

PRESTo uses 3-component accelerometric data which acquisition is based on SeedLink (http://www.iris.edu/data/dmc-seedlink.htm), a robust and widely used protocol for waveform data transmission. The system employs the phase detector and picker algorithm Filter Picker (FP), optimized for real-time seismic monitoring and EEWS, in order to detect an incoming seismic event (Lomax et al., 2012).

FP is a general purposes, broadband phase detector and picker algorithm, which has been designed to operate stably on continuous, real-time data streams, and produce realistic time uncertainty on the picks, for real-time seismic monitoring and earthquake early warning. FP is a computationally highly efficient algorithm that operates on discretized time-series with little or no pre-processing, which may be a broadband data stream as output from a digitizer without filtering or mean removal. The algorithm principle consists of a relatively simple multiband signal processing, which allows decomposing the original signal in a pre-determined set of band-passed time series with different center periods. These latter are in turn used to compute a set of characteristic functions that can be combined or analyzed independently to detect a phase arrival and declare a trigger. Picks are produced as soon as the arrival waveform is available, making FP particularly suitable also for EW applications.

The measured P-wave arrivals at every station are analyzed to determine whether they are coherent with the propagation from a common source. This analysis criterion is based on the coincidence of a certain number of picks within a given time window, dependent on the average station spacing (Satriano et al., 2011).

1.2.2 Earthquake location

The earthquake location of PRESTo is based on RTLoc algorithm (Satriano et al., 2008). This real time algorithm provides a probabilistic estimation of the hypocenter location and origin time using

information from both triggered and not-yet-triggered stations. The technique uses the formulation based on the equal differential time (EDT) surfaces (Font et al, 2004). These latter are open surfaces in the Earth whose points are characterized by an equal differential travel time from a pair of stations. The location algorithm draws an EDT surface for each pair of stations and searches for the hypocenter in the area crossed by the largest number of EDT surfaces. As the number of triggered and not-yet stations increases, the volume bounded by the EDT surfaces decreases and the location converges to a standard EDT location (Satriano et al., 2011).

1.2.3 Magnitude estimation

PRESTo provides a real-time magnitude estimation using the algorithm RTMag (Lancieri and Zollo, 2008). It is based on the empirical correlation law between the P and the S peak displacement, measured on the first seconds of low-pass-filtered signal after the phase arrival, and the final earthquake magnitude (Satriano et al., 2011). This relation consists in a pre-determined regression, dependent on the seismic phase and on the length of the considered time window, generally 2 or 4 seconds for the P phase and 1 or 2 seconds for S wave. In this study we considered the relationship estimated by Lancieri and Zollo (2008), who used the *European Strong-Motion Database* (ESD) and the *Japanese K-Net/Kik-Net strong motion network data-set*. The Peak displacement is computed immediately after the event detection and its first location. At each time step the measurement of Peak Displacement for every station and time window provides the magnitude estimation, following a Bayesian approach. This estimation is continuously updated in correspondence of the arrival of new signal from the stations, and when the hypocenter location and uncertainty respect to the previous instant changes.

1.2.4 Peak ground shaking prediction and alarm messages at target sites

PRESTo is able to predict the Peak Ground Acceleration (PGA), the Peak Ground Velocity (PGV) and the instrumental Intensity (I) at each configured target site using regional Ground Motion Prediction Equations (GMPE), dependent on the magnitude and epicentral distance (Satriano et al., 2011). PGA, PGV and I, as well as their uncertainties, are calculated as soon as the first magnitude and epicentral distance predictions are available, and they are updated whenever the source parameters estimation change.

During the occurrence of an energetic event, the evolutionary estimates of location, magnitude and peak ground motion at a target site are communicated to a list of users.

The user can choose the sites to alert and several associated parameters like the alarm format, the transmission protocol and the ground motion threshold above which to send an alarm (Satriano et al., 2011).

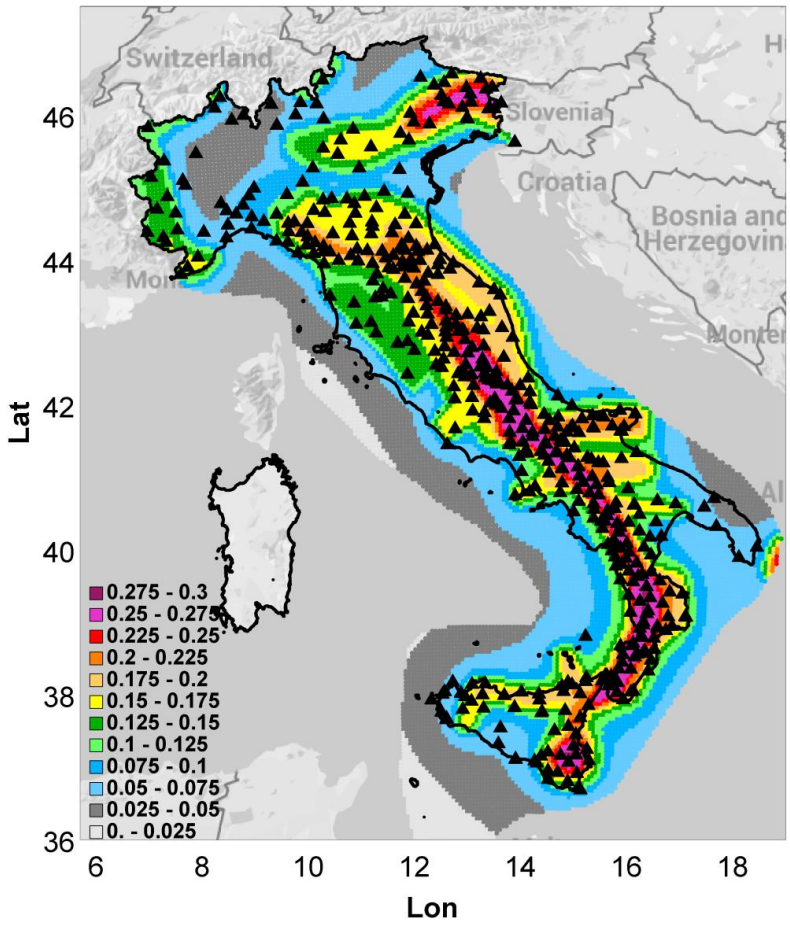

Figure 1.2: Seismic hazard map for Italy showing the peak ground acceleration values that have a 10% chance of being exceeded in 50 years (http://esse1-gis.mi.ingv.it/s1_en.php, redrawn), and the RAN-Italian Accelerometric Network (black triangles).

1.3 The Italian Accelerometric Network RAN

The Italian strong motion network consists of about 500 digital strong motion stations with data telemetry and time synchronization by GPS. It covers all the higher seismic hazard regions of the Italian territory with a 20-30 km mesh step (figure 1.2), and frequently its stations are located within urban areas. The network is managed by Dipartimento della Protezione Civile (DPC) and its recorded data are collected, validated and organized in the public database ITACA 2.0 (Luzi et al., 2008; Pacor et al., 2011). In the RAN network 198 stations are located into electric transformation

booths of the Italian electric company "ENEL Distribuzione", and 330 have been built in free field (2014 update). The free field station data-loggers are mainly Etna or Basalt Kinemetrics with a dynamic range(19-24 bits) and are equipped with three components FBA23 or Episensor sensors. The stations within the electric booths are made up with Syscom motion processor units (www.syscom-instrument.com), REFTEK 130 data-loggers and FBA23 strong motion sensors. All the instruments have a ±1 g full-scale range, the time synchronization by GPS and data telemetry by General Packet Radio Service(GPRS) digital data transmission. Currently, the RAN stations begin to record the seismic event if the 10^{-3} g threshold is exceeded and they stop when the ground motion amplitude is equal to the pre-event level. Subsequently, the recordings are sent by GPRS to the DPC center. Furthermore, during the occurrence of an earthquake, the RAN stations transmit in real time to the DPC by short message service (SMSs) the PGA values and the timing of the seismic event for a very rapid estimate of the ground shaking level. The RAN data centre is placed in the DPC headquarter (Rome, Italy) and it controls the network efficiency and the strong motion data production by the software package "Antelope", provided by Boulder Real Time Technologies (BRIT, http://www.brtt.com).

2. Methodologies of EEWS performance assessment for RAN Network

In this thesis the potential of a nation-wide EEWS for Italian territory has been explored using the integration of the RAN Network and the PRESTo software. This feasibility study has been conducted considering two different strategies based on real and synthetic data. The two analyses are described in the following sections.

2.1 Analysis based on real data

In this analysis, the off-line mode of the PRESTo software has been applied on the RAN recordings correspondent to the moderate to strong earthquakes that occurred in Italy the last decade. The seismic waveforms have been selected from the project ITACA 2.0 web-page (Luzi et al., 2008; Pacor et al., 2011), where the recordings are made freely available. In particular, we analyzed the data relative to the 40 events having local magnitude larger than 4.5 occurred in the Italian territory during the period 2002-2013 (figure 1.6a).

In this case, the performance of the RAN-PRESTo system has been evaluated in terms of its capability to provide epicentral location, magnitude and the time of first alert, defined as the difference between the first P-wave arrival and the instant at which the first source parameters

estimation is made available. In particular, in order to take into account the trade-off between the number of available data in real-time and the precision of the early warning estimates, two different time parameters in the off-line mode have been considered for the RAN-PRESTo performance evaluation. The first time parameter is the instant t_{alert} at which a fixed number of RAN stations (generally from 3 to 6) detects the event, and its minimization can provide alert messages characterized by high lead-time and well-constrained earthquake location to target sites (Picozzi et al., 2015a). The second time parameter corresponds to the instant $t_{0.5}$ at which the uncertainty interval associated to the evolutionary magnitude estimation is smaller than 0.5 magnitude units (m.u.). This parameter can be considered, in first approximation, as an indication of the stability of magnitude estimation provided by the system and it can assume a different value for each event, being essentially dependent on the network geometry.

Zone	M_{min}	M_{max}	ν	B	Z_{eff}
901	4.3	5.8	0.045	1.133	8
902	4.3	6.1	0.103	0.935	10
903	4.3	5.8	0.117	1.786	9
904	4.3	5.5	0.050	0.939	7
905	4.3	6.6	0.316	0.853	8
906	4.3	6.6	0.135	1.092	8
907	4.3	5.8	0.065	1.396	8
908	4.3	5.5	0.140	1.408	10
909	4.3	5.5	0.055	0.972	10
910	4.3	6.4	0.085	0.788	10
911	4.3	5.5	0.050	1.242	8
912	4.3	6.1	0.091	1.004	7
913	4.3	5.8	0.204	1.204	13
914	4.3	5.8	0.183	1.093	13
915	4.3	6.6	0.311	1.083	8
916	4.3	5.5	0.089	1.503	6
917	4.3	6.1	0.121	0.794	7
918	4.3	6.4	0.217	0.840	13
919	4.3	6.4	0.242	0.875	8
920	4.3	5.5	0.317	1.676	6
921	4.3	5.8	0.298	1.409	7
922	4.3	5.2	0.090	1.436	13
923	4.3	7.3	0.645	0.802	8
924	4.3	7.0	0.192	0.945	6
925	4.3	7.0	0.071	0.508	4
926	4.3	5.8	0.061	1.017	4
927	4.3	7.3	0.362	0.557	9
928	4.3	5.8	0.054	1.056	13
929	4.3	7.6	0.394	0.676	13
930	4.3	6.6	0.146	0.715	13
931	4.3	7.0	0.045	0.490	10
932	4.3	6.1	0.118	0.847	13
933	4.3	6.1	0.172	1.160	10
934	4.3	6.1	0.043	0.778	10
935	4.3	7.6	0.090	0.609	13
936	3.7	5.2	0.448	1.219	3

Table 1.1 : Characterization of the seismic sources corresponding to the ZS9 seismic zonation (Meletti et al., 2008), according to Barani et al. (2009). For each zone the following information is provided: minimum (M_{min}) and maximum magnitude (M_{max}), annual rate of earthquake occurrence for M_{min} (ν) and negative slope of the Gutenberg-Richter relationship (*b*), and the 'efficient depth', e.g. the bottom depth of the crustal layer within which the frequency distribution of the events is considered uniform (Z_{eff}). See Figure 1.3 for the distribution of the zones.

2.2 Analysis based on synthetic data

In the following part, synthetic simulations have been considered in order to extend the performance analysis of the RAN-PRESTo system to the whole national territory, also including potentially damaging earthquake (M_L>6.5) scenarios. The analysis consisted in considering for the Italian territory a regular grid in which each node represents a virtual location of a seismic source. In particular, the grid is the same one adopted for the INGV seismic hazard map in Italy (a node each 0.05° x 0.05°) and it has been assumed that every virtual source can produce a ground shaking equal to the maximum value estimated for the seismic zone (ZS) that contains the source. In order to characterize the sources for the Italian territory, the ZS9 seismogenic zonation (Meletti et al., 2008) and the seismic parameters correspondent to each zone (Barani et al., 2009) have been considered (Table 1.1). Furthermore, the depth of each source has assumed to be equal to the 'efficient depth', defined as the bottom part of the layer where 90% of the events in the single ZS occurs (Gruppo di lavoro MPS 2004, Table 1.1).

These synthetic seismic sources have been grouped into four classes, called Macro-Zones (MZ), based on the maximum magnitude expected for each ZS (Figure 1.3). They consisted in ZS having maximum magnitude equal or larger than 6.5, comprised between 6 and 6.5, between 6 and 5, and equal to 5. In particular, the last MZ is constituted by all the nodes not belonging to the first three MZ, for which the maximum magnitude value is assumed equal to 5.

For the four described MZ, the results and their discussion are reported in the following sections.

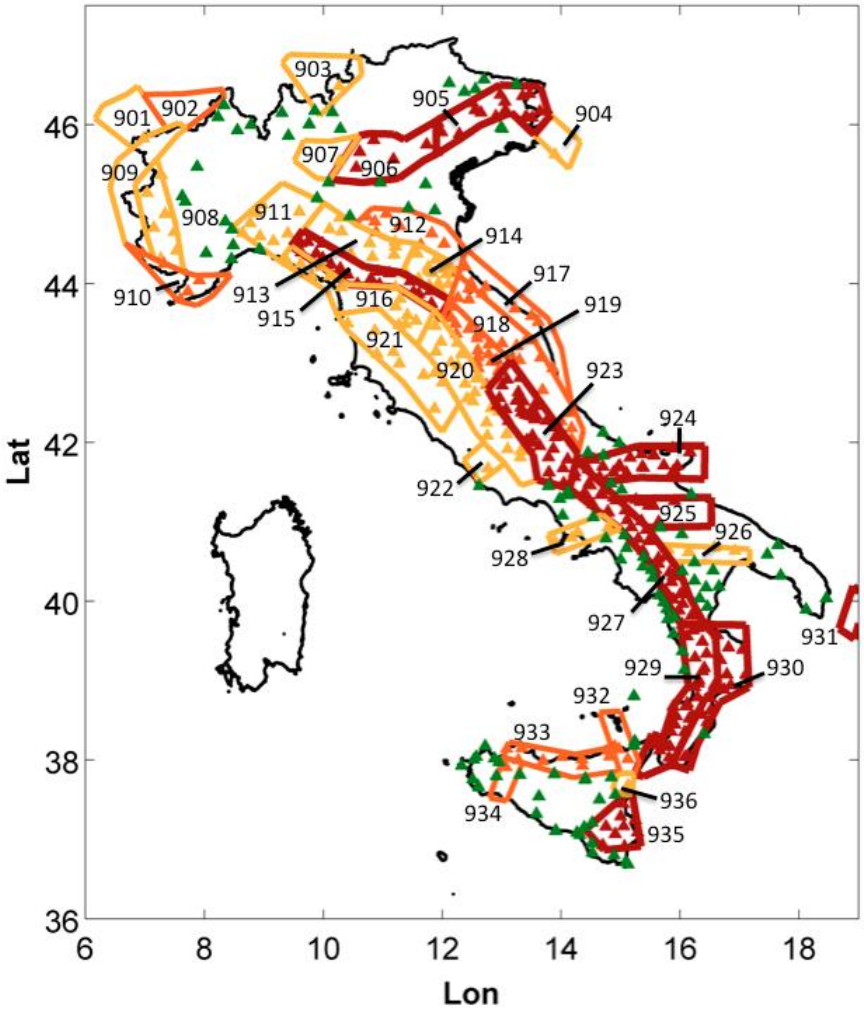

Figure 1.3: Distribution of RAN stations in the seismic macro-zones (MZ). These MZ are obtained by gathering seismic zones (ZS) with $M_{max} \geq 6.5$ (red); with M_{max} between 6 and 6.5 (orange); M_{max} between 6 and 5 (yellow); and finally, RAN stations outside of all ZS (green), which have been assigned to the fourth MZ. The numbers refer to the ZS listing in Table (1.1), according to Barani et al. (2009).

2.2.1 Network geometry criteria

The stations distribution has a crucial role for the effectiveness of the EEWS, because it determinates the rapidity of a network to issue an alert (Picozzi et al., 2015a). In order to estimate the network performance in terms of this last quantity, the first parameter studied in this analysis is the first alert time. Considering the synthetic seismic signal of each source and the velocity models proposed by Li et al., (2007) this parameter has been measured.

The second parameter analyzed for the EEWS performance evaluation is the dimension of the Blind Zone (BZ). The BZ is defined as the area where the destructive S-waves reach the target before an alert is issued and then no lead-time is available for safety action. This last parameter depends both on the network geometry, such as the first alert time, and operational parameters like telemetry and computation. In this analysis the computation of the BZ takes into account the sum of three delays. The first contribution is the first alert time that in this study corresponds to the trigger of 3 and 6 RAN stations. The second delay is related to the telemetry and computation, and it is assumed equal to 2 seconds, according to the value measured for PRESTo at the ISNet accelerometric network (Southern Italy) over a long period of testing (Satriano et al., 2011, Picozzi et al., 2015a). The last contribution is associated to the 2 seconds of P-wave needed by RTMag algorithm to estimate the magnitude.

Finally, the sum of these three contribution has been converted in the radius of the BZ multiplying it for the average S-wave velocity, derived by the Li et al., (2007)'s velocity model.

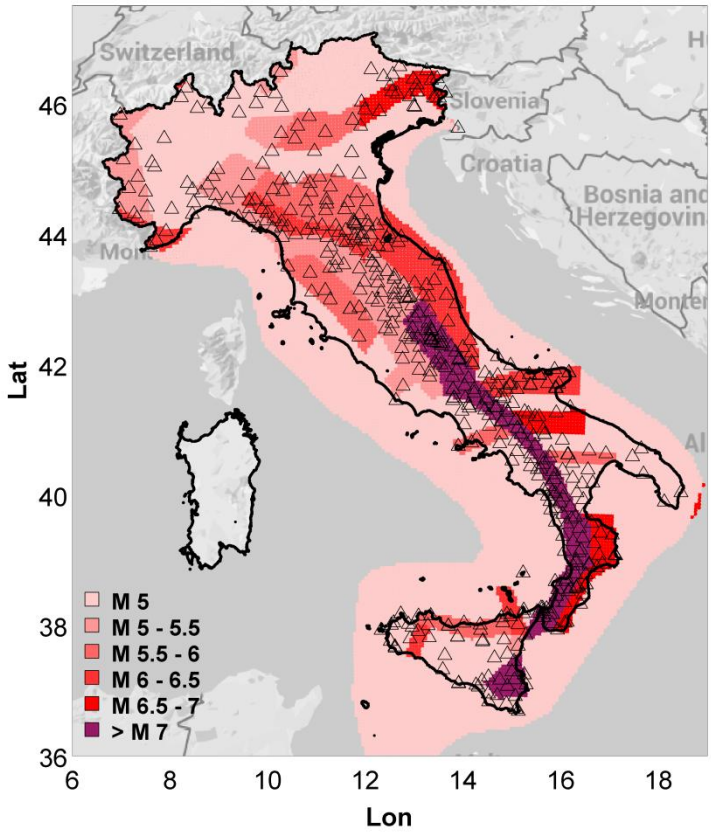

Figure 1.4: Magnitude values corresponding to the 10% probability of occurrence in 50 years with respect to which the EEWS RAN-PRESTo is tested.

2.2.2 Network geometry and reference scenario criteria

Taking into consideration the ZS proposed by Meletti et al.(2008) and the seismic parameters of each ZS proposed by Barani at al.(2009), we defined for each grid node a reference earthquake as the event having a magnitude corresponding to the 10% probability of occurrence in 50 years (figure 1.4). For those nodes that were not included in any ZS, we forced the magnitude to be equal to 5. This analysis, taking into account intense earthquakes, allows to evaluate the performance of a nation-wide EEWS for potentially damaging events, which are the same event considered by the legislator to define the reference ground motion within the Italian seismic building code (Picozzi et al., 2015a).

The main parameters derived to quantify the benefit and the efficiency of an EEWS in Italy are the BZ and the estimated Damage Area (DA) for each node (figure 1.5). The DA is defined as the area where the peak ground velocity (PGV) is greater than 6.1 cm/s, which corresponds to the lower bound of the EMS Intensity class VII (Faccioli & Chiauzzi, 2006; Grünthal et al., 1998). The selection of this last threshold allows to consider the widest region that suffers damage, providing a minimization of the number of missed alerts. The dimension of the damage area has been obtained calculating PGV on the surface using the earthquake reference parameters of each node and the Akkar and Bommer (2007a) GMPE relationship. In order to take into account the variability of PGV values observed in the experimental data, three different DA values have been considered. They correspond to the average PGV, the average PGV plus and minus one standard deviation (σ) of the GMPE regression. In the case where DA is larger than BZ, the ring (circular band) related to the difference between radii of DA and BZ, has been defined as the "Early Warning Zone" (EWZ). Within this zone the lead-time ranges from 0 at the circular border of BZ up to a maximum positive number, function of the DA area extension. In order to allow an effective implementation of early warning operations within the EWZ, the lead-time value should take into account the time necessary for safety procedures and the time of alert delivery. The transmission of the alert message can have duration of a few tens of milliseconds as measured at the ISNet Network (Satriano et al, 2011). On the contrary, the duration associated to the execution of safety procedures is strongly dependent on the user training, and to the efficiency of the automatic protective operations. Although this aspect is very important, to evaluate the effectiveness of an operational EEWS is beyond the aim of this thesis.

Finally, given the EWZ associated to a node, we also estimated the number of municipalities falling within it, in order to quantify the number of potential beneficiaries of the RAN-PRESTo EEWS alert.

a)

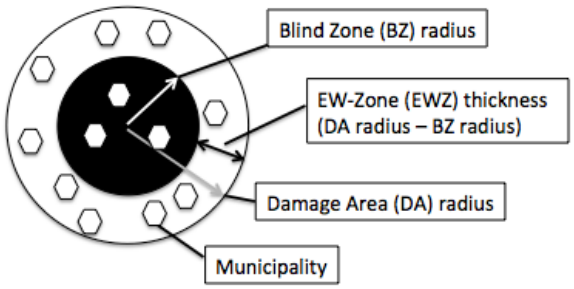

b)

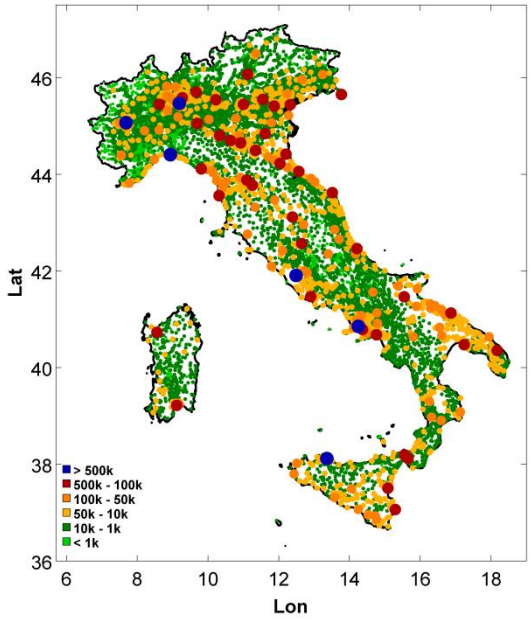

Figure 1.5: a) Schematic representation of the parameters adopted for quantifying the PRESTo-RAN EEWS performance. b) Municipalities and the relevant 2011 post-census resident population in thousands (http://demo.istat.it).

2.2.3 Gutenberg-Richter derived sequences

The last part of the analysis has been centered on the capability of the RAN-PRESTo EEWS to predict the earthquake location and magnitude using only the recordings of a small number of

stations. With this aim, a grid of synthetic sources has been considered for the whole Italian territory and first ten sets of synthetic P-wave arrival times have been computed for every grid node. These recordings have been obtained using the four velocity models for P- and S-waves provided by Li et al., (2007). Furthermore, two random sources of uncertainty have been added to the synthetic data. The first contribution consists in a random error that takes into account the uncertainty for each velocity models layer estimated by Li et al., (2007). The second contribution is a temporal shift around the synthetic arrival time, having a Gaussian distribution with a standard deviation equal to 1 s. Then, the PRESTo performance has been evaluated on these data in terms of epicentral location, using RTLoc algorithm.

The source characteristics of each node are determined by the seismic hazard parameters of the ZS containing the node. For each grid node, ten earthquake sequences have been generated with a magnitude interval of 0.5 magnitude units, following the Gutenberg-Richter (GR) distribution. In particular this earthquake sets have been built considering a virtual testing period of 50 years and the correspondent moment magnitude M_W ranges between 5 and the maximum value associated to ZS (i.e., M_{max} in Table 1.1). For each source-node, the relationship between the Peak Displacement (PD) and the magnitude, derived by Lancieri and Zollo (2008), has been used to obtain random values of the PD for the first three triggered stations. These values, correspondent to signal windows of 2/4 seconds for P-wave and 2 seconds for S-wave, have been selected within the uncertainty bounds of the regressions. The variability of the observed P-wave peak measurements have been reproduced in the simulated data considering the uncertainties of the Lancieri and Zollo (2008) relationships and on the real-time earthquake location. On these data the RTMag performance for the magnitude prediction has been evaluated counting the number of cases in which the magnitude estimation is contained within the interval $[M_{W(BULL)}-0.5, M_{W(BULL)}+0.5]$ around the ITACA 2.0 bulletin value $M_{W(BULL)}$.

3. Applications and results

In the following sections the application and the results of the three described analyses are presented**.** Figure (1.3) shows that the stations density is much higher for the group of ZS having the highest seismic hazard. This observation is not surprising, because RAN was designed and developed throughout the years to cope with the past and actual seismicity distribution. We found that within the highest seismic hazard zone, MZ-I (Figure 1.3), the stations density is one per 308 km^2 (i.e., corresponding to an average inter-stations distance of about 17.6 km). This value is similar to that of the Japan accelerometric network one (i.e., average inter-stations distance of about

19 km). The MZs II, III and IV have a stations density equal to one every 544, 622, and 1134 km^2 (i.e., average inter-stations distance equal to 23.3, 24.9 and 33.7 km), respectively.

3.1 PRESTo performance on RAN real data

The real-time PRESTo functioning has been simulated for 40 earthquakes by using the RAN Network recordings (figure 1.6a). These events have magnitude between 4.3 and 6.3 and occurred during the period 2002-2013 in the Italian territory. For most of these earthquakes, the high RAN density allows obtaining with PRESTo an earthquake location that differs less than 10 km from the epicenter provided by ITACA 2.0, even when only 3 stations have triggered (figure 1.6b). At this instant, the performance of PRESTo in estimating the magnitude M_{EW} has been assessed. We observed that a significant overestimation (e.g. a false alarm) of the ITACA bulletin moment magnitude (i.e. $M_{EW}>M_{W(BULL)}+0.5$) have been registered in the 12.5% of the events, while an underestimation (e.g. a missed alarm) has been observed in the 15% of the events (where $M_{EW}<M_{W(BULL)}-0.5$) (Figures 1.6c and 1.6e). In the remaining 72.5% of cases the first magnitude estimation is reliable (i.e. $M_{W(BULL)}-0.5 <M_{EW} < M_{W(BULL)}+0.5$) and provided within 2-3 seconds after the first P-wave arrival. These results have been obtained without taking into account the time necessary for data telemetry, which, as discussed, we assume being 1 second in agreement with what observed operating the ISNet network.

The analysis results show that 2-3 seconds after the first alert time are sufficient to obtain a general convergence of the magnitude estimates M_{EW} towards $M_{W\ (BULL)}$ (Figures 1.6d and 1.6f). In particular, considering the magnitude estimates at the $t_{0.5}$, the percentages of false and missed events decrease to 2.5 % and 10% respectively, while in the 87,5% of cases the magnitude predictions are very close to $M_{W(BULL).}$

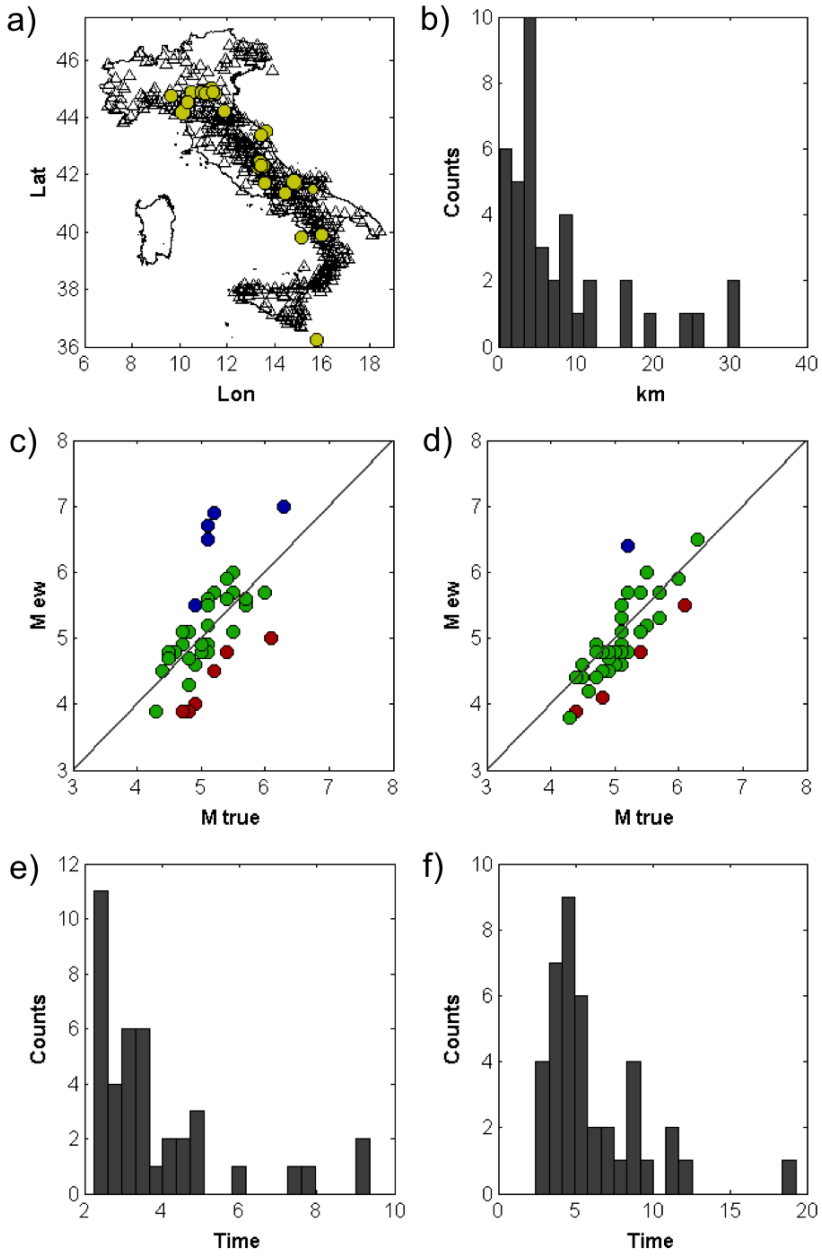

Figure 1.6: Results of the PRESTo playbacks with RAN recordings of forty earthquakes having magnitudes larger than 4.5 that occurred in Italy during the period 2002 – 2013. a) RAN stations (triangles) and epicentres (yellow dots). b) Error in epicentral estimation. c) Comparison of Magnitude values estimated within the early warning timeframe M_{ew} (i.e., when 3 stations have triggered) and from bulletin, M_{true}: difference within 0.5 units (green), M_{ew} larger than M_{true} plus 0.5 unit (blue), M_{ew} less than M_{true} minus 0.5 units (red). d) same as c), but at the instant when the uncertainty associated with M_{ew} is less than 0.5 units. e) Seconds needed by the PRESTo system for the first M_{ew} estimation. f) Same as e), but for the instant when the uncertainty associated with M_{ew} is less than 0.5 units.

3.2 First Alert Time and Blind Zone

The influence of the stations distribution on EEWS performance has been assessed considering the first alert time and the blind zone size for the cases of three and six triggered stations.

Using only 3 stations, the first alert time is smaller than 5 seconds for most of the synthetic sources along the Apennine chain (figure 1.7a). Its average value for the four MZs are reported in Table (1.2), and they range from a minimum of 3.7 seconds for MZ I (higher seismic hazard) to a maximum of 11.4 seconds for the source-nodes not included in any seismic zone (MZ IV). Considering 6 stations (figure 1.7b), the first alert time varies between 5.3 and 14.3 seconds in correspondence of the MZ I and MZ IV, respectively (Table 1.2). Since the RAN's density is generally high throughout the Italian country, the EW performance with the use of 6 stations doesn't change significantly along the Apennine with respect to the previous case and the first alert time is almost equal to 5. On the contrary, a worsening of the performance has been observed in the North-Eastern Italy and in some parts of Sicily, where the first alert time increases to values included between 5 and 10 seconds (compare figures 1.7a and 1.7b).

In the case of three triggered stations, the BZ radius is smaller or equal to 25 km for most of the ZSs and it is confined within 40 km (figure 1.7c), with exception of two areas in the Alps region (Northern Italy). Its averaged value, that ranges between 23 km and 42 km for the MZ I and MZ IV respectively, is reported in Table (1.2). Similarly to the case of the first alert time, the BZ radius tends to increase using six trigged stations (figure 1.7d), varying overall between 29 and 52 km (Table 1.2). In spite of this, passing from 3 to 6 used stations, in most of Italian regions the BZ radius is still confined within 30 km.

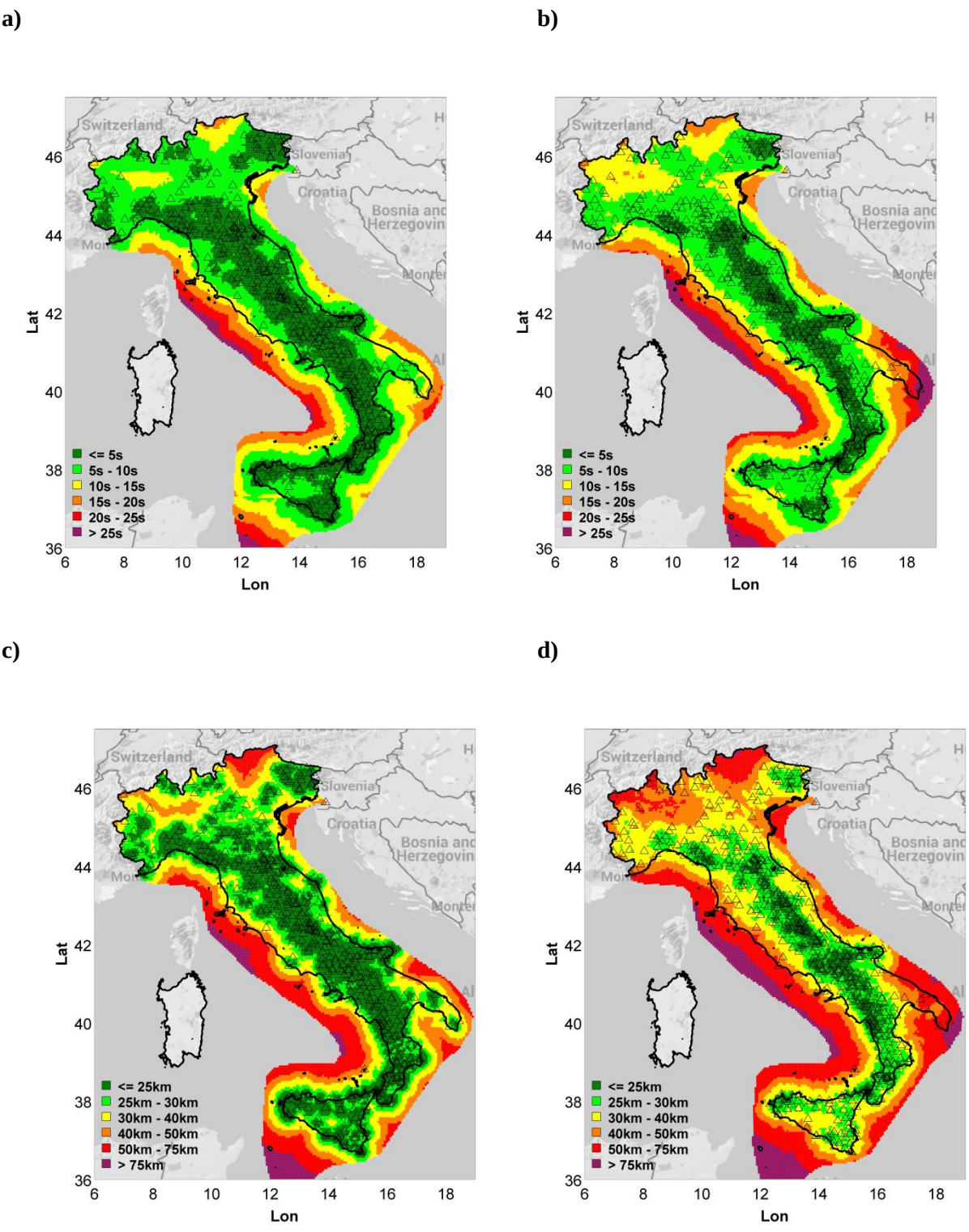

Figure 1.7: Distribution of the first alert time and the blind zone radius for the grid of synthetic sources derived from the PSHA map for Italy. a) and b) first alert time for 3 and 6 RAN triggered stations, respectively. c) and d) Same as a) and b), but for the blind zone radius.

Parameter	N. of triggered stations	I	II	III	IV
Time 1st Alert (s)	3	3.7	4.5	5.0	11.4
Time 1st Alert (s)	6	5.3	6.4	7.1	14.3
BZ radius (km)	3	23	25	26	42
BZ radius (km)	6	29	32	34	52

Table 1.2: Average of the EEWS performance parameters for the four MZ and a different number of triggered stations. Time is estimated off-line, and does not include that needed for telemetry and computation.

3.3 EEWS performance for reference earthquake scenarios

In this analysis the occurrence of the 1980 Irpinia earthquake (MS 6.9, Bernard and Zollo, 1989) has been simulated. For this event the BZ and the lead-times distributions have been calculated (figure 1.8b) and compared with the Observed Macroseismic field after the earthquake (Guidoboni et al., 2007; data available from http://emidius.mi.ingv.it/DBMI11/, Locati et al., 2011) considering the actual RAN configuration (figure 1.8a). In particular, for the municipalities having an assigned macroseismic intensity I_{MCS} equal or larger than VII (i.e. from moderate up to very high damage) we assumed that an EEWS was operational. The results show that the lead-time was smaller than 5 seconds for 53 municipalities, between 5 and 10 seconds for 73 municipalities, between 10 and 20 seconds for 112 municipalities and larger than 20 seconds for 24 municipalities. This scenario study for the 1980 Irpinia earthquake shows that an EEWS could hypothetically have provided an alert to about 262 municipalities affected by damage. Among these localities 136 would have benefited of a lead time larger than 10 seconds (Picozzi et al., 2015a). Furthermore, the damage area (DA), the blind zone (BZ), and the early warning zone (EWZ) dimensions have been derived for this event, at the instant when three stations triggered (Figure 1.8b, Table 1.3). Considering the actual high RAN density in the Irpinia region, the estimated BZ value is about 20 km and the municipalities contained within it is 31 (Table 1.3). Despite this localities couldn't be alerted, the EWZ radius, equal to 56 km, would have allowed 414 municipalities to benefit a EEWS warning message (Table 3, Figure 8b). It's interesting to note that the number of municipalities within the EWZ, obtained by the mean PGV values of the Lancieri and Zollo (2008)'s GMPE, is comparable to the number of localities having $I_{MCS} \geq$ VII. In this EWZ the maximum lead-time derived is 18 seconds (Table 1.3).

In order to consider the worst scenario for the Irpinia earthquake, the EWZ has been also derived adding the uncertainty σ of the Lancieri and Zollo (2008)'s regression to the correspondent mean PGV values. In this case the number of municipality included within EWZ increases to 847.

a)

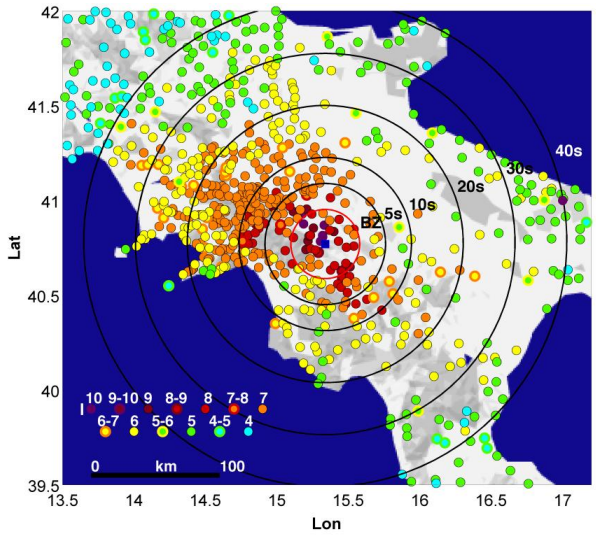

b)

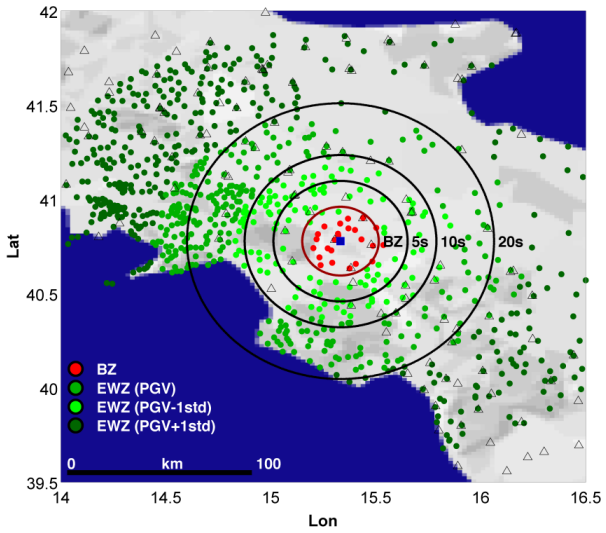

Figure 1.8: a) Macroseismic intensity of the November 23, 1980 Irpinia Earthquake (M_W 6.9) from Guidoboni et al., 2007 (data available from Locati et al., 2011). Epicentre (blue square), the circles indicate the BZ (red line) and distribution of LT (i.e., 5, 10, 20, 30 and 40 seconds, black line). b) Municipalities within the BZ (red) and the EWZ (different green tone for the average PGV, and +/- 1 standard deviation, corresponding to the macroseismic intensity of level VII) for three triggered stations and the scenario mimicking the South Italy 1980 Irpinia Earthquake (M_W 6.9). LT circles are as in a).

Region	BZ (km)	EWZ (km) *mean PGV (-σ; +σ)*	Lead Time (s) *mean PGV (-σ; +σ)*	N.Munic. Blind Zone	N. Munic. EWZ *mean PGV (-σ; +σ)*
Irpinia	20	56 (25; 110)	18 (8; 36)	31	414 (124; 847)

Table 1.3: EEWS performance for the 1980 Irpinia scenario.

This analysis has been extended to the reference earthquakes defined in the section 2.2.2 for all the grid nodes that cover the Italian territory, using three and six triggered stations (Table 1.4). Considering only three stations (Figure 1.9), the EWZ radius and lead-time values are null for the MZ II, III and IV. This result is due to the low value of the maximum magnitude expected in those regions, which, given the current RAN distribution, determinates DA with dimension comparable to the BZ one. Therefore, in low or moderate seismic hazard areas, the use of the on-site EEWS would be more appropriate (Picozzi et al., 2015a). On the other hand, in the higher seismic hazard regions (MZ I) significant EWZs and lead-times are always available during the occurrence of large magnitude earthquakes (Table 1.4), both considering three and six triggered stations. Furthermore, for the source-nodes having magnitude larger than 6.5 (compare with figure 1.4), the EWZ dimension is on average 85 km using three triggered stations (figure 1.9, Table 1.4). The maximum lead-time in these EWZs is larger than 25 seconds, and then, the number of municipalities that might potentially benefit of a warning message is equal to 493 (Table 1.4).

a)

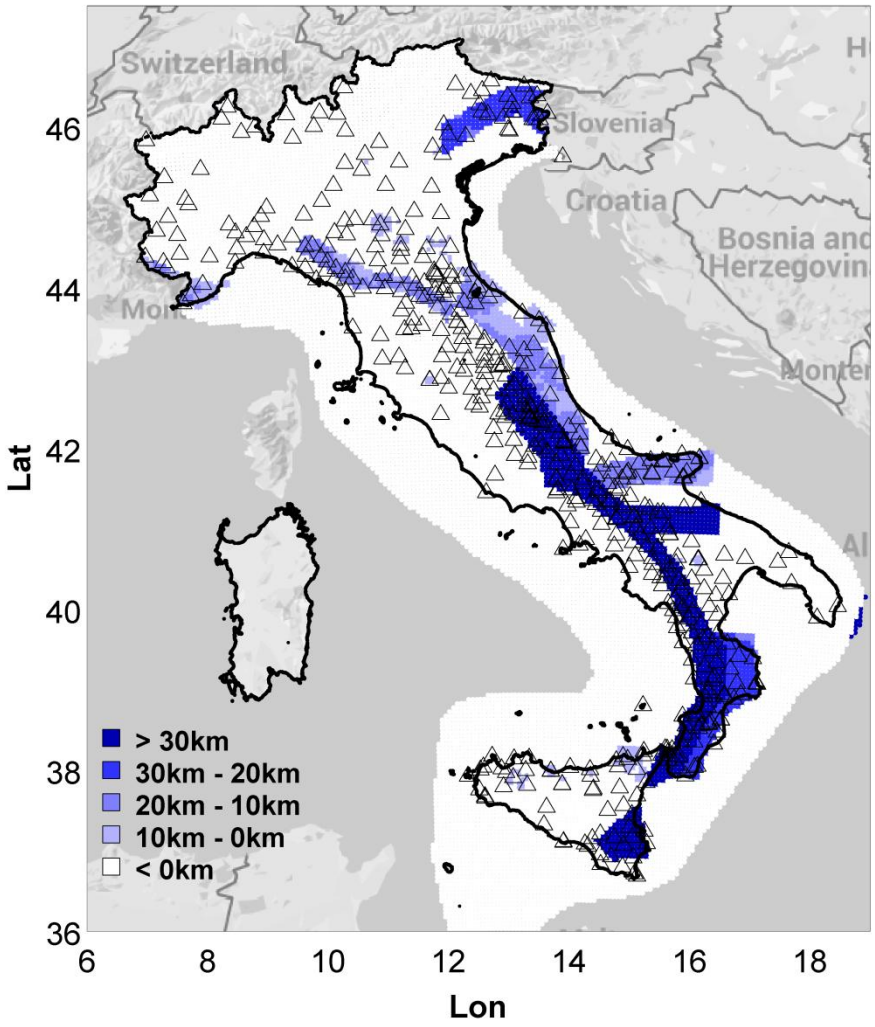

Figure 1.9: Overview of the EW parameters performance for reference events (i.e., with a magnitude > 5 having 10% probability of occurrence in 50 years) for three triggered stations: a) Radius of the Early Warning Zone; b) Maximum lead-time; c) Number of municipalities within the Early Warning Zone.

b)

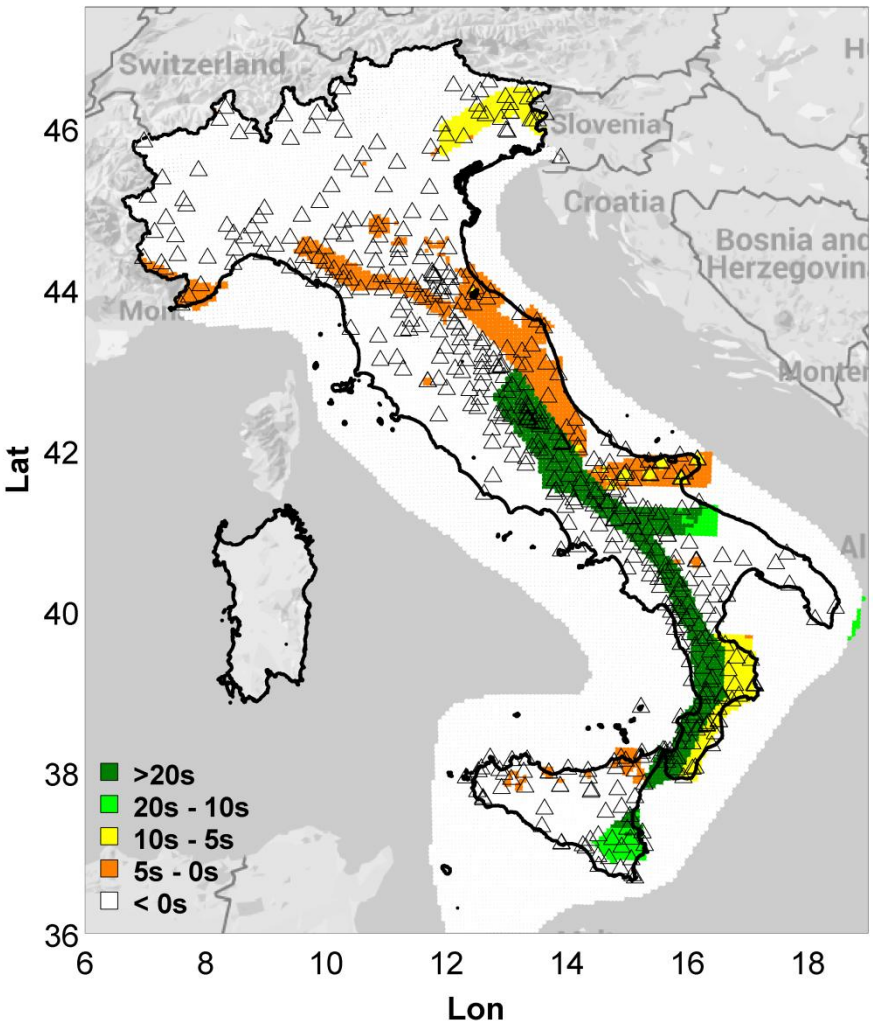

Fig. 1.9 - *continued*

c)

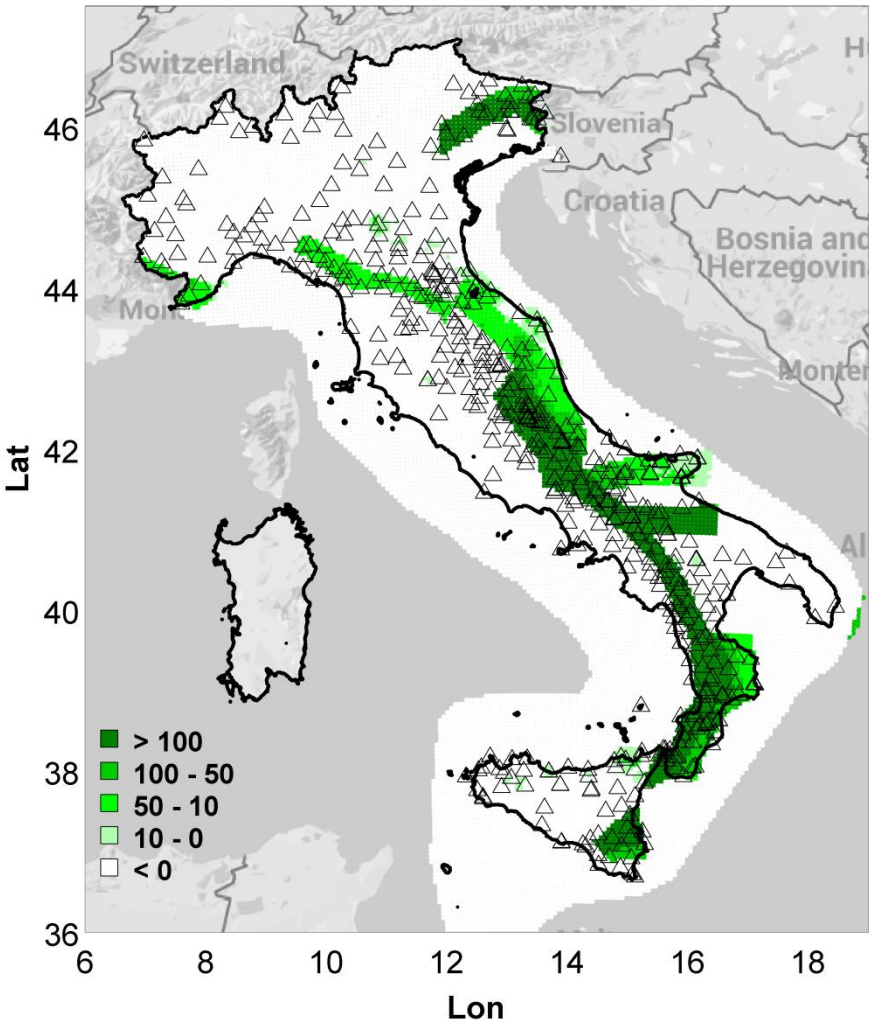

Fig. 1.9 - *continued*

Parameter	**N. st.**	**MZ I** ***mean PGV*** ***(-σ; +σ)***	**MZ II** ***mean PGV*** ***(-σ; +σ)***	**MZ III** ***mean PGV*** ***(-σ; +σ)***	**MZ IV** ***mean PGV*** ***(-σ; +σ)***
EWZ width (km)	3	85 (41; 150)	2 (<0; 24)	<0	<0
EWZ width (km)	6	77 (36; 144)	<0 (<0; 17)	<0	<0
Lead-Time (s)	3	26 (13; 47)	<0 (<0; 8)	<0	<0
Lead-Time (s)	6	24 (11; 46)	<0 (<0; 5)	<0	<0
N. Municip.	3	493 (226; 915)	None (None; 89)	None	None
N. Municip.	6	472 (205; 894)	None (None; 69)	None	None

Table 1.4: Average of the EEWS performance for the four MZ obtained considering for each grid node a magnitude having a 10% of probability of occurrence in 50 years.

a)

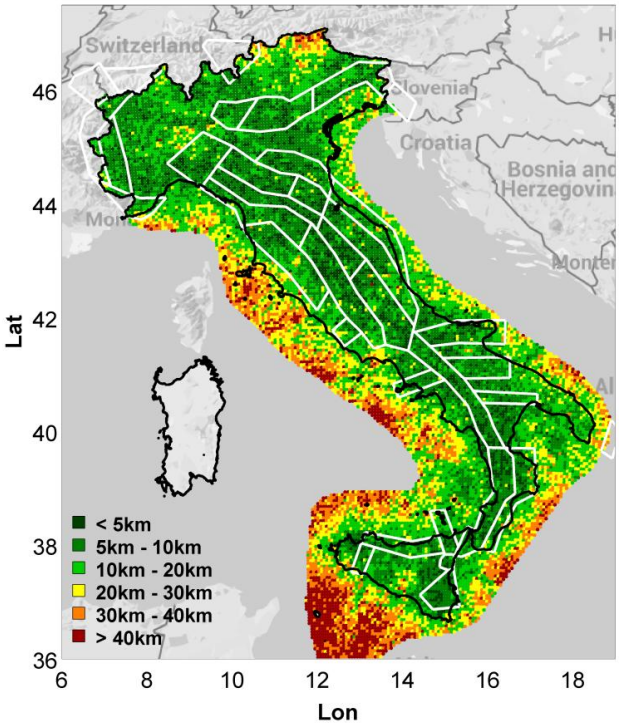

b)

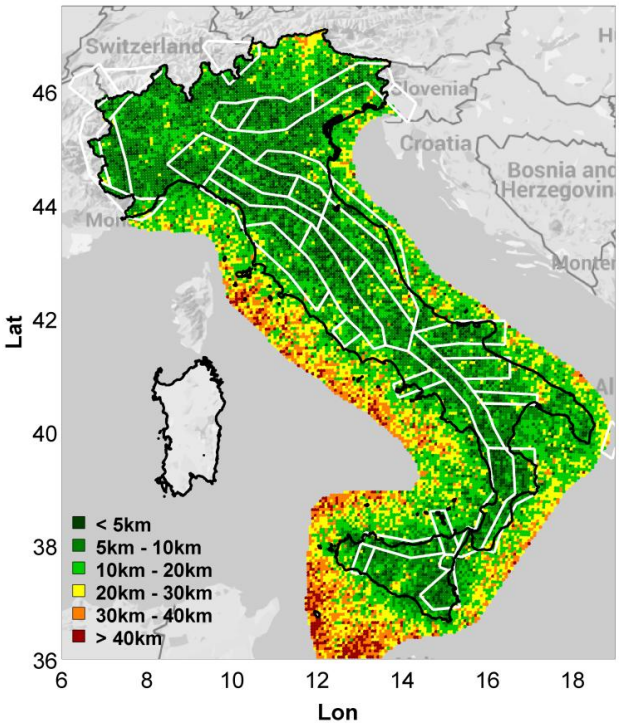

Figure 1.10: RTLoc performance on synthetic data at the national scale in terms of average epicentral error. a) three triggered stations, b) six triggered stations. Boundaries of the ZS are shown as white lines.

N. of stations	MZ I	MZ II	MZ III	MZ IV
3	8.1	9.	9.7	20.3
6	8.7	9.4	10.5	18.1

Table 1.5: Average RTLoc epicentral errors (in km) for the four MZ.

3.4 EEWS performance for the earthquake location and magnitude estimation

The average epicentral error related to ten simulations of the RTLoc algorithm for each source-node of the grid has been calculated (figure 1.10) and grouped for the four MZs (Table 1.5). The results of this analysis indicates that for most of the Italian territory the epicentral location error at the first alert time ranges from 5 to 10 km, while it is larger than 20 km for off-shores sources and a few, small, on-land regions. These results are in good agreement with the epicentral location errors obtained by PRESTo on real RAN Network recordings (Figure 1.6b).

A performance based on the RTMag technique has been evaluated for the 1980 Irpinia earthquake scenario using three triggered stations (figure 1.11). In particular, P- and S-wave PD values have been randomly derived from the Lancieri and Zollo (2008)'s relationship for ten seismic sequences used as input for RTMag (figures 1.11a and 1.11b). The results of this analysis show that the absolute value of difference between the RTMag estimates and the real magnitude values is equal or smaller than 0.5 u.m. for most of cases and it never exceeds 1 u.m (figure 1.11c).

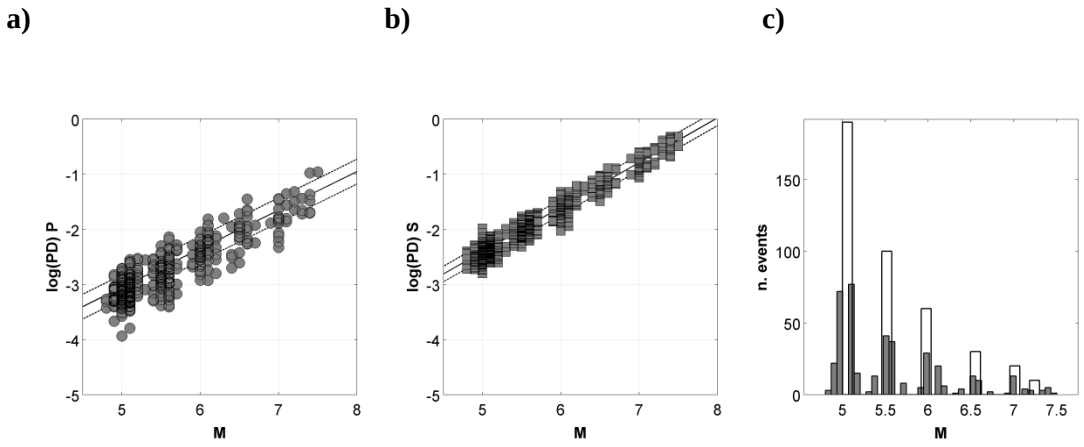

Figure 1.11: Results of the RTMag analysis on synthetic data derived from the simulation of the seismicity related to ten fifty years sequences in the same area of the 1980 Irpinia Earthquake. a) P-waves displacement peaks for a 4 second time window (grey dots), Pd-M relationships proposed by Lancieri and Zollo (2008) +/-

1 st. dev. (black lines). b) Same as a), but for S-waves peak displacement in a 2 second window. c) Histogram of the input (white bars) and output (gray bars) magnitude estimation.

Performance	***MZ I***	***MZ II***	***MZ III***	***MZ IV***
Success	97.1	95.9	95.8	71.5
False	1.4	1.5	0.7	2.6
Missed	1.5	2.6	3.5	25.9

Table 1.6: Average RTMag success, false, and missed rate (in %) for the four MZ when three triggered stations are used.

The same performance analysis has been conducted for the reference earthquakes associated to each synthetic sources on the whole Italian territory, considering both three and six RAN triggered stations. The results indicate that almost in every region of Italy the magnitude estimates differ less than +/- 0.5 u.m. from the real value for about the 90 % of simulations. The percentage of reliable magnitude estimates by RTMag is obviously higher with 6 triggered stations respect to the case in which 3 stations are considered. In this last case the percentage for which RTMag estimates differ less +/- 0.5 u.m. from the real value is comprised between 75% and 50% for three zones (figure 1.12a). These are two areas are in the Alps region (North Italy) and one area in Sicily (South Italy) and they are characterized by a low station density and a low seismic risk. Furthermore, figure (1.12c) shows that within the regions characterized by the worst performance of RTMag, the number of misses alarms (i.e., $M_{EW}<M_{W(BULL)}-0.5$) is larger than the false alarms one (i.e., $M_{EW}>M_{W(BULL)}+0.5$). Although in these areas the RAN-RTMag system tends to underestimate the magnitude of intense earthquake, it is able to provide reliable estimates in the regions with higher seismic hazard (compare Figure 1.2 and 1.12a). The results of this analysis are summarized for the four MZs in the table 1.6. In particular, the percentage of reliable magnitude estimates is above the 95% for MZ I and MZ III, while the RAN-RTMag system underestimates on average the real magnitude value (i.e., missed events) in 2.5% of the cases and overestimates (i.e., false events) in the remaining cases. On the other hand, in the MZ IV the reliable estimate rate is 71.5%, while the false and missed events rate is 2.6% and 25.9%, respectively.

Respect to the use of three triggered stations, the RTMag performance slightly improves when 6 stations are considered (compare Figure 1.12a and 1.12b) and its percentage of reliable magnitude estimations is larger than 95% in most of the country. Similarly to Figure (1.12c), Figure (1.12d) shows that in the areas where RTMag is less efficient, the real magnitude value is generally

underestimated. In table (1.7) the average percentage of the EW reliable magnitude estimates for the four MZ is showed, indicating a performance improvement when more stations are considered. In fact, in that case the reliable magnitude percentage ranges between 98% and 85%, the underestimation percentage between 0.6 % and 13% and the overestimation percentage between 0.4% and 14%.

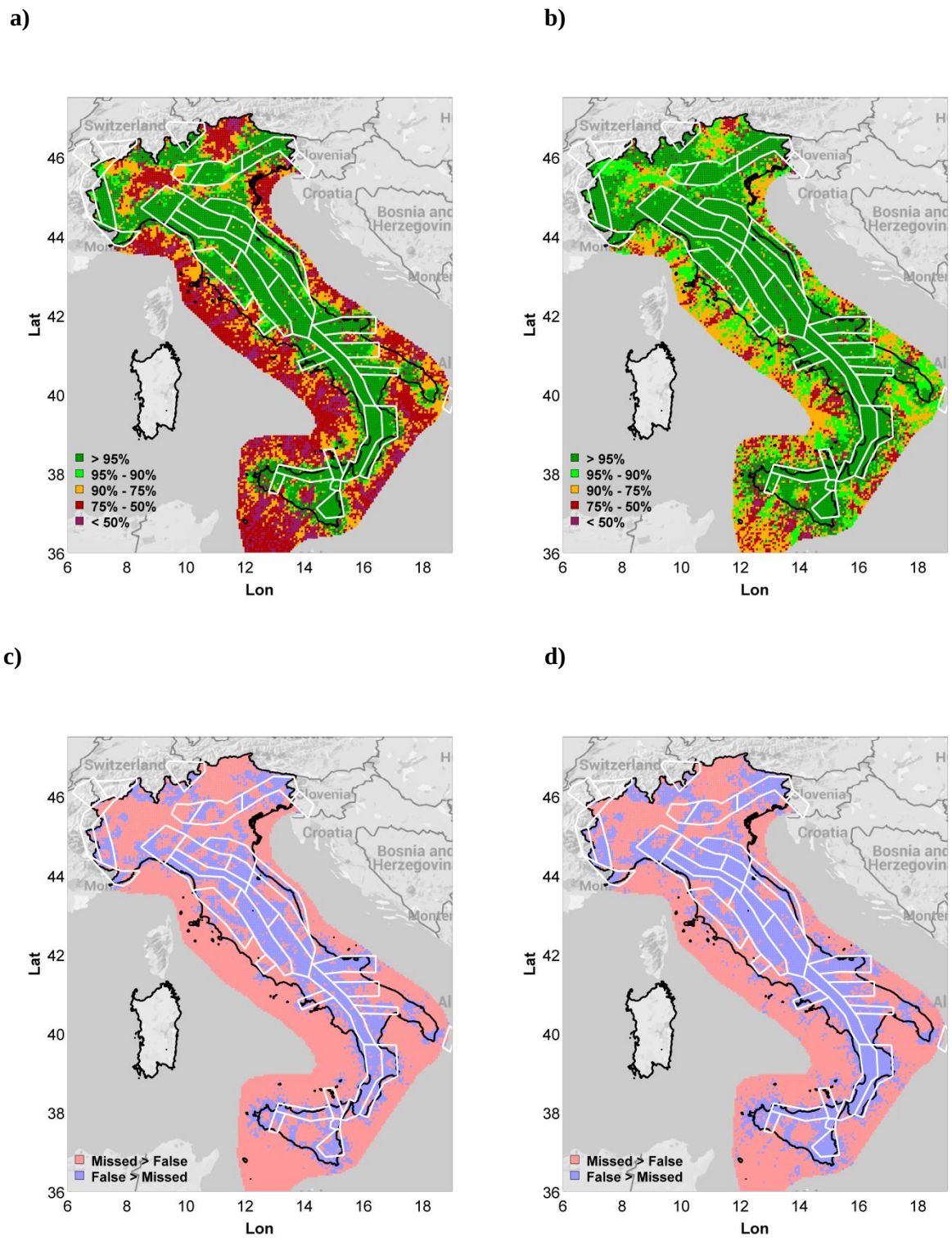

Figure 1.12: RTMag performance at the national scale from the simulation of ten fifty-years long seismic sequences according to the Gutenberg-Richter parameters of the ZS: a) percentage of success (i.e. M_{ew} included within the range M_{true} +/- 0.5 unit) for three triggered stations; b) same as a), but for six triggered

stations; c) distribution of underestimated and overestimated M_{ew} predictions for three triggered stations; d) same as c), but for six triggered stations. Boundaries of the ZS are represented by white lines.

Performance	***MZ I***	***MZ II***	***MZ III***	***MZ IV***
Success	98.2	97.8	98	85.6
False	1.2	1.2	0.4	1.4
Missed	0.6	1	1.6	13

Table 1.7: Same as Table (1.6), but for the case of six triggered stations.

3.5 Discussion and Conclusions

The previous sections presented the results of a feasibility study for an EEWS conducted by using real and synthetic data. The aim of scientific work was to assess the performance of a nation-wide earthquake early warning system in Italy based on the RAN network and the EW software platform PRESTo.

The performance analysis of the PRESTo regional scheme integrated with the RAN Network focused on the real-time estimation of earthquake location and magnitude.

Despite the fact that predicting the ground motion severity at target sites is the final outcome of an EEWS, this issue has not been included in the performance assessment of the RAN-PRESTo system because such an analysis would mostly depend on the uncertainty associated to the chosen GMPE.

It is worth noting that, although most of the EEWS software as PRESTo implicitly adopts the point source assumption, in case of large magnitude events (i.e., M > 6.5), the finite extent of the fault must be properly accounted for, along with directivity effects, and the source mechanism. In fact, these factors could have a dominant role on the ground motion at near-source target sites. A complementary approach, such as the threshold-based EW method proposed by Zollo et al., (2010, 2014) and Colombelli et al., (2012), would allow accounting, as a first approximation, for the source finiteness. In particular, it allows directly to map the Potential Damage Zone using the early P-wave peak displacement and characteristic period measurements at the near-source stations.

The performance of a nation-wide RAN-PRESTo EEWS was first evaluated by off-line simulations using seismic real-data. They correspond to forty moderate earthquakes that occurred during the last ten years in Italy and recorded by the RAN Network. In particular, the RAN network capability of providing fast earthquake location and magnitude estimations has been assessed. Furthermore, the

time at which this information is available, respect to the first P-wave arrival at the RAN stations, has been obtained. Concerning the epicentral location, the results indicate that using only three triggered stations, the retrieved epicenter differs from the bulletin ones less than ten kilometers in most cases.

It is worth noting that using the Pd-M relationship proposed by Lancieri and Zollo (2008), location errors within 50 kilometers correspond to errors in magnitude smaller than 0.5 units. The magnitude estimation with three stations, which would be available within three to four seconds after the first P-wave arrival, is reliable in 72.5% of cases, while it overestimates and underestimates the bulletin value in the 12.5%, and in the 15% of cases, respectively.

When further two or three seconds of signal are used, allowing an analysis with more stations, the percentage of reliable magnitude estimations increases to 87.5%, while the overestimation (i.e., false alarm) and the underestimation (i.e., missed alarms) rates became 2.5%, and 10%, respectively.

The analyzed strong motion data are relevant for some of the most active seismogenic Italian areas in the history. In this study it has been deducted that they provide a clear indication that the integrated RAN-PRESTo EEWS might have a great potential to issue a rapid alert during the occurrence of moderate and large earthquakes.

The analyses with synthetic data confirmed that the density of RAN stations in seismogenic zones has an important and direct impact on the EEWS performance, both in terms of geometrical and physical parameters of the source. Indeed, under the assumption of a fixed delay in the data telemetry and computation, it has been observed that the stations distribution constrains the first-alert time to be around 4 and 5.5 seconds in the high seismic hazard areas for the cases of three and six triggered stations, respectively. Furthermore, the blind zone in these areas has radius equal about to 25 and 30 kilometers when three and six stations have triggered, respectively. Such dimensions of blind zones indicates that a regional EW approach, such as the one explored in this study, would provide lead-times greater than zero only for events having magnitude larger than 6.5. These large threatening events, even if they occur less frequently than the smaller ones, are capable of generating great losses both in human and economic terms. For this reason, taking example from Japan and California experience, a country like Italy prone to large seismic hazard should employ all the existent seismic risk mitigation tools and strategies, including an EEWS.

The EEWS performance analysis of this study, based on reference earthquake scenarios, indicates that for large earthquakes in the higher hazard zones, the EWZ sizes would be in the order of eighty kilometers, the maximum lead-time around twenty-five seconds. Furthermore, the number of municipalities for which an alert would be useful is about five hundreds. These results have been

compared with the macroseismic intensity field observed after the 1980 Irpinia Earthquake and the LT distribution, theoretically estimated for this event considering the actual RAN geometry (Figure 1.8). In particular, it has been found that several tens of municipalities with I_{MCS} >= VII had a LT between 10 and 40 seconds. Moreover, several hundreds of municipalities are within the zone that observed I_{MCS} value between V and VII. In this area, where the shaking perception was high but no significant damages were observed, an EEWS's alert could be useful to inform the population about the impending earthquake, and to mitigate the panic effect.

The analysis focused on the network capability to provide fast and reliable estimations of earthquake location and magnitude using only three and six stations indicates that: a) location errors larger than 20 kilometers affect mainly offshore sources; b) the combination of a dense seismic network such as the RAN and a robust location algorithm, as RTLoc in PRESTo, allows EW locations with errors in the range between five and ten kilometers along most parts of the Italian territory; c) location errors obtained from synthetic data analyses are in good agreement with those obtained using PRESTo simulations on real RAN acceleration recordings; d) with respect to the location errors obtained considering six stations, the use of only three stations provides slightly better EEWS results, obtaining smaller blind zones (Figure 1.7). This last observation is confirmed by the average epicentral error of the MZ I, II, and III (Table 1.5). These findings are considered to be related to the stations density, to the use of both triggered and not-triggered stations in RTLoc, and to the level of noise associated the picks of the triggered stations. Indeed, in the regions where the RAN has a relatively high density, we found that, using three noise-biased picks combined with the existence of many nearby not-triggered stations, the location estimate is more robust than the case when six noise-biased picks are used.

The performance analysis of the RAN-RTMag system shows that the use of both three and six stations led to a very high percentage of success (>95%) in estimating accurate location and magnitude, over most of the Italian high seismic hazard areas (Table 1.6 and 1.7, Figure 1.12a and 12b). The results of this study indicate that if an integrated EEWS such as RAN-PRESTo would be operational, by using only the closest three stations to the epicenter, a moderate or large event potentially occurring in the greater part of the country, could be rapidly detected (i.e., in less than 5 seconds). Furthermore, at the detection instant, sufficiently accurate estimations of location and magnitude of these events could be obtained (i.e., in more than 95% of the cases). Considering the seismicity observed in the last forty years in Italy, we expect that a RAN-PRESTo EEWS would be successful and capable of delivering useful warning for most of them. In particular, analyzing 67 events with M > 5 in the ITACA 2.0 database, recorded during the period 1972 -2013 by RAN, (of

which 9 had a M_W larger than 6) for 59 of them the percentage of EW reliable magnitude estimates, obtained by PRESTo simulations, is 87.5%.

In areas with lower seismic hazard, the expected magnitude of the events is smaller (between 5 and 6) and the maximum extent of the potential damage area (i.e., I_{MM} >= VII) has the same size of the blind zone (i.e., lead-time < 0). In these cases, two possible strategies can be followed: 1) to decrease the blind-zone dimension by increasing the network density, 2) to integrate the EEWS with the on-site methods. Although on-site single station analyses do not provide the earthquake location and magnitude estimates, the relationship between P-peak ground motion (i.e. Pd, peak displacement; Pv, peak velocity, and Pa, peak acceleration) and the incoming S-wave ground shaking (PGV, PGA) is robust. Increasing the station density and adopting on-site EEWS strategies would therefore reduce the blind-zone area, and thus increase the extent of the early warning zone.

In our approach the lead-time estimate is based upon the first S-wave arrival time as obtained from the earthquake location. However, we point out that this value likely underestimates the time available for automatic/individual security actions, since rarely first S-arrivals are associated with the strongest ground shaking. In addition, the failure of building structural/non structural elements may take some time and not be contemporary to the strong ground shaking. From the practical point of view, the effective implementation of a protective measure against the earthquake effects is possible only when the lead-time is larger than the time required to execute the safety operations.

Considering the current high RAN density in the highest hazard ZSs of Italy, if a long-term program for the implementation of a nation-wide EEWS in Italy would start, in addition to upgrading the network to enable real-time data telemetry, we advice to take into account any important aspects. In particular, as a first step, we suggest increasing the stations density in areas classified at the moment with a lower seismic hazard, especially in northern Italy and in Sicily region, for which now we observed the worst EEWS performance.

Furthermore, the decade long experience of an operational EEWS in Japan outlines the primary importance of the training and education of the EW users on the seismic risk and on the protective measures that could be taken within a few seconds after an EW alert. In particular, training exercises should be specifically tailored for the different users. Related to this topic, we mention two studies. The first, is a study committed by the Governor's Office of Emergency Services in California aimed at defining, in agreement with users belonging to the institutional sector (i.e., education, health care, emergency response agencies of state and local government, and utilities and transportation lifelines), the actions that these organizations could take when a lead-time of 10 seconds are available (Goltz, 2002 and Table 1.8). The second study is a pilot experimentation of an EEWS in Italy (Picozzi et al., 2015b), where it has been verified by drill tests that the protection of

students at schools (i.e., duck and cover before the S-waves arrival) is among the possible actions to take in a relatively short time (< 10 sec; a video presenting the drill can be seen at http://www.rissclab.unina.it/en/experiments/710-early-warning-applicationa-at-school).

Education:	**Emergency Services:**
-notify teachers with mobile phones	-turn off computer
-shut off gas	-send alert to fire department command center
-alert custodial staff to secure building	-warn the community
-shut off machines, move away from lab equipment	-make sure everyone is out of elevators
-notify security to be on alert	-activate backup
-get mobile phones	-alert field workers
-move clear of potentially falling objects	-shut down equipment
	-evacuate bottom floor
	-stop hazardous work
	-secure equipment
Health Care:	**Utilities & Transportation:**
-shut off equipment	-start automatic sms
-secure supplies	-shut down computers
-secure patients	-shut down gas
-shut off gas	-alert drivers
-stop surgeon activities	-control traffic signals
-shut off water	-put information on the computer
-stop elevators	

Table 1.8: Examples of actions that could be taken when 10 seconds warning time are considered (modified from Goltz, 2002).

PART II – An IV2 based On-Site methodology for Italy

The EEW nation-wide feasibility study for Italy, assessed in the first part of thesis, showed that a system given by the combination of the RAN network and the software PRESTo is theoretically capable of providing reliable estimates of epicenter location and magnitude after a few of seconds only the arrival of P-wave at the 3 to 6 RAN stations. On the other hand, we have found that adopting this EEW regional approach, given the RAN stations density, the Blind Zone (BZ) radii would be in average 25 km, which for most of the earthquakes occurring in Italy would also correspond to areas with higher damage. An integration of Regional and On-Site EEW systems, associated to the use of 1 to 2 seconds P-wave time windows, might in principle allow implementing rapid safety operations even in the BZ areas of the regional approach.
Consequently, the second part of thesis focused on On-site EEW systems, and explored the possibility of using new proxies for the prediction of the S-wave ground motion.
In the fourth and in the fifth chapter, the basic concepts of the on-site EEW approaches are introduced and the seismic parameters related to the structural damage are explored. In the sixth chapter, the analysis procedure carried out on the same seismic RAN database used for the EEW nation-wide feasibility study is described and the new on-site strategy is presented. In the seventh chapter the performance of our method is evaluated on the two independent Osservatorio Sismico delle Strutture (OSS) and INGV Strong Motion Database (ISMD) datasets. Furthermore, the results of the methodology applied on the M_W 6, 29th May 2012 Emilia earthquake (Northern Italy) have been compared with the intensity values measured in a macroseismic survey in the epicentral area after the event.

4. The On-Site Early Warning Approach and the analyzed data bases

4.1 The On-Site Early Warning approach

An on-site EEWS consists in one or more seismic sensors, located directly at the target site. In this approach the beginning part of the ground motion (mainly P-wave) recorded at the site is used to

predict the incoming ground motion (mainly S and surface waves)at the same site (Satriano et al, 2010, figure 1). In this case, lead-time is theoretically defined as the time interval between the P- and the S- wave arrival at the target (figure 2.1) . To this time interval, some seconds should be added in order to take into account event detection and computation. Similarly to the case for the regional approach, it increases with the epicentral distance, due to the growing travel-time difference between the slower S-wave front and the faster P-wave one. An on-site EEW system can provide a useful lead-time in the regional EEW Blind Zone, even if it can be much smaller than the average regional lead-time.

Among the on-site EEW methods, the UrEDAS system (Nakamura, 1988) is able to estimate the earthquake location and magnitude from a single station. In particular, the on-site or threshold based approach of EEW PRESTo, is able to provide the local alert level as a common single-station system. The "threshold-based" method is essentially based on the real-time, joint measurement of peak displacement PD and average period τ_c in first 3 seconds of P-wave. This last parameter is defined by the square root of the ratio between the integral of the squared displacement and the integral of the squared velocity (Wu & Kanamori, 2005, 2008). As PD is considered a proxy for the Peak Ground Velocity (PGV), the τ_c parameter can give important indications on the magnitude of the occurring earthquake. The measured value of PD and τ_c are compared to threshold values and a local alert level is assigned at each recording site, based on a decision table (Zollo et al, 2010; Colombelli et al., 2012).

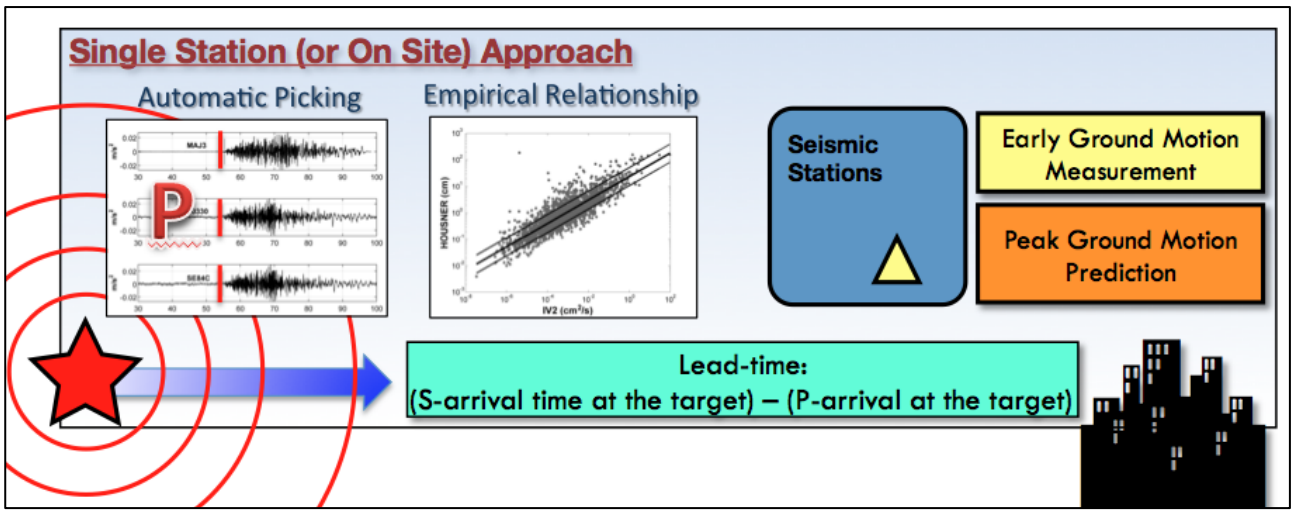

Figure 2.1: Schematic representation of the on-site approach for EEW (modified from *Satriano et al.*, 2011). Note, this is the maximum theoretical lead-time, discounting processing and transmission time.

4.2 The Accelerometric Networks and Data bases

4.2.1 Calibration Data Set: The Italian Accelerometric Network

The RAN consists of about 500 digital strong motion stations with data telemetry and time synchronization by GPS and covers all the higher seismic hazard areas of Italy with a 20–30 km mesh step (Figure 2.2). The RAN data are collected, validated, organized, and made available by the ITACA 2.0 database (Luzi et al., 2008; Pacor et al., 2011).

The RAN database consists of about 5000 strong motion records of 170 earthquakes with M_L>4 that occurred in Italy from 1997 to 2013 which have been used to calibrate the new EEW on-site relationships presented in the following sections. In order to reduce the effect of noise in the analysis, we have selected 2200 recordings having a signal-to-noise ratio higher than 80 (Figures 2.2a and 2.2b). The selected recordings span hypocentral distances from less than 10 km to a maximum of 300 km, and magnitudes M_L from 4 to 6.3, with most records acquired at hypocentral distances of less than 60 km. Most importantly, this data set includes the mainshock and the largest aftershocks of the M_W 6.3, L'Aquila and the M_W 5.9 Emilia earthquakes, which occurred in April 2009 and May 2012, respectively.

Figure (2.2c) shows the number of recordings available for the RAN stations. Clearly, the stations having the higher number of recordings are those located in Central and Northern Italy because of the great number of aftershocks of L'Aquila (2009) and Emilia (2012) earthquakes.

4.2.2 Testing Data Sets: The "Osservatorio Sismico delle Strutture" and the INGV Real-Time Strong Motion Data

The OSS is a strong motion network, which, similarly to the RAN, is owned and managed by the DPC, which aims to study the behavior of 124 civil structures in Italy during the occurrence of potentially damaging earthquakes (Dolce, 2012). Of the total, 116 stations are installed on buildings (e.g., schools, municipalities, hospitals, churches, sport centers, and historical buildings), 7 on bridges, and 1 on a dam. As with the RAN, the OSS stations are located in the highest seismic risk and vulnerability areas (Dolce, 2012; http://www.protezionecivile.gov.it/jcms/it/osservatorio.wp).

The ISMD is the first Italian real-time Strong-Motion web portal, designed and developed by several INGV Working Groups. The aim of the ISMD is the real-time archiving, processing, and distribution of strong-motion data recorded by the INGV and partner networks, with the necessary information for the use of published records (Massa et al., 2014). The automatic system on which the ISMD portal is based checks the quality of raw accelerograms, archives, and processes the data in real time to provide rapid estimations of the main strong motion parameters of a seismic event. Within a few minutes after the earthquake, the system publishes on the website (http://ismd.mi.ingv.it/) a real-time report of the event (e.g., event and waveform metadata, seismic response of recording sites, comparisons between observed and predicted data), accelerogram waveforms, as well as the related response spectra. In the present configuration, the INGV strong-motion network consists of 400 stations and covers central northern Italy (in particular, the Po Plain and the southern central Alps), the entire Italian Apennine chain, the Calabrian Arc, and eastern-southern Sicily.

The OSS and ISMD data have been used to test the performance of the developed on-site EEW procedure (Figures 2.2e and 2.2f). This testing data set consists of 30 strong motion records of the OSS database related to eight earthquakes that occurred in Italy from 2009 to 2014 and 190 ISMD recordings corresponding to 11 seismic events that occurred in Italy from 2014 to 2015. The magnitude range of the OSS events is M_L 4–6.0, and most of the data has hypocentral distances between 10 and 50 km. The IMSD events have a magnitude range of M_L 3.5–5.5 and hypocentral distances smaller than 200 km.

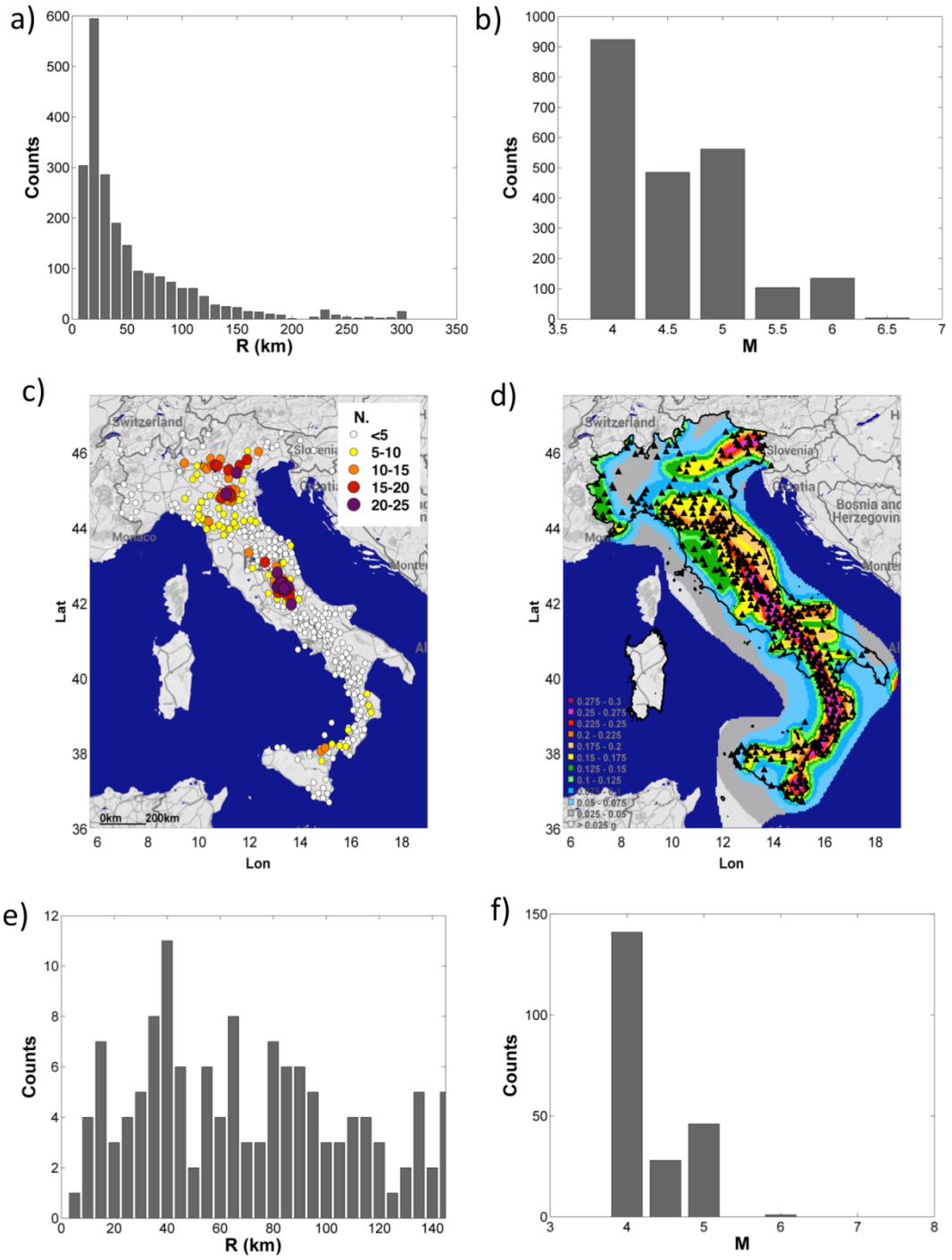

Figure 2.2: The ITACA Calibration data set and the OSS and ISMD testing data sets. a) Distribution of ITACA records in terms of hypocentral distance. b) Distribution of ITACA recordings in terms of Local Magnitude. c) Number of recordings used for the single ITACA station: Number smaller than 5 (green circle), between 5 and 10 (yellow circle), between 10 and 15 (orange circle), between 15 and 20 (red circle) and larger than 20 (dark violet circle). D) Seismic hazard map for Italy showing the peak ground acceleration values that have a 10% chance to being exceeded in 50 years (http://esse1-gis.mi.ingv.it/s1_en.php, redrawn) and the RAN Network (black triangles). e) Distribution of OSS and ISMD records in terms of hypocentral distance. f) Distribution of OSS and ISMD records in terms of Local Magnitude.

5. The Analyzed Parameters

The ITACA data set has been used to estimate the P-wave EEW parameters PD and IV2, as well as the ground motion parameters PGV and I_H, considering the entire traces and the macroseismic intensity (IM) exploiting empirical relations.

5.1 Earthquake Early Warning Parameters

The analysis for the estimation of the EEW parameters follows the procedure proposed by Zollo et al. (2010) and consists of sensitivity correction, P and S phase identification and manual picking, and single and double integration to obtain the velocity and displacement records. The EEW parameters have been estimated considering a P-wave window on the vertical component having a variable length, depending on the S-wave arrival, with a maximum width of 3 s. In order to exclude the S- wave contribution for the near source stations, all P- and S- wave picks have been carried out manually.

The PD is measured, according to Kanamori (2005), on band-pass-filtered displacement using a causal Butterworth high pass filter with a cutoff frequency of 0.075 Hz and two poles to remove the long-period drift after the double integration.

Several authors have shown that the distance attenuation-corrected, low-frequency PD is well correlated with earthquake magnitude. On the other hand, the uncorrected PD is correlated as well with the peak ground shaking (e.g., PGV and PGA), and therefore it has become over the last 10 years the most used parameter in both regional and on-site EEW applications (e.g., among others, Kanamori (2005), Wu and Zhao (2006), Zollo et al. (2006), Allen (2007), Zollo et al. (2010, 2011), and Colombelli et al. (2014)).

The integral of the squared velocity (IV2) is defined as follows:

$$IV2 = \int_{t}^{t+\Delta t} v(t)^2 \, dt \qquad (2.1)$$

where the integral is computed over a window of length Δt after the first P arrival time and v^2 is the ground motion velocity squared.

As discussed by Kanamori et al. (1993), when computed on direct S-waves, IV2 is related to the energy radiated by the earthquake and, as discussed by Boatwright and Fletcher (1984), it includes

information about the energy radiated by the advancing rupture on the fault plane. Therefore, IV2 provides direct, although partial, insight into the physics of the earthquake rupture (Festa et al., 2008).

Festa et al. (2008) first investigated the use of IV2 computed on P-wave time windows in EEW for real-time magnitude estimation exploiting a data set of Japanese earthquakes. Similarly, Lancieri et al. (2011) investigated the behavior of IV2 estimated from P- and S-wave time windows on the aftershock sequence of the Tocopilla event of November 2007 (M_W 7.8) in northern Chile. Both Festa et al. (2008) and Lancieri et al. (2011) reported a stable correlation between the logarithm of IV2 and the catalogue magnitude over a wide magnitude range. It is worth noting that Festa et al. (2008) observed a saturation of the parameter for magnitudes around M_W 6.5 when estimated on a 4 s P phase time window and a 2 s S phase time window. On the contrary, Lancieri et al. (2011) observed, as for PD, that the IV2's trend did not show saturation up to M_W 7.8.

5.2 PGV and I_H

In this study the peak ground velocity (PGV) has been inferred from the maximum amplitude on the highpass-filtered horizontal components of the ground motion velocity records.

The Housner intensity is defined as the area under the pseudovelocity spectrum PSV(T, ξ) of the seismogram (Housner, 1952):

$$I_H = \int_{T_{inf}}^{T_{Sup}} S_V(T, \xi)\, dt \qquad (2.2)$$

where T is the period and ξ is the fraction of critical damping in computing the PSV (Chiauzzi et al., 2012). The I_H is used in engineering and seismological studies to characterize the damage level suffered by a structure (Chiauzzi et al., 2012). Following Masi et al. (2010), I_H has been estimated considering the period range 0.01 s to 2 s and adopting the value of 5% for the fraction of critical damping. Furthermore, I_H has been obtained for each seismic trace as the quadratic sum of the integral of the horizontal component's pseudovelocity spectrum.

Both PGV and the I_H have been estimated considering the full length of the seismic traces.

5.3 Macroseismic Intensity: MCS and EMS-98 Scales

The macroseismic intensity is a parameter that quantifies the strength of shaking at any place during an earthquake as a function of its observed effects (Musson et al., 2009). The two intensity scales most used in Italy are the Mercalli-Cancani-Sieberg (MCS) (Sieberg, 1930) and the European Macroseismic Scale (EMS-98) (Grünthal, 1998). The MCS involves the addition of 2° to the earlier 10° Mercalli scale (Cancani, 1904), in order to deal with very strong earthquakes, and it was reformulated by Sieberg in 1912 (Faenza and Michelini, 2010). The EMS-98, which is a modification of the 12° Medvedev, Sponheuer, and Kàrnìk (MSK) scale, has been defined with the aim of making the MSK scale to more appropriate modern building types and advances in macroseismology (Musson et al., 2009). MCS and EMS-98 generally describe in the same way the macroseismic intensity (Codermartz et al., 2003; Musson et al., 2009; Chiauzzi et al., 2012), although experience seems to show that MCS intensity assignments are frequently higher than those in EMS-98 for the same data (Musson et al., 2009). However, in the following, we will consider the MCS and EMS-98 macroseismic intensities to be equivalent.

Recent studies have derived for Italy linear relationships between PGV and macroseismic intensity expressed by MCS (Faenza and Michelini, 2010) and between the I_H and macroseismic intensity in EMS-98 (Chiauzzi et al., 2012). In particular, Chiauzzi et al. (2012) identified the I_H equal to 0.18 m as the value corresponding to the V-VI EMS-98 Intensity (I_{EMS-98}), that is to say the threshold above which a structure starts to suffer damage.

These authors defined a bilinear regression between I_{EMS-98} and I_H, splitting the data set where I_H is smaller and greater than 0.18 m, and used it as a rapid damage assessment proxy.

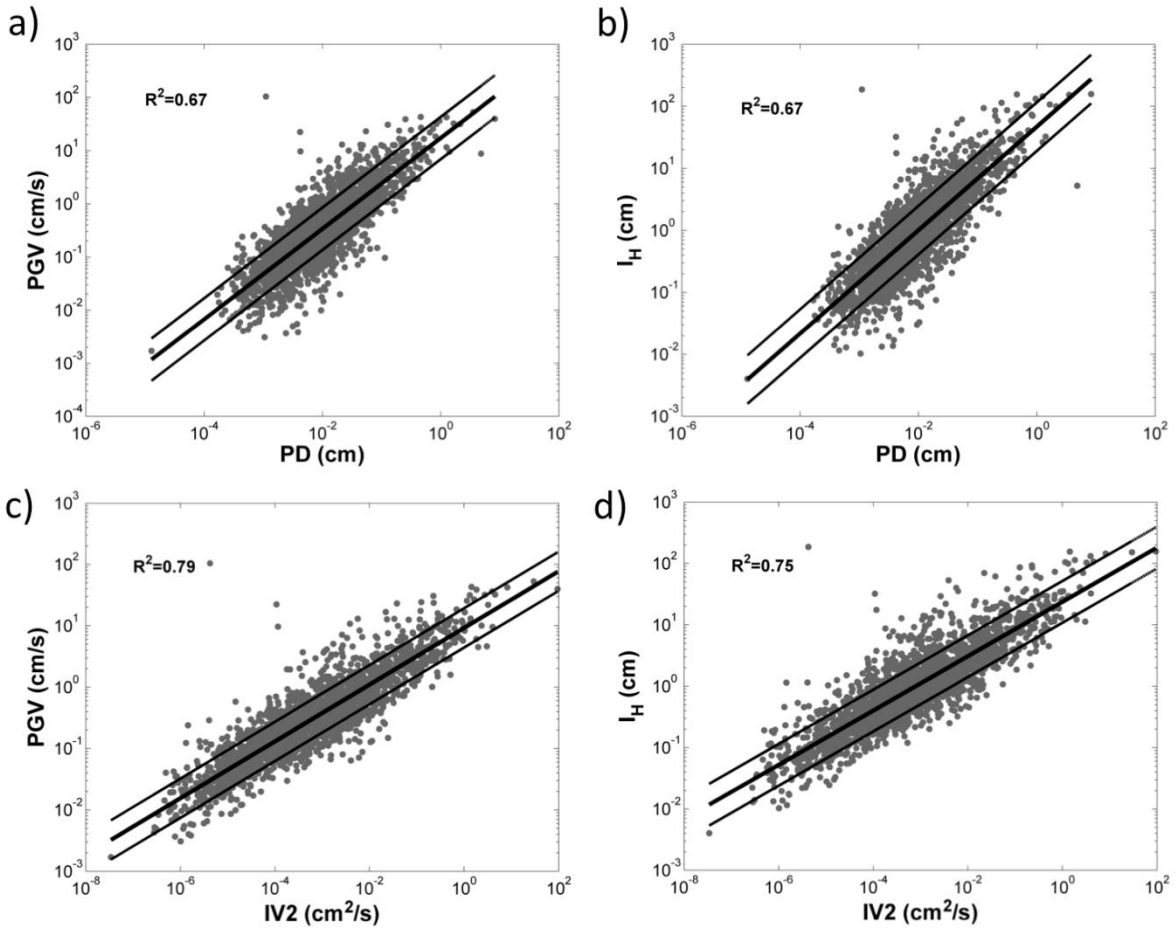

Figure 2.3: PGV (a,c) and I_H (b,d) as a function of early warning parameters PD (a,b) and IV2 (c,d gray dots) with the obtained regressions (thick black line) and the correspondent +/- 1 sigma lines (thin black line) (see Table 2.1).

6. Analysis Procedure

6.1. EEW Parameters Versus PGV and I_H

Ordinary least squares regressions between the EEW parameters (P_{EEW}) PD and IV2 and the ground motion parameters (P_{GM}) PGV and I_H have been computed using the ITACA data set. For this purpose, we used a linear relation between the logarithms in base 10 of both quantities:

$$\log_{10}(P_{EEW}) = A + B \log_{10}(P_{GM}) \qquad (2.3)$$

Figure (2.3) and Table 2.1 show the results of the analysis. Interestingly, both PD and IV2 correlate very similarly with both PGV and I_H.

Concerning the relationship between PGV and PD, the coefficients of equation (2.3) that have been found from the ITACA data set are in rather good agreement with those obtained by Wu and Kanamori (2008) and Zollo et al. (2010) for recordings from Japan, Southern California, and Taiwan, and for Japan, Taiwan, and Central Italy, respectively.

Indeed, the differences of the coefficients A and B of equation (2.3) found in this work with respect to Zollo et al. (2010) are 5% and 16%, respectively.

Similarly, considering the work of Wu and Kanamori (2008) they differ by 25% and 8%, respectively. On the other hand, differences of the same order between the A and B coefficients are found also comparing directly the relations of Wu and Kanamori (2008) and Zollo et al. (2010) (i.e., 17% and 26%). The differences among the coefficient values may be attributed to the different data sets used in these analyses and, in particular, the epicentral distance range. The epicentral distance for Wu and Kanamori (2008) and Zollo et al. (2010) is less than 60 km, while in our work it reaches up to 300 km.Considering the superior capability of I_H compared to PGV to correlate the severity of seismic events with building structural damage (Masi et al., 2010), we found these results very promising for EEW purposes.

The standard deviations and R^2 coefficients computed for the different regressions indicate that IV2 correlates better than PD with the ground motion parameters (Table 2.1). Moreover, considering that IV2 correlates similarly with PGV and I_H and that this latter parameter is considered a more effective parameter than PGV to correlate the severity of seismic events with building structural damage (Masi et al., 2010), in the following sections we consider the relationship between IV2 and I_H to be of primary concern.

EW Param.	A	B	σ	R^2
PD vs. PGV	1.23	0.85	0.40	0.67
PD vs. I_H	1.67	0.83	0.39	0.67
IV2 vs. PGV	0.96	0.46	0.32	0.79
IV2 vs. I_H	1.37	0.44	0.34	0.75

Table 2.1: Parameters of Eq.(2.3) standard deviation and R^2 coefficient for different combination of EEW and strong motion parameters.

6.2. Variable Time Analysis Window

Due to the large variability in the station-to-hypocenter distances, the above regressions have been calculated on data related to different time window lengths (TWL). To investigate the dependence of the IV2 versus I_H relationship on the TWL, the data have been divided in four groups: TWL

smaller than 1 s, between 1 and 2 s, between 2 and 3 s, and equal to 3 s. As a first approximation, considering average P- and S-wave velocities equal to 5 km/s and 3 km/s, respectively, the TWL groups correspond to hypocentral distance less than 7.5 km, from 7.5 km to 15 km, from 15 km to 22.5 km, and equal to or greater than 22.5 km, respectively. Figure (2.4) shows the distribution of IV2 for the different TWL groups with respect to the best fit relation, ±1 standard deviation, obtained considering the whole data set (Table 2.1). We observe that for each TWL group, most of the data are confined within 1 standard deviation of the best fit line. Therefore, to a first approximation, the

effect of the time window dimension seems to be negligible for the explored magnitude and distance range and suggests that, with respect to regional EEW approaches, using P-wave time windows between 1 and 2 s for computing IV2 would allow to reduce the blind-zone dimension.

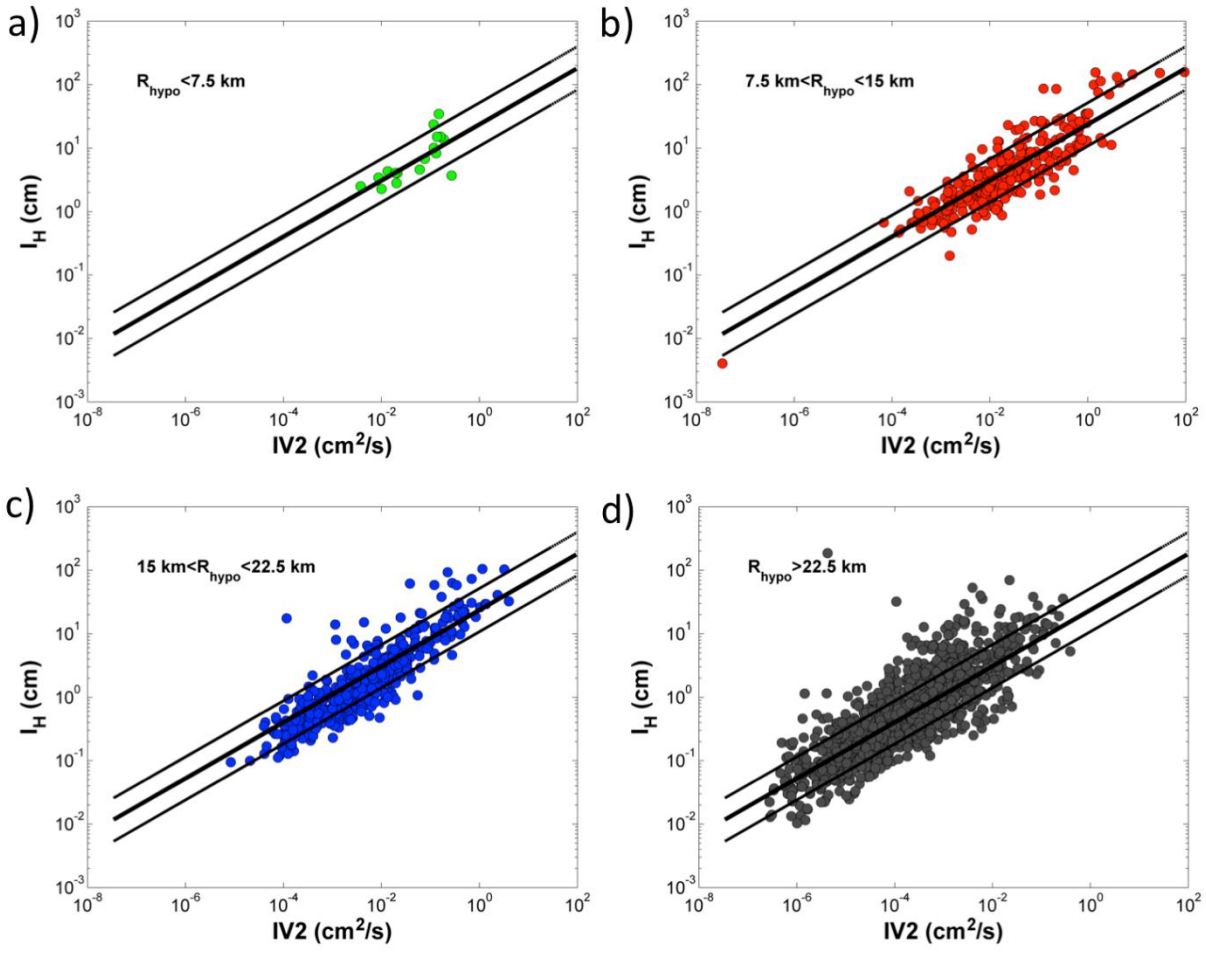

Figure 2.4: Housner Intensity values as a function of IV2 for different P-wave time window lengths (TWL), the regression line (thick black lines) +/- 1 standard deviation (thin black lines) obtained considering all data (see Figure 2.3). a) TWL smaller than 1 second (green dots). b) Same as a), but between 1 and 2 seconds (red dots). c) Same as a), but between 2 and 3 seconds (blue dots). d) Same as a), but TWL equal to 3 seconds (grey dots).

6.3. The Method: IV2 Versus Macroseismic Intensity

Similarly to Zollo et al. (2010), the relationships between EEW and ground motion parameters PGV and I_H (Figure 2.3 and Table 2.1) could be used, once a proper threshold for the "damage" or "no-damage" states has been defined (e.g., PGV larger than 6.1 cm/s (Faccioli and Cauzzi, 2006) and I_H larger than 0.18 m, which correspond to the lower bound of the European Macroseismic Scale Intensity class VII (Grünthal, 1998)) to deliver real-time alerts at target sites during earthquakes and before the S-waves reach the sites. However, in this work we take a step further and explore the possibility of predicting the macroseismic intensity directly from IV2. Our procedure is grounded on the idea of exploiting the relations existing between IV2 and I_H and between I_H and IM, in order to predict IM directly from IV2 estimates.

Chiauzzi et al. (2012) derived a two-branch relationship between unbinned I_H and 0.5 units binned IM, fixing a value of I_H equal to 0.18 m to mark the change between the two. The first relation for I_H less than 0.18 m, which refers to IM less than VI, is characterized by a high R squared coefficient ($R^2 = 0.88$). The second one, for I_H equal to or greater than 0.18 m, has a different slope and an R^2 equal to 0.60. Moreover, the number of data having I_H less than 0.18 m is about 3 times greater than those with I_H equal to or greater than 0.18 m. Because the considered distribution of data is so uneven and dealing with an a priori threshold for the selection of the I_H-IM relation to use in real-time analysis might lead to high errors in case of misselection, we decided to undertake a new regression analysis. Our decision was also influenced by the observations of Bakun and Scotti (2006), who highlighted that in case of heterogeneous distribution, quality, and completeness of macroseismic data, binning the data contributes to reducing the biases in the regression model. Therefore, we used the 0.5 units binned IM and the 50th percentile of I_H distribution for each IM class to derive a new single-line relationship. Figure (2.5a) shows the observed IM, the I_H, the 50th percentiles, and the best fit line to these latter values, which is characterized by an R^2 equal to 0.91, plus the ±1 standard deviation relations ($\sigma = 0.46$). The new I_H versus IM relation has the following form:

$$IM = 7.95 + 2.27 \log_{10}(I_H) \qquad (2.4)$$

Then, equation (2.4) has been used to estimate IM from the I_H values obtained for the ITACA data set. Therefore, these latter IM values have in turn been used to derive a novel direct relationship with IV2. Differently from equation (2.4), in this case each IM class is characterized by a large

distribution of IV2 values, and therefore the fit has been done considering directly the IV2 data. The new relation, shown in Figure (2.5b), has the form

$$\mathrm{IM} = 6.48 + 0.95 \log_{10}(\mathrm{IV2}) \qquad (2.5)$$

and is characterized by an R^2 equal to 0.71 and σ equal to 0.79.

Equation (2.5) provides IM values in a continuous form; thus, similarly to Chiauzzi et al. (2012), we approximate the IM values to the nearest macroseismic intensity adopting a step of 0.5 intensity units.

Furthermore, we adopted also an alternative procedure for obtaining IM values from PD estimates. In particular, we estimated PGV from PD using equation (2.3) and the parameters in Table (2.1). Then, the PGV values were in turn used to estimate IM using the relationship proposed by Faenza and Michelini (2010), which has been adopted by the INGV for computing shake maps after an event. The steps of the second procedure are those that, in our opinion, many users would follow to assess IM from PD in EEW time frames. Therefore, we considered it as a kind of "standard" approach, and we used it to assess the performance of the procedure based on IV2.

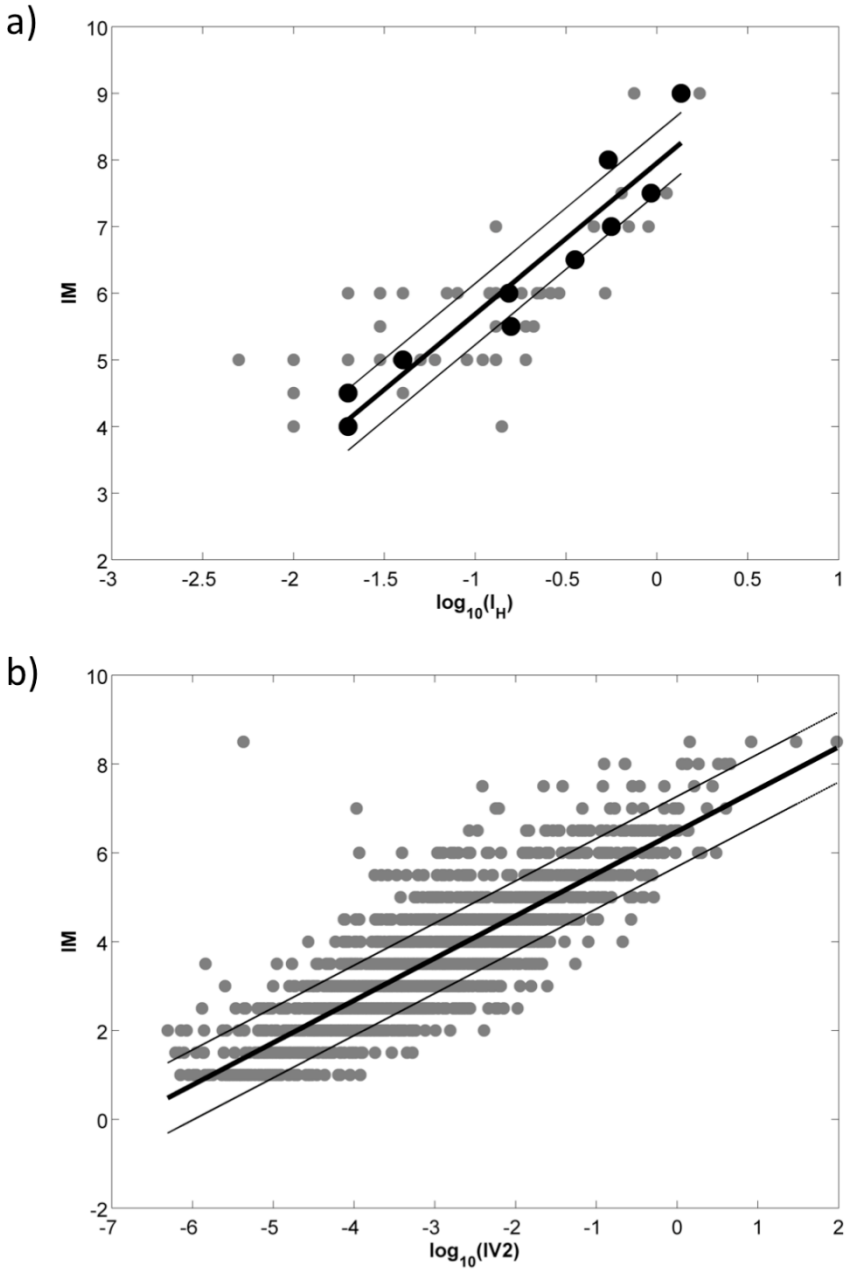

Figure 2.5: a) IM values reported as a function of Housner Intensity (gray dots) obtained by Chiauzzi at al. (2012), 50th percentiles data (black dots), best-fit regression (thick black line) and +/- 1 sigma (thin black line). b) IM values obtained by Eq.(2.4) versus IV2 (gray dots), best-fit regression, Eq. (2.5), (thick black line) and +/- 1 sigma (thin black line).

7. Applications and Results

7.1 Applications to OSS and ISMD Data Sets

In order to verify the performance of equation (2.5) for the prediction of IM within EEW time frames, we tested it using the recordings from the OSS and ISMD data sets. To this purpose, first, we used equation (2.4) to derive IM estimates from I_H measures for both data set. Therefore, these IM values have been compared with the prediction of IM obtained from IV2 estimates and equation (2.5) (Figures 2.6a and 2.6b). Similarly, for the sake of consistency, we used the relationship proposed by Faenza and Michelini (2010) to obtain IM estimates from the observed PGV values, and we compared them with the IM prediction obtained from the PD estimates (Figures 2.6c and 2.6d). Figure 2.6 shows that IM predicted by IV2 is mostly confined within ±1 units of the reference IM (i.e., the 85% of the data).

On the contrary, in the case of IM predicted by PD, only 61% of the values are within ±1 units of the reference IM. Unfortunately, the two data sets at hand are rather poor for IM values equal to and greater than VI. However, we found it interesting that in the range IM II and VII, the two IM prediction procedures do not show any biases with respect to increasing observed intensity.

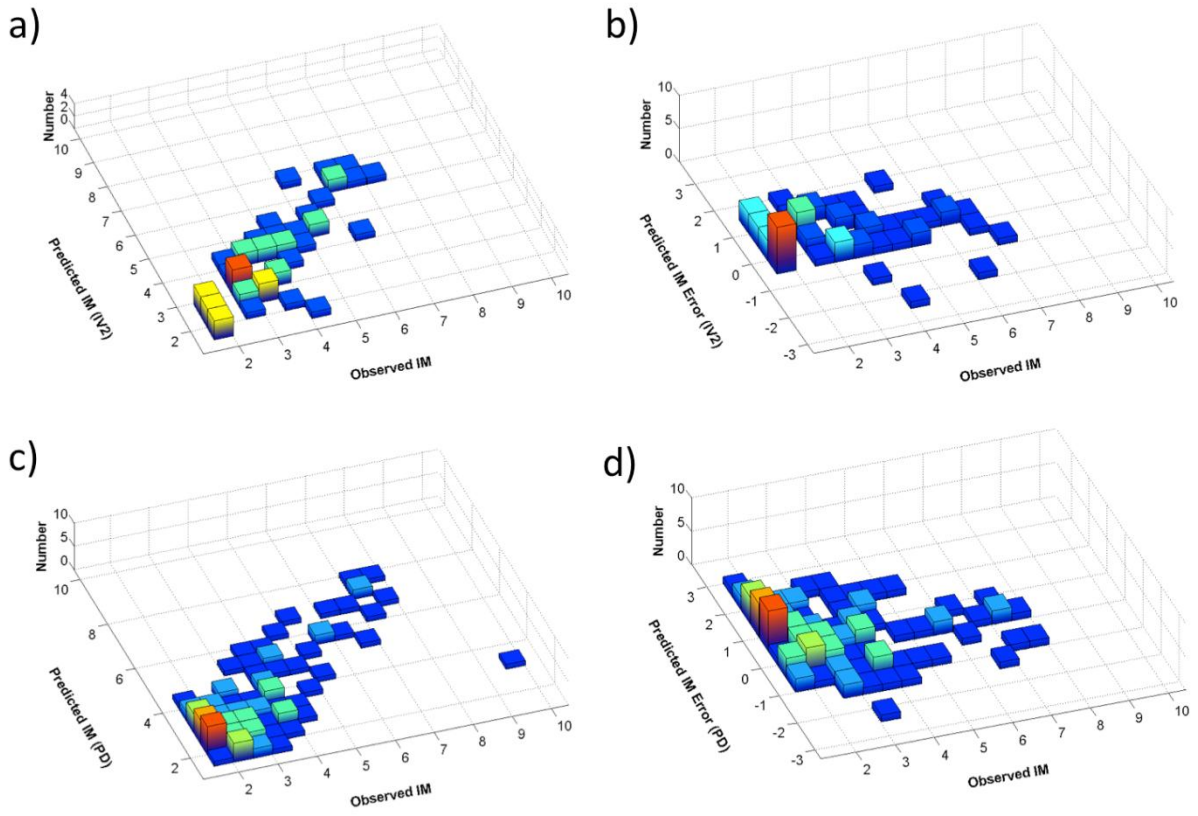

Figure 2.6: a) predicted IM, obtained from IV2, as a function of the observed IM(reference IM). b) Residuals between predicted IM, obtained from IV2, and the observed IM(reference IM). c) the same as a), but for the IM predicted from PD and PGV. d) the same as c), but for the IM predicted from PD and PGV.

7.2 Applications to the 29 May 2012Emilia 5.8 M_L Earthquake

7.2.1 The 2012 Galli's Macroseismic Survey

This section presents the results obtained from applying the procedures for predicting IM to the data of the Mw 6.0 earthquake (Quick Regional Centroid Moment Tensor, 2012) that struck the Emilia Region (Italy) on 29 May 2012. In particular, our IM predictions from IV2 have been compared with those obtained by Galli et al. (2012) by means of a macroseismic survey of the epicentral area. It is worth noting that the IM values provided by Galli et al. (2012) refer to the cumulated damage suffered by the municipalities in the area after the whole earthquake sequence, which besides the second mainshock that we considered, included the first mainshock M_W 6.1 which occurred

on 20 May 2012 and at least 11 events with $M_L \geq 4.5$. However, in the following analysis we assume that the IM estimates from Galli et al. (2012) are, at least in the first approximation, directly comparable with our EEW estimates. Our choice of considering the second mainshock instead of the first one is due only to the very limited number of accelerometric stations that were installed in the epicentral area on 20 May 2012.

In order to avoid any possible bias due to the distance between the stations where we have estimated IM from IV2 and PD (IM_{EEW}) and the sites where Galli et al. (2012) assessed the macroseismic intensity (IM_{OBS}), we have limited the comparison to 16 sites with station to surveyed site distances less than 1 km (Table 2.2). The selected sites are characterized by IM_{OBS} from V to VII (Figure 2.7a and Table 2.2) and distances within about 50 km from the epicenter. Figure 2.7b shows the IM_{EEW} derived from IV2. The EEW intensity map presents a distribution of IM with increasing distance from the epicenter that is in rather good agreement with the observed intensity map (Figure 2.7a), with, at a first glance, underestimations and overestimations mostly of the order 0.5 to 1 intensity unit.

Figure 2.7c shows the IM_{EEW} map derived from PD estimates. Also, in this case, the IM distribution is qualitatively in good agreement with that of Figure 2.7a, even if for the two closest sites at the epicenter we have found that IM is overestimated by 2 units (Table 2.2).

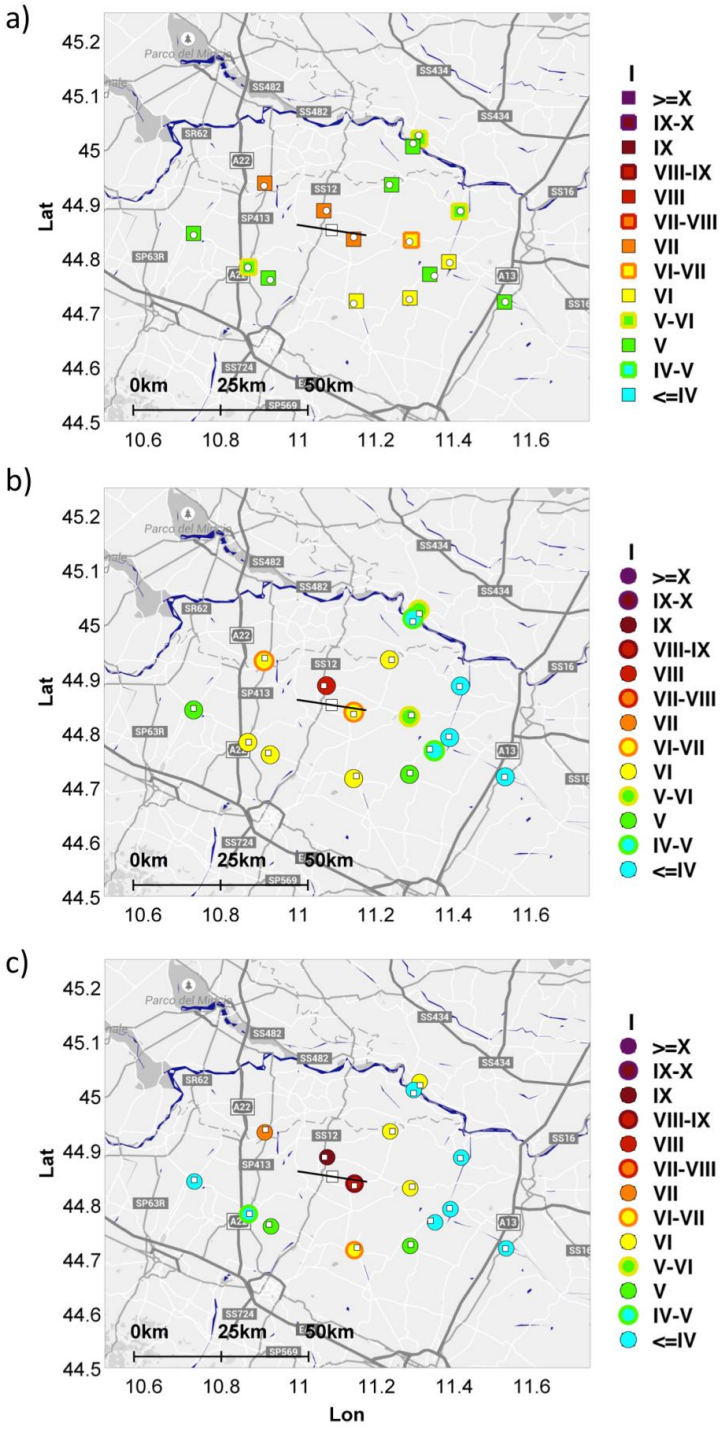

Figure 2.7: a) Observed macroseismic intensities from Galli et al. (2012) for the M_W 6 May 29th 2012 Emilia Earthquake (coloured squares), stations for which the intensity has been predicted (white dots) (see Table 2.2). b) Same as a), but with predicted intensities from IV2 (coloured dots), and locations of observed intensities (white squares). c) Same as b), but with predicted intensities from PD (coloured dots), and locations of observed intensities (white squares).

We have analyzed the distribution of residuals between IM_{EEW} and IM_{OBS} with respect to the epicentral distance and the azimuth (Figure 2.8). Interestingly, when IV2 is used to predict IM, the residuals are mostly within ±1 intensity units, with the exception of three stations in the distance range 25 to 40 km, and azimuth equal to about N100°E (Figures 2.8a and 2.8b). This direction is compatible with the results of Convertito et al. (2013), which estimated a dominant rupture direction for the 29 May 2012 event of around N300°E. Therefore, the underestimation of IM at those three stations is likely to be related to a directivity effect of the source and these results suggest the need to further explore the use of IV2 as a parameter for characterizing the directivity effects in EEW applications.

A similar analysis of the residuals has been carried out for the PD-derived IM estimates (Figures 2.8c and 2.8d). In this case, we observe that IM_{EEW} estimates tend to overestimate the observed IM at short epicentral distances by the order of two intensity units and to underestimate them by up to four intensity units at larger distances (Figure 2.8c). Similarly to IV2, the largest underestimation of IM occurs for the azimuth at around N100°E (Figure 2.8d).

Figure 2.9a shows the IM_{EEW} map for the 29 May 2012 Emilia earthquake, considering stations within 100 km from the epicenter. Of course, as the IV2 values are the same as those used to calibrate the IV2-to-IM relationship, our concern in this result is not the specific value obtained for the IM_{EEW} estimates but rather on the overall trend in the intensity predictions and the value that such a EEW product might have. Indeed, we think that besides the EEW application, such kinds of IM_{EEW} maps would be an important piece of information for real-time risk assessment and rapid response procedures, as suggested by Picozzi et al. (2013).

This issue is even more important considering that standard monitoring networks are equipped with modern broadband sensors, which lead them to saturate within a radius of the order of 100 km from the epicenter and hamper immediate response (Faenza et al., 2011). The procedure proposed in this study would overcome this kind of problem and could be adopted also with velocimetric networks, because it relies on P-waves signal analysis. Real time maps like that of Figure 2.9a would therefore assist the Civil Protection to act immediately according to the severity of the situation.

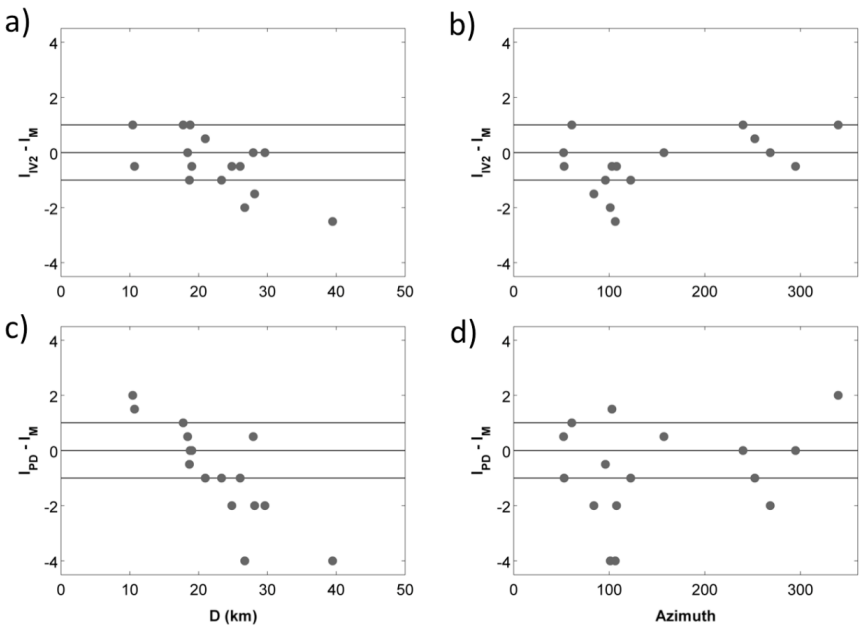

Figure 2.8: Distribution with distance and azimuth of the residuals between the intensity predicted by IV2 (a and b) and PD (c and d) with respect to the observed ones by Galli et al. (2012), (see Figure 2.7).

RAN Latitude	RAN Longitude	Hypocentral Distance (km)	IM (IV2 derived)	IM (PD derived)	Latitude Obsserved IM	Longitude Observed IM	Observed IM	Distance RAN vs. Observed IM (km)
44.9320	10.9120	19.4	6.5	7	44.9372	10.9139	7.0	0.60
44.8864	11.0728	11.0	8	9	44.8864	11.0660	7.0	0.54
44.8380	11.1430	11.3	6.5	8.5	44.8341	11.1425	7.0	0.44
44.8297	11.2867	19.0	5.5	6	44.8326	11.2917	6.5	0.51
44.7234	11.2867	23.6	5	5	44.7259	11.2880	6.0	0.30
44.7157	11.1428	18.8	6	6.5	44.7205	11.1497	6.0	0.76
44.7910	11.3904	27.0	4	2	44.7926	11.3883	6.0	0.24
44.8860	11.4180	28.4	4	3.5	44.8849	11.4157	5.5	0.22
45.0250	11.3110	28.2	5.5	6	45.0187	11.3122	5.5	0.71
44.7823	10.8703	21.3	6	4.5	44.7825	10.8724	5.5	0.18
44.7190	11.5340	39.6	2.5	1	44.7187	11.5320	5.0	0.16
44.8419	10.7306	29.9	5	3	44.8447	10.7303	5.0	0.31
44.9340	11.2350	18.1	6	6	44.9341	11.2409	5.0	0.47
45.0100	11.2958	26. 3	4.5	4	45.0044	11.2954	5.0	0.62
44.7668	11.3508	25.1	4.5	3	44.7697	11.3389	5.0	0.99
44.7594	10.9276	19.1	6	5	44.7628	10.9226	5.0	0.55

Table 2.2: Comparison of IM predicted and observed by Galli et al. (2012) after the M_W 6 May 29th 2012 Emilia Earthquake for RAN stations and localities within 1 km of distance (see Figure 2.7, and Section 7.2.1 for details).

7.2.2 The potential benefit of IM prediction

In order to assess the potential benefit of the IM predictions obtained by our procedure, we estimated the arrival time of the PGV for each station that recorded the 29 May 2012 Emilia earthquake. Therefore, we computed the lead time as follows: arrival time PGV - (arrival P-wave time + P window time + computation time).

The P window time used for the analysis is selected to be equal to 2 s, which according to our results represents, for a M_W 6 event, a good compromise between the requirement of being fast and the need to obtain robust IV2 estimates. The computation time is assumed to equal 1 s based on experience with PRESTo and regional EEW analyses (Satriano et al., 2011). For the computation of the lead time, instead of using the S-wave arrival, we have selected the PGV arrival time because this latter parameter is one of the main ones responsible for structural and nonstructural damages. Therefore, for EEW purposes, we consider the PGV arrival as the maximum time within which an end user can implement protective measures. As examples of protective actions, we considered "duck and cover," and moving away from windows or equipment. According to EEW drills realized in schools in southern Italy (Picozzi et al., 2015b), trained students need between 3 and 5 s to take cover under desks. Therefore, Figure 2.9b shows for each of the stations used in the analysis the distribution of lead times less than 5 s, between 5 s and 10 s, and greater than 10 s. Despite at a few stations where we observe incoherent PGV arrival times, which might be due to local site or noise conditions, the overall trend clearly suggests that for distances greater than about 20 km, trained users might have had more than 5 s to implement protective measures aiming at reducing their exposure to risk of injury. Figure 2.9c shows the localities for which Galli et al. (2012) made the macroseismic survey, while Figure 2.9d shows which of these sites are at a distance less and greater than 20 km (i.e., lead times smaller and greater than 5 s) from the fault responsible for the 29 May 2012 event. Comparing Figures 2.9c and 2.9d, we observe that lead times greater than 5 s would have been available only for localities with macroseismic intensities equal to or less than VI. The information about the population living in each locality (Galli et al., 2012) lead us to estimate that around 190,000 inhabitants would have not benefited from the 5 s we consider necessary to cover and duck (i.e., the blind-zone area for the specific EEW action considered). However, it is worth considering that most of these people could have benefited from EEW alerts if instead of directly responding to the alert, we considered EEW automatic mitigation actions (e.g., automatic turnoff of gas burners). Indeed, in this case, assuming 1 s for the implementation of the automatic procedures, the EEW alerts could have been exploited already at distances from the fault greater than about 5 km and hence useful also for those sites affected by greater damage. Finally, we have

estimated that considering the sites with a lead time larger than 5 s, about half a million inhabitants would have potentially benefited from this lead time by having the time necessary to reduce their exposure

to injury for secondary effects (e.g., fall of objects, broken glass, or staying away from dangerous machines) and not to panic.

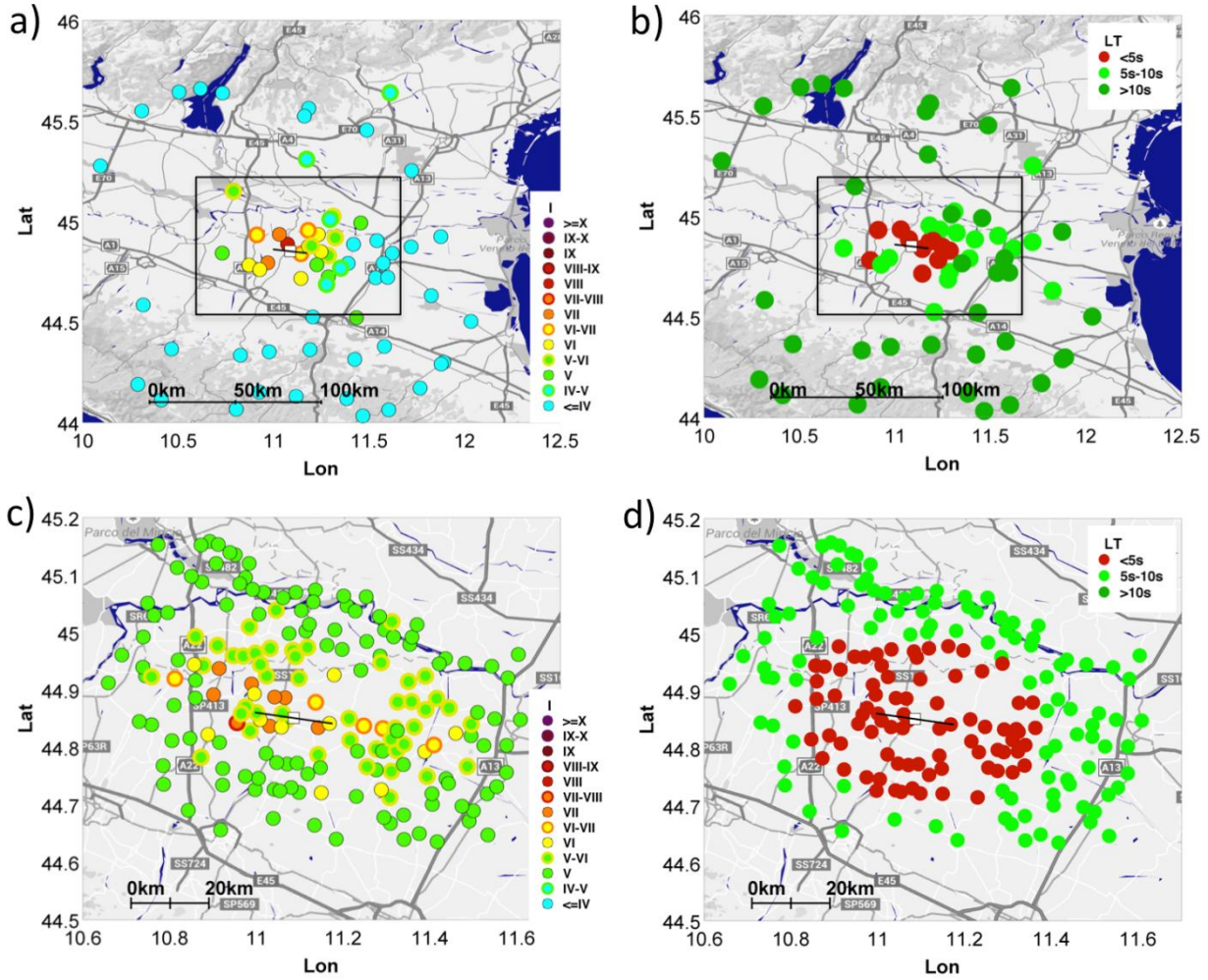

Figure 2.9: a) Predicted macroseismic intensities from IV2 for the M_W 6 May 29th 2012 Emilia Earthquake (coloured squares). b) Distribution of lead-time (LT) for the same sites shown in a). where LT is grouped in values smaller than 5 s (red dots), between 5 s and 10 s (light green dots), and greater than 10 s (dark green dots). The rectangular border (black line) contains the area surveyed by Galli et al. (2012) and shown in c) and d). c) Macroseismic intensity field from Galli et al. (2012) (redrawn). d) Same area as b), but LT computed for the sites surveyed by Galli et al. (2012).

7.3 Discussion and Conclusions

This work presents the results of a novel procedure based on the use of the parameter IV2 measured on P waves, aiming at the prediction of the macroseismic intensity for on-site EEW systems.

First, we have shown that IV2 correlates better than PD with both PGV and I_H, the latter considered by engineers a better proxy for rapid damage assessment. The relationship between IV2 and I_H could therefore be used to discriminate in real time and before the arrival of S-waves if a site is going to be adversely affected or not, and thus has the potential to become a key relationship in the design of on-site EEWS.

We have verified that for events having magnitudes around M_W 6, which in Italy occur roughly every 10 to 20 years and are responsible for considerable damage, even the availability of only 1 s of P-wave signal would provide I_H estimates confined within ±1 standard deviation of the IV2-I_H relation. Therefore, we found that with respect to regional EEW approaches (Picozzi et al., 2015a), IV2 might lead to blind zone with reduced dimensions. Of course, it is worth noting that our results are representative of the magnitude range characterizing the data set at hand, and for larger magnitude events, as observed for PD, we expect that IV2 will be prone to saturation effects. This is an issue that will be certainly investigated in future studies by exploiting data sets with broader magnitude and distance ranges. It is worth noting, however, that the data set used in this study to calibrate the relationships between IV2, I_H, and IM is well representative of Italian seismicity, as also discussed by Picozzi et al. (2015a).

The second part of the work focused on deriving and testing a new relationship between IV2 and the IM for EEW purposes. The new IV2-IM relationship, which has been tested on independent data sets from those used for its calibrations, showed better performance for the prediction of IM than a procedure based on estimating PGV from PD, and in turn use PGV for estimating the intensity by the Faenza and Michelini (2010) relationship.

Indeed, considering two different data sets, we have seen that in the 85% of the cases the IM predicted by IV2 were within ±1 unit of the reference IM. With respect to this issue, future studies will be devoted to assessing our procedure on data sets covering a larger magnitudes range.

Applying the IV2-IM relationship to the recordings of the M_W 6, 29 May 2012 Emilia earthquake, we have seen that IV2 allows us to obtain a prediction of the IM field in good agreement with the one observed by Galli et al. (2012).

Our results suggest that IV2 is a good proxy for the prediction of the IM in EEW applications. As discussed, besides EEW, the real-time maps of the predicted IM would be valuable pieces of

information for assisting Civil Protection to act immediately, according to the severity of the situation. Finally, we have discussed the applicability of the IM_{EEW} maps for EEW purposes by taking into consideration, as example, the mitigation action of duck and cover of users after the alerts. As discussed, trained users might reduce their exposure to the seismic risk in about 3 to 5 s. Therefore, in the case of the considered 2012 Emilia scenario, about half a million persons could have potentially benefited from such EEW information to reduce their risk of injury
and to minimize panic five or more seconds before the arrival of the maximum ground motion.

PART III – Real-time estimation of energy magnitude in EEW

In the previous chapter, the capability of the IV2 parameter to predict the ground motion intensity at a target site has been assessed. The importance of the IV2 parameter is related to the fact that when measured on P- and S-wave, it is directly connected with the energy irradiated by the source (hereinafter, E_S).

In this part of thesis, a new regional P-wave based EEW strategy for the real-time estimation of E_S released during an ongoing earthquake is presented. The approach we propose exploits the IV2 parameter and aims to characterize the earthquake size in terms of Energy Magnitude (hereinafter, M_E). The procedure here proposed, despite its general character, is calibrated using a database of Italian earthquake recordings. Therefore, despite in the following we show that the procedure works well also on a couple of Japanese earthquakes, we point out that, similarly to the M_L scale, for different regions the IV2 versus M_E relationship should be parameterized on local recordings.

Respect to the Moment Magnitude (hereinafter, M_W), one of the most used parameter in regional EEWS, the E_S can provide important information on the dynamic properties of the rupture process (i.e., stress drop, Moment Rate function), and M_E better reflect than M_W the high frequency component of the earthquake signal, which is strictly correlated to the structural damage in the epicentral area. In the eighth chapter, the main concepts of the E_S and M_E are explored, while in the ninth chapter the analysis procedure and the IV2 based methodology are described. In the tenth chapter, the performance of the method is first evaluated considering the same data set used for calibrate it and, subsequently, by comparing its results with the teleseismic measurements of M_E realized according to the procedure proposed by Di Giacomo et al. (2010) for 8 earthquakes of the L'Aquila, 2009 and the Emilia, 2012 seismic sequences. Finally, a test of the procedure has been performed considering two Japanese earthquakes with similar M_W (i.e., ~7), but different teleseismic M_E.

8. The Seismic Energy and the Energy Magnitude

8.1 The Seismic Energy

The energy involved in a seismic event consists mainly in 5 contributions (Kanamori et al., 1993): the strain energy change W, the heat loss during faulting H, the potential energy due to the deformation E_p, the energy for creation of fractures E_c, and the energy radiated in seismic wave E_S. The radiated seismic energy E_S, even if it represents only a small portion part of the energy budget of the earthquake, it is an important physical parameter connected to the dynamic characteristics and to the complexities of rupture process of the earthquake. Furthermore, because of the difficulty to determine the absolute tectonic stress in the crust with seismological methods, E_S is the only part of the energy budge that can be derived from seismic data (Kanamori et al., 1993).
The parameter E_S depends on the variation of stress condition during the rupture process on the fault (Rudnicki and Freund, 1981):

$$E_S = \int_{-\infty}^{+\infty} \int_{S} \left[-\sigma_{ij}\gamma_j \dot{u}_i\right] dS\, dt \qquad (3.1)$$

Where $\dot{u}_i$ is the particle velocity, σ_{ij} the stress change associated with the fault displacement u_i , γ_j the unit vector normal to the surface S and pointing outward from the source, and *t* the time. This definition is valid in the far-field approximation, i.e., the radius of surface S is much larger than the dimension of the seismic source. According to Rudnicki and Freund (1981), the equation (3.1) is equivalent to the expression formulated by Haskell (1964), widely used in seismology:

$$E_S = \int_{-\infty}^{+\infty} \int_{S} \rho\left[\alpha \dot{u}_\alpha{}^2 + \beta \dot{u}_\beta{}^2\right] dS\, dt \qquad (3.2)$$

Where ρ is the crustal density, α and β the P- and S-wave velocity in the medium, $\dot{u}_\alpha$ and $\dot{u}_\beta$ the far-field velocity records of P- and S-wave, respectively. In this expression, the velocity records have to take into account the correction for the energy loss related to geometrical spreading and the anelastic attenuation of the body waves during the propagation from the source to the receivers.

Considering the moment rate function $\dot{M}(t)$, the displacement $u_{\alpha,\beta}$ of the particle produced by P- and S-wave fronts in far-field approximation can be written as(Aki and Richards, 1980):

$$u_\alpha(t) = \frac{R_\alpha(\theta,\phi)}{4\pi r\alpha^3}\dot{M}(t) \qquad (3.3)$$

$$u_\beta(t) = \frac{R_\beta(\theta,\phi)}{4\pi r\beta^3}\dot{M}(t) \qquad (3.4)$$

Where r is the source-receiver distance and $R_\alpha(\theta,\phi)$ and $R_\beta(\theta,\phi)$ the radiation patterns for P- and S-waves, respectively. Replacing the equations (3.3) and (3.4) in the expression (3.2), and using the Parseval's identity E_S can be expressed in the frequency domain (Venkataraman and Kanamori, 2004a):

$$\begin{aligned} E_S &= \left(\frac{1}{15\pi\rho\alpha^5} + \frac{1}{10\pi\rho\beta^5}\right)\int_{-\infty}^{+\infty} \left|\widehat{\ddot{M}(f)}\right|^2 df \\ &= \left(\frac{2}{15\pi\rho\alpha^5} + \frac{1}{5\pi\rho\beta^5}\right)\int_{0}^{+\infty} \left|\widehat{\ddot{M}(f)}\right|^2 df \\ &\approx \left(\frac{2}{15\pi\rho\alpha^5} + \frac{1}{5\pi\rho\beta^5}\right)\int_{f_1}^{f_2} \left|\widehat{\ddot{M}(f)}\right|^2 df \qquad (3.5) \end{aligned}$$

Where f is the frequency and f_1 and f_2 are the lower and the upper bound of the integration, respectively. Then, E_S, in the far-field approximation, is proportional to the time derivative of the moment rate function $\dot{M}(t)$. It is worth noting that the equation (3.5), useful for a simpler correction of the frequency dependent attenuation effect, is valid for a point source approximation (i.e., the signal wavelengths are much smaller than the source to receiver distance and neglecting directivity effects).

Although E_S has been always considered a fundamental parameter to characterize the earthquake source, since its direct calculation from the seismic recordings is not straightforward, the use of E_S has been rather limited. In order to obtain a first, even if rough, estimation of the energy released by the source, a linear relationship between E_S and the surface wave magnitude, proposed by Gutenberg and Richter (1956a,b), was widely used.

In the recent years, the worldwide development of seismic networks, equipped with high quality digital broadband seismometers, has stimulated the development of new approaches for the direct measurements of the Seismic Energy. In this context, three main strategies have been applied to estimate E_S (Singh and Ordaz, 1994). They consist in computing E_S from: (1) the source-time function retrieved from body wave modeling (Vassiliou and Kanamori, 1982; Kikuchi and Fukao, 1988), (2) the spectra of teleseismic broadband P waves (Boatwright an Choy, 1986) and (3) the broadband near-source recordings either in the frequency or in the time domain (Thatcher and Hanks, 1973; Bolt, 1986; Shoja-Taheri and Anderson, 1988; Kanamori et al., 1993).

Recently, Lomax et al. (2007) and Di Giacomo et al. (2010) proposed new approaches for the estimation of E_S, and in turn M_E, considering P-waves signals at teleseismic distance. These approaches presents two main advantages with respect to methods that rely on S-waves: 1) the earlier P-wave arrival allows a rapid earthquake magnitude determination and 2) the energy loss of P-wave is much smaller than the S-wave one.

8.2 The estimation of Seismic Energy by using the Magnitude scales

The concept of magnitude scale was developed over past decades in order to provide information about a particular aspect earthquake source (Di Giacomo et al., 2010).

The first magnitude scale linked to the physical characteristics of the earthquake, independently of its effects, was the local magnitude M_L, which has been introduced by Richter (1935) with the aim to obtain an estimation of the amount of energy released by the seismic source.

In the following years, the magnitude concept evolved (Gutenberg, 1945a,b,c; Gutenberg and Richter, 1956a,b), and other magnitude scales have been introduced with the use of teleseismic recordings, but always keeping the basic idea to obtain information on the energy release of the seismic source. In particular, this intention is testified by the so-classical Gutenberg-Richter relationships:

$$\log_{10}(E_S) = 2.4\, m_B - 1.2 \qquad (3.6)$$

$$\log_{10}(E_S) = 1.5\, M_S + 4.8 \qquad (3.7)$$

where E_S is the seismic energy (Haskell, 1964) measured in Joule, m_B is the body-wave magnitude calculated between about 2 and 20 s (Abe, 1981) and M_S is the surface wave magnitude measured at periods around 20 s.

After the introduction of the seismic moment M_0 (Aki, 1966), the moment magnitude scale M_W, proposed by Kanamori (1977) and Hanks & Kanamori (1979), has been used to indicate the energy amount involved in an earthquake. This modern and popular scale is related to the seismic moment $M_{0,}$ a well-defined physical parameter of the source defined as:

$$M_0 = \mu A \overline{D} \qquad (3.8)$$

where μ is the rigidity, A the rupture area and $\overline{D}$ the average displacement on the fault surface.
In the M_W formulation, Kanamori (1977) expressed the seismic energy E_S as:

$$E_S = \left(\frac{\Delta\sigma}{2\mu}\right) M_0 \qquad (3.9).$$

In this case, under the condition of complete stress drop, E_S corresponds to the strain energy drop W. The condition of complete stress drop is verified when the final average stress σ_1 and the frictional stress σ_f are identical (Orowan, 1960). It is worth noting that this assumption may be not valid, because final stress σ_1 can be larger than σ_f (partial stress drop, Brune, 1970) or smaller than σ_f (frictional overshoot, Savage and Wood, 1971). In addition, Kanamori (1977), assuming μ equal to 3-6 $\times 10^4$ MPa in the source area and a stress drop confined between 2 and 6 MPa for very large earthquakes, obtained from equation (3.9):

$$\frac{E_S}{M_0} = 5 \times 10^{-5} = \text{constant} \qquad (3.10)$$

By the condition (3.10) and the changing M_S for M_W in the equation (7), Kanamori (1977) defined the Magnitude Moment M_W as:

$$M_W = (\log_{10}(M_0) - 9.1)/1.5 \qquad (3.11)$$

where, M_0 given in N·m. The scale defined by (3.11) is widely used in the seismological applications as ShakeMap and seismic hazard studies (Di Giacomo et al., 2010).
Recently Choy and Boatwright (1995) introduced a new magnitude scale: *Energy Magnitude* M_E. This scale has been obtained from the equation (3.7) in a similar way to that one used by Kanamori (1977) to derive $M_{W.}$ In particular Choy and Boatwright (1995) measured E_S directly from the recordings and they reported it as a function of M_S, and they substituted M_S with M_E. Then, they

calculated by a standard least-square regression, the best fitting line with the prescribed slope of 1.5 as in the equation (3.7), and they substituted M_S with M_E. As a result, they obtained a new value of the intercept respect to the equation (3.7) one, equal to 4.4.

Initially, Choy and Boatwright in 1995 retained the original constant of the Gutenberg-Richter equation (3.7) for consistency with other older types of magnitude, defining M_E as:

$$M_E = \left(\frac{2}{3}\right)\log_{10}(E_S) - 3.2 = \frac{\log_{10}(E_S) - 4.8}{1.5} \qquad (3.12)$$

With E_S measured in Joule. In their following works, they used the intercept of their new regression, modifying the formula (3.12) in (Choy et al., 2006):

$$M_E = \left(\frac{2}{3}\right)\log_{10}(E_S) - 2.9 \qquad (3.13a)$$

equivalent to:

$$M_E = \frac{\log_{10}(E_S) - 4.4}{1.5} \qquad (3.13b)$$

In particular, the equation (3.13b) is recommended by Bormann et al. (2002), because the equation (3.13a) can be affected by rounding errors of 0.1 magnitude units (Di Giacomo et al, 2010). Currently, the equation (3.13b) is accepted as standard also at the National Earthquake Information Center (NEIC) of the U.S. Geological Survey (USGS).

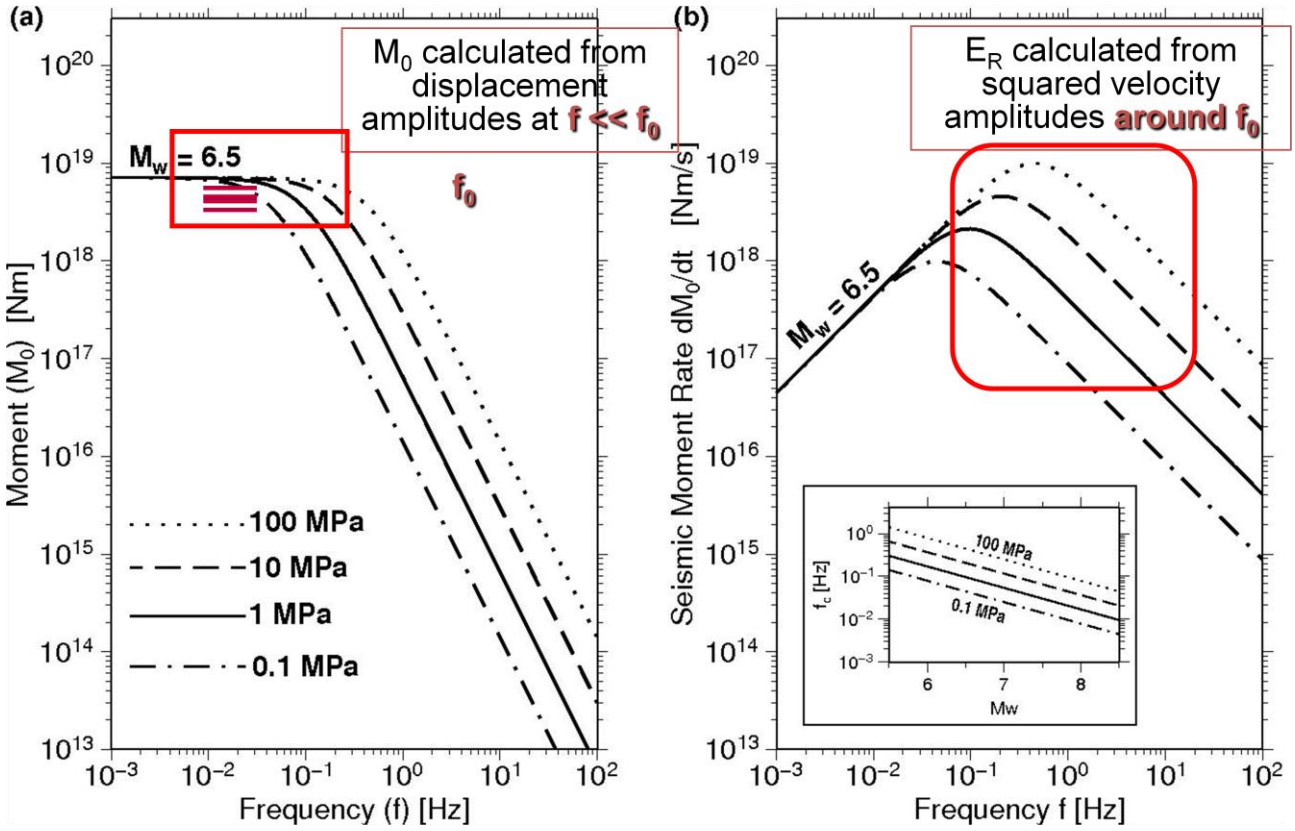

a) **b)**

Figure 3.1: Moment (a) and Moment rate function (b) spectra relative to Brune model (figure from Di Giacomo et al., 2010). The red squares identify in both cases the frequency band associated to the higher energy contribution.

8.3 The comparison between M_W and M_E

Nowadays M_W is considered as the best parameter to evaluate the earthquakes damage potential. Despite this, M_W provides only limited information about the earthquake source, especially on the high frequency content (Beresnev, 2009). This contribution of the source function is fundamental for the evaluation of an earthquake shaking potential and it is strictly related to the structural damage in the epicentral area. In particular Beresnev (2009) affirmed that*: "It is clear even intuitively, though, that the low-frequency measure, such as the moment (or magnitude), can only provide limited information about the source process. The moment, by its definition, is determined by the final slip on the fault. The way the slip reaches its final state cannot be recovered from the*

value of the moment, and the more detailed slip history must be "recorded" in the higher-frequency content of the spectrum."

In contrast to M_W, the Energy Magnitude M_E is sensitive to the variation of the stress conditions governing the earthquake process (Equations 3.1 and 3.13b), which determinates the amount of energy transferred to seismic waves (Di Giacomo et al., 2010).

Assuming a Brune (1970) source model, Figure (1a) shows M_0 as a function of frequency for events having the same M_W but different stress-drop. As Beresnev (2009) pointed out, the frequency content of M_0 is mainly constituted by low frequency components much smaller than the corner frequency f_0 (Figure 3.1a), that for S-wave spectrum is equal to:

$$f_0 = \mathrm{c}\,\beta\left(\frac{\Delta\sigma}{M_0}\right)^{1/3} \qquad (3.14)$$

where c is a constant equal to 0.49. For this reason, according to Beresnev (2009), M_W results a parameter insensitive to the release of seismic energy in the high frequency range.

On the contrary, Figure (3.1b) shows that in the Moment Rate function the frequencies having the largest amplitude are those localized around the corner frequency f_0. It is interesting to note that, from equation (3.14), f_0 is related to the dynamic parameter $\Delta\sigma$. Therefore, the moment rate function $\dot{M_0}(t)$ is a parameter capable of providing information about the dynamic properties of the source and the temporal evolution of slip function on the rupture surface. Indeed, from equation (3.13b) the Energy Magnitude M_E is strictly related to the Seismic Energy E_S, that according to the equation (3.5) is proportional to the moment rate function $\dot{M}(t)$.

For these reasons, the M_E scale can provide important indication on the dynamic parameters of the earthquakes, and it can be complemented with M_W in order to obtain a detailed characterization of the earthquake source (Di Giacomo et al., 2010).

9. The Analysis procedure

9.1 Used Databases

9.1.1 Calibration Dataset: ITACA Database

The database used for the calibration of a IV2 versus M_E relationship for regional EEW consists of about 900 accelerometric recordings of RAN Network (i.e., please, see the previous chapters for details on the RAN network). In particular, the database consists of 29 earthquakes occurred in Italy between 1997 and 2013, having moment magnitude between 4 and 6.3 (figure 3.2a). These events correspond to the Umbria-Marche (1997) and L'Aquila (2009) seismic sequences in Central Italy, and to the Emilia (2012) sequence in Northern Italy. The selected hypocentral distance interval of this traces ranges from 0 to 100 km (figure 3.2b).

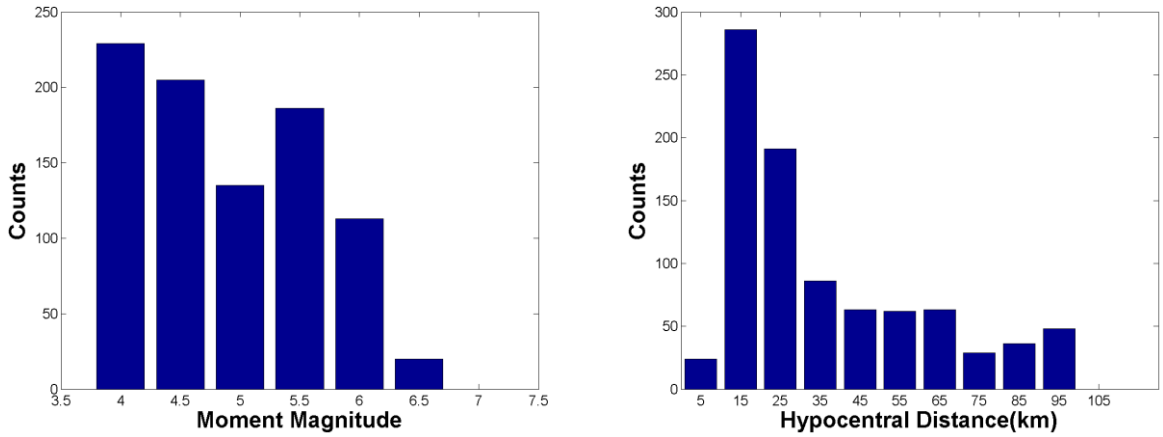

a) **b)**

Figure 3.2: Calibration data set: ITACA recordings reported as a function of Moment magnitude (a) and hypocentral distance(b).

9.1.2 Testing Dataset: Kik-net and K-NET Databases

Aiming to test the procedure for the estimation of M_E on a dataset different from that used to calibrate the IV2 vs. M_E relationship, we have considered the recordings of two Japanese seismic events, the Iwate-Miyagi (2008) and the Miyagi-Oki (2008) earthquakes, having M_W 6.9 and 7.0, respectively. The waveforms have been extracted from the Kik-net and the K-NET on-line databases (http://www.kik.bosai.go.jp/ and http://www.k-net.bosai.go.jp/). The analyzed data set consists of 100, three-component strong-motion accelerometer records, having hypocentral distance between 0 and 100 km (Figure 3.3).

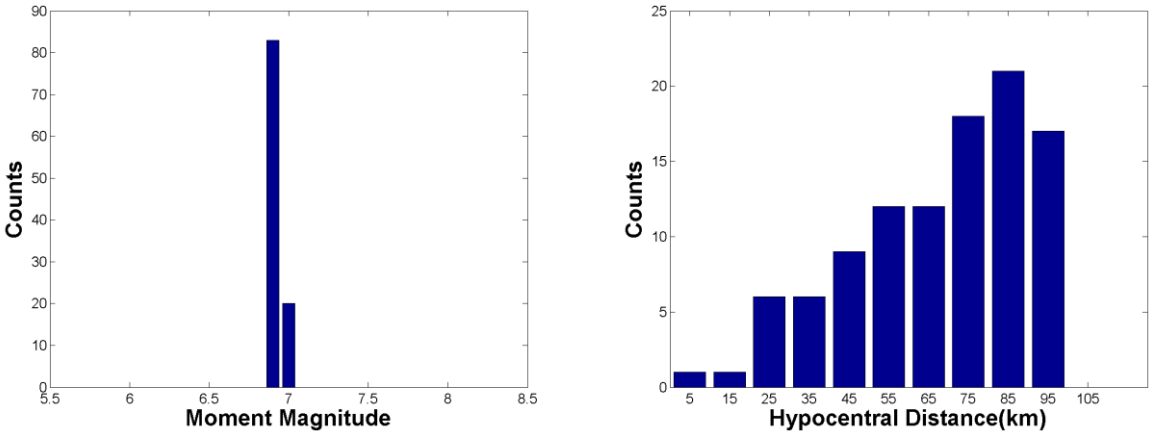

a) **b)**

Figure 3.3: Data base for method Blind Test: Kik-Net and K- NET recordings reported as a function of Moment magnitude (a) and hypocentral distance (b).

9.2 IV2 vs Seismic Energy

9.2.1 IV2 and Seismic Energy Calculation

The procedure for the estimation of M_E is grounded on the capability of the IV2 parameter to predict the overall amount of E_S released by an earthquake, or being anyhow a good proxy of E_S when measured on P-wave recordings. The use of IV2 in EEW is not new. In fact, Festa et al.(2008) and Lancieri et al.(2011) have already investigated the use of IV2 in regional EEW approaches to estimate M_W. In particular, Festa et al. (2008) used signal windows of 4 seconds of P wave and of 2 seconds of S-wave, while Lancieri et al.(2011) used 4 seconds of P-wave. In both works, a saturation effect dependent on the signal window length has been observed for magnitude greater than M_W 6.5 and M_W 7.6, respectively. In this work, with the aim to avoid as much as possible the saturation effects, the estimation of IV2 has been carried out at each station considering the entire available P-wave signal on the vertical component between the P-wave and S-wave arrival times.

In order to obtain a linear relationship between IV2 and E_S, we have calculated the theoretical value of E_S for 29 earthquakes recorded by the RAN network considering the source parameters (i.e., corner frequency f_0, the seismic moment M_0, the stress drop $\Delta\sigma$) estimated by Bindi et al. (2004, 2009) and Castro et al.(2013). In particular, we have computed the theoretical displacement Brune (1970) spectrum $U(\omega)$ for P- and S-wave by:

$$U(\omega) = \frac{R_{\theta\varphi}^{C} F}{4\pi\rho c^3 R} \frac{M_0}{1 + (\frac{\omega}{\omega_0})^2} \qquad (3.15)$$

where $R_{\theta\varphi}^{C}$ is radiation pattern, F is the free-surface coefficient (equal to 2), c is the velocity seismic phase, R is the distance source to receiver (assumed equal to 1 km), ω is the pulsation and $\omega_0 = 2\pi f_0$.

Subsequently, we have computed the theoretical seismic energy contribution for both P- and S-waves at the reference hypocentral distance of 1 km, using the formula of Boatwright and Fletcher (1984):

$$E_S = \frac{4\pi\rho c R^2}{F^2} \frac{1}{\pi} \int_0^{\infty} \omega^2 |U(\omega)|^2 d\omega \qquad (3.16)$$

where, E_S is given in Joule and R is equal to 1 km.

It is worth noting that, in order to allow dimensional consistency, the seismic energy E_S provided by equation (3.16) is associated with a sphere centered in the hypocenter with radius equal to 1 km, instead of the point source.

The obtained P-wave energetic contribution $E_S^{(P)}$ is about the 8% of the S-wave theoretical energy $E_S^{(S)}$. This percentage is nearly compatible to the P-wave energy fraction calculated by Haskell (1964), equal to 4%. The overall $E_S^{(TOT)}$ is given by:

$$E_S^{(TOT)} = E_S^{(P)} + E_S^{(S)} \qquad (3.17)$$

Then, the resultant theoretical seismic energy $E_S^{(TOT)}$, correspondent to the 29 analyzed earthquakes has been associated to the P-wave derived IV2 values observed for the same events. In particular, as shown in the following section, a linear regression has been calculated reporting IV2 measurements as a function of the theoretical seismic energy $E_S^{(TOT)}$ and the hypocentral distance R.

9.2.2 Regression Analysis

Taking as reference the functional adopted by several recent works on GMPEs (e.g., Akkar and Bommer, 2007b; Atkinson & Boore, 2006; Campbell 2003), the relation between IV2 and E_S has been studied by a multiparametric regression approach. Similarly to the relationship between the P-wave peak displacement and M_W, here we aim to define a relationship between IV2 and E_S that can be used by regional EEW approaches. Therefore, considering the IV2 estimates obtained at network's stations, we have sought the optimal correction for the attenuation of IV2 with the hypocentral distance.

With respect to the popular attenuation function used in EEW (e.g. Zollo et al., 2006), here the hypocentral distance range has been subdivided in 10 non-overlapping intervals having width equal to 10 km, and for each of them a specific attenuation coefficient C_i has been derived. The considered functional for the multi-parametric regression is:

$$\log_{10}(\mathrm{IV2}) = A + B\log_{10}(E_S) + \sum_{i=1}^{N}\sum_{j=1}^{D} C_i W_{ij} \qquad (3.18)$$

where, E_S indicates $E_S^{(TOT)}$, N is the number of attenuation coefficients (equal to 10), D is the number of data (equal to 900). Furthermore, W is N×M matrix that is equal to 1 if the j-th IV2 measurement has a hypocentral distance value included in i-th distance interval, and null otherwise. This working scheme is easy to implement in real-time operations, since the matrix W selects the appropriate attenuation correction factor for the IV2 value as soon as the first real-time hypocentral estimation is available.

Given the high number of parameters, we forced the coefficient C_1 to be equal to 0, in order to well-constrain the regression analysis. This condition implies that data having hypocentral distance smaller than 10 km are not corrected for the geometrical spreading effect. The obtained coefficients A, B and C_i of the equation (3.18) are reported in Table 3.1. The calculated regression, shown in figure 3.4a, has a R^2 correlation coefficient equal to 0.76, while its standard deviation is 0.58. This value is comparable to the uncertainty of the regressions between IV2 and moment magnitude derived by Festa et al. (2008) and Lancieri et al. (2011).

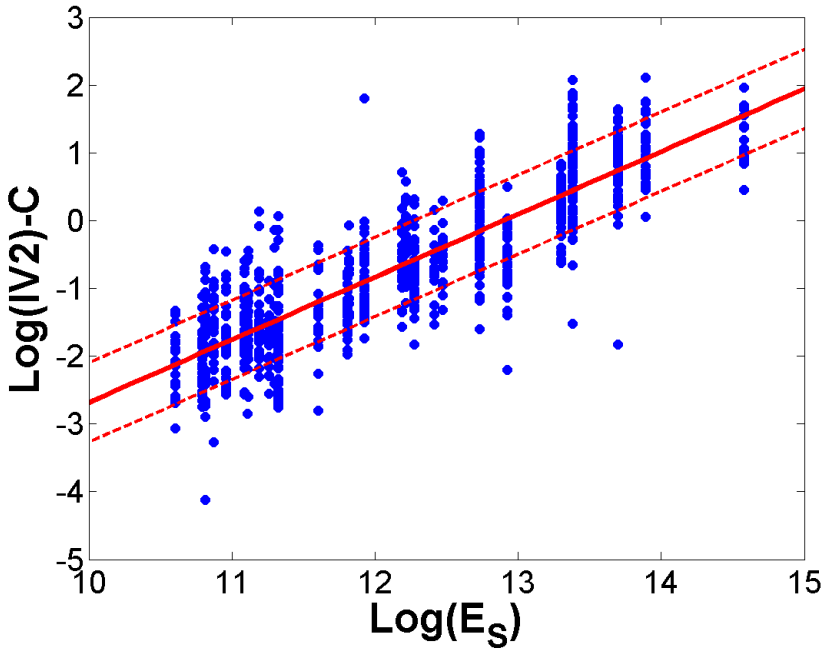

a)

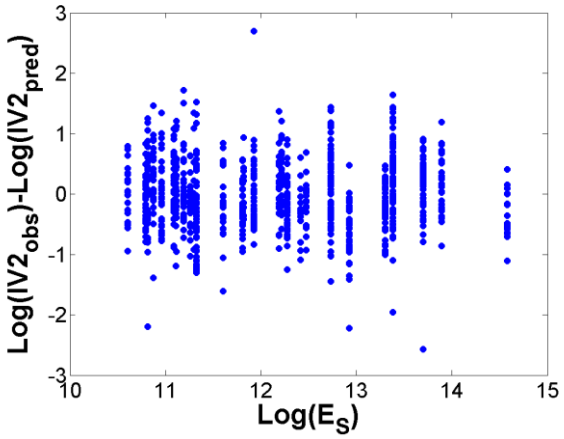

b)

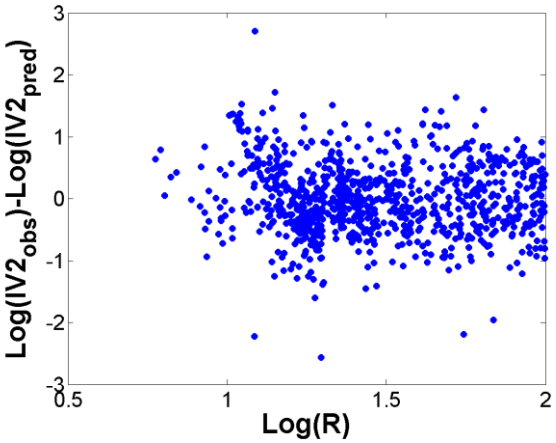

c)

Figure 3.4: IV2 values, corrected for C attenuation coefficients, are shown as a function of theoretical seismic energy, calculated from the source parameters of Bindi et al.(2004, 2009) and Castro et al.(2013). In addition, the regression of eq.(18) (thick red line) is reported with his standard deviation (dashed red lines) (a). The residuals of the eq.(18) are shown as a function of theoretical seismic energy (b) and hypocentral distance (c).

Figure 3.4b and 3.4c show the regression residuals as a function of theoretical E_S and the hypocentral distance. In both cases, we observe that residual distribution is, in first approximation, uniformly centered on the null value.

In order to check the stability of the regression and to obtain the accuracy of the obtained parameters the bootstrap statistical method (Efron, 1979) has been used. In particular, this technique allows deriving the standard errors for the coefficient regressions by using the a random sampling with replacement of the original dataset. In Table (3.1) the mean value and the standard deviation of the parameter A, B and C_i (Equation 3.18), obtained with 10000 random samplings of original dataset, are reported. In particular, we observe that all the regression parameters are consistent with the correspondent mean values calculated by the bootstrap method. Furthermore, the standard deviations associated to the A and B coefficients are the 2% of their correspondent mean values, while in the case of C_i coefficients the percentage is 5% (table 3.1).

Parameters	Parameters Regression Values	Bootstrap Mean Values	Bootstrap Standard deviations
A	-11.9346	-11.9317	0.2536
B	0.9250	0.9246	0.0199
$\mathbf{C_1}$	0	0	0
$\mathbf{C_2}$	-1.1337	-1.1317	0.1042
$\mathbf{C_3}$	-2.0005	-1.9982	0.1023
$\mathbf{C_4}$	-2.4591	-2.4568	0.1105
$\mathbf{C_5}$	-2.5476	-2.5452	0.1297
$\mathbf{C_6}$	-2.6797	-2.6768	0.1273
$\mathbf{C_7}$	-2.8661	-2.8625	0.1213
$\mathbf{C_8}$	-2.6658	-2.6627	0.1318
$\mathbf{C_9}$	-2.7752	-2.7719	0.1370
$\mathbf{C_{10}}$	-2.5938	-2.5918	0.1203

Table 3.1: Values of regression parameters A, B and C_i, reported with the correspondent mean values and their standard deviations, obtained by using the Bootstrap method (Efron, 1979) on the calibration dataset.

9.3 Magnitude Energy estimation method

In this section a method for the real time estimation of M_E is presented. In recent regional EEW studies, as Lancieri and Zollo (2008), the moment magnitude M_W is estimated by reversing the regression equation of the Peak displacement (measured on 4 seconds of P-wave and 2 seconds of S-wave), written as a function of M_W and hypocentral distance. With a similar approach, our method provides an estimation of E_S from the IV2 measured on P-wave window recordings.

Therefore, considering equation (3.18), the real-time EEW prediction of seismic energy $E_{S(EW)}$ is obtained by the formula:

$$\log_{10}\left(E_{S_{(EW)}}\right) = \frac{\log_{10}(IV2) - \sum_{i=1}^{N}\sum_{j=1}^{D} C_i W_{ij} - A}{B} \qquad (3.19)$$

As discussed, Eq.(3.19), can be used in real-time operations, that is to say, the evolutive estimate of the hypocentral position provided by a regional EEW location algorithm can be used to select for each station the most adequate attenuation coefficient C_i and to correct the IV2 measurements.
Therefore, considering the equation (3.13b), the EEW magnitude energy estimation $M_{E(EW)}$ is calculated by the expression:

$$M_{E_{(EW)}} = \frac{\log_{10}(E_{S_{(EW)}}) - 4.4}{1.5} \qquad (20)$$

According to the procedure commonly adopted by EEWS for estimating M_W, we estimate $M_{E(EW)}$ of an event as the average value of the $M_{E(EW)}$ predictions obtained at the single recording stations provided by equation (3.20). It is worth noting that, at the present, factors as the focal mechanism earthquake, the source directivity and the local site effects are not taken into account in (3.19).

10. Applications and Results

The performance of the methodology described in the previous chapter has been assessed considering first the same data base used to calibrate it, focusing on the results for the 6th April 2009 L'Aquila (M_W 6.3) and the 29th May 2012 Emilia earthquakes (M_W 6.0). Furthermore, the M_E estimates obtained by our method have been compared with the teleseismic measurement of M_E obtained applying the procedure proposed by Di Giacomo et al. (2010) for 8 Italian earthquakes, correspondent to the strongest events of the L'Aquila (2009) and Emilia (2012) seismic sequences. Finally, a test of the proposed procedure has been carried out considering 2 Japanese earthquakes, both having M_W 7.0 but different stress-drop, which corresponds to different amount of E_S.

10.1 Performance on the Calibration Data Set

As first testing of the procedure for the estimation of M_E, and to check if our data are able to retrieve the model assumed for this study (i.e., Eq. 3.18), we assessed the new EW procedure on the same RAN data used to derive the equation (3.18). In figure (3.5a), we compare the theoretical and EEW M_E computed for the 29 seismic events of the calibration dataset. The theoretical energy magnitude ($M_{E(THEO)}$) is obtained using the source parameters provided by Bindi et al. (2004, 2009), and Castro et al. (2013), and considering the Eqs. (3.15), (3.16), (3.17) and (3.13b). The EEW energy magnitude $M_{E(EW)}$ is derived by the IV2 measurements and the Eqs. (3.19) and (3.20).

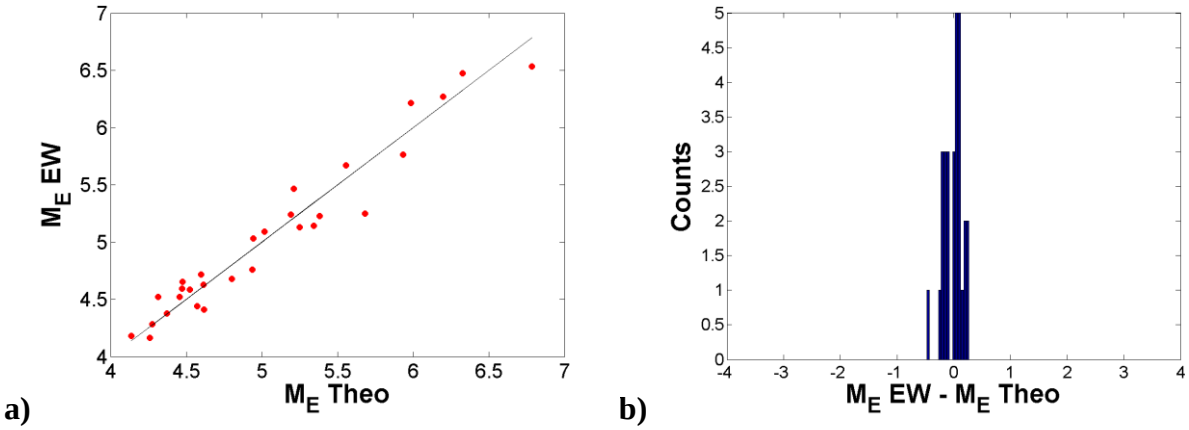

Figure 3.5: a) Average $M_{E(EW)}$ and $M_{E(THEO)}$ values. b) Histogram of the residuals.

Figure (3.5b) shows that residuals computed for the two M_E estimates are smaller than 0.3 unit of magnitude (u.m.) for the 96,5% of events.

In addition to this analysis, we have focused our attention on the residuals obtained for the two strongest and better recorded seismic events that struck the Italian territory in the last 10 years: the 6th April 2009 L'Aquila (M_W 6.3) and the 29th May 2012 Emilia (M_W 6.0) earthquakes. In particular, Figure (3.6) shows for the two events the azimuthal distribution of the RAN stations around the epicenter and the M_E residuals for each recording station with respect to the hypocentral distance and azimuth. In particular, the difference between the magnitude energy estimate $M_{E(EW)}$ at each recording station and the theoretical value $M_{E(THEO)}$ calculated for the event are shown as a function of hypocentral distance (figure 3.6c and 3.6d), azimuth (figure 3.6e and 3.6f) and the number of stations (Figure 3.6g and 3.6h). Considering Figure (3.6h) concerning the M_W 6.0 Emilia earthquake (2012), we observe that the residuals have distribution almost Gaussian and having a mode indication that the $M_{E(EW)}$ estimate overestimate the $M_{E(THEO)}$ of 0.4 m.u. Considering that for

this event is characterized by a rather dense and homogenous distribution of stations in both distance and azimuth, we believe that the difference between $M_{E(EW)}$ and $M_{E(THEO)}$ is not due to the focal mechanism, while it could be related to directivity effects hypothesized by other authors (Convertito at al., 2013).

Considering the M_W 6.3 L'Aquila Earthquake, we noted that $M_{E(THEO)}$ is underestimated of 0.3 u.m. (figure 6g). In this case the distribution of residuals is peculiar, being all residuals smaller that zero. We hypothesize that this result is due to the low density and heterogeneous distribution of the stations around epicenter, which together with the focal mechanism of the earthquake, having a strike angle parallel to Apennine direction, likely bias the IV2 measurements, and in turn the $M_{E(EW)}$ estimates. In view of these observations, in the next future we will further investigate the correlation between the focal mechanism and IV2 estimates in order to set-up automatic procedure for correcting the $M_{E(EW)}$ estimates on the basis of the azimuthal coverage of the stations.

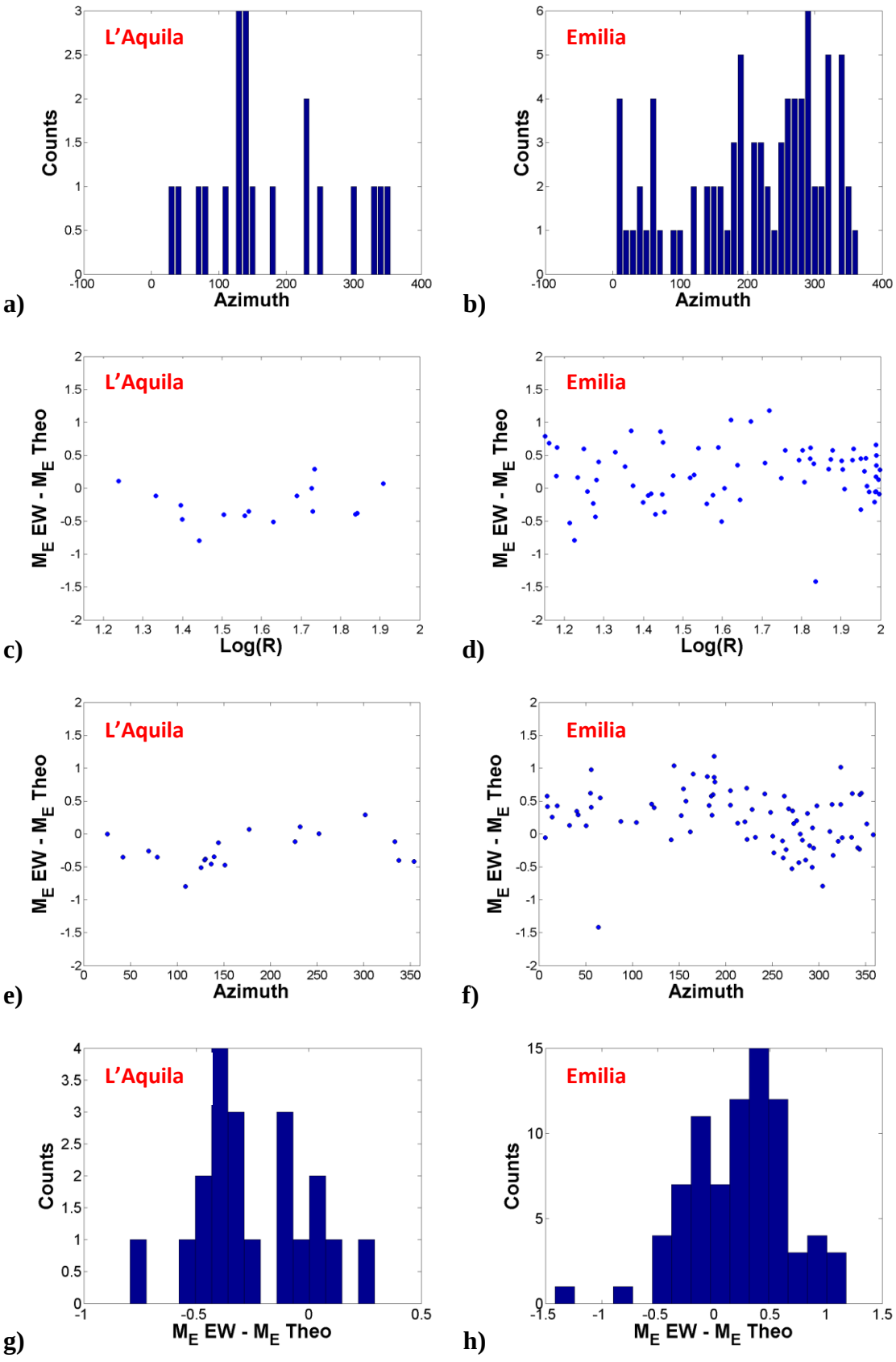

Figure 3.6: Method performance on (M_W 6.3) 6th April 2009 L'Aquila (a-c-e-g) and (M_W 6.0) 29th May 2012 Emilia (b-d-f-h) earthquakes: azimuthal distribution of the stations around the epicenter (a-b); difference

between EW magnitude estimates at stations and event theoretical M_E value shown as a function of hypocentral distance (c-d), azumith (e-f) and number of event recordings (g-h).

10.2 Performance considering M_E teleseismic measurements

In this section the results of our EEW methodology are compared with the energy magnitude M_E calculated using the approach proposed by Di Giacomo et al. (2010) for the largest and more recent 8 earthquakes of our dataset. In particular, these events correspond to the mainshock and the more intense aftershocks of L'Aquila (2009) and Emilia (2012) sequences. The procedure proposed by Di Giacomo et al. (2010) for estimating M_E exploits teleseismic P-wave recordings, and equations (3.5) and (3.13b), after having corrected the P-wave amplitude for the attenuation by means of theoretical spectral amplitude decay function for periods between 1 s and 16 s.

Figure (3.7a) and Table (3.2) shows the comparison between the $M_{E(EW)}$ and the M_E measurement provided by Di Giacomo et al. (2010) (hereinafter, $M_{E(TEL)}$) for the 8 considered seismic events. Although, the comparison has been performed on a very limited number of events, we observed that the M_E estimations provided by our method are rather in good agreement with the values provided by Di Giacomo et al, (2010). In particular, the $M_{E(EW)}$ estimates overestimates on average the $M_{E(TEL)}$ teleseismic measurements of around 0.3 u.m.(Figure 3.7b).

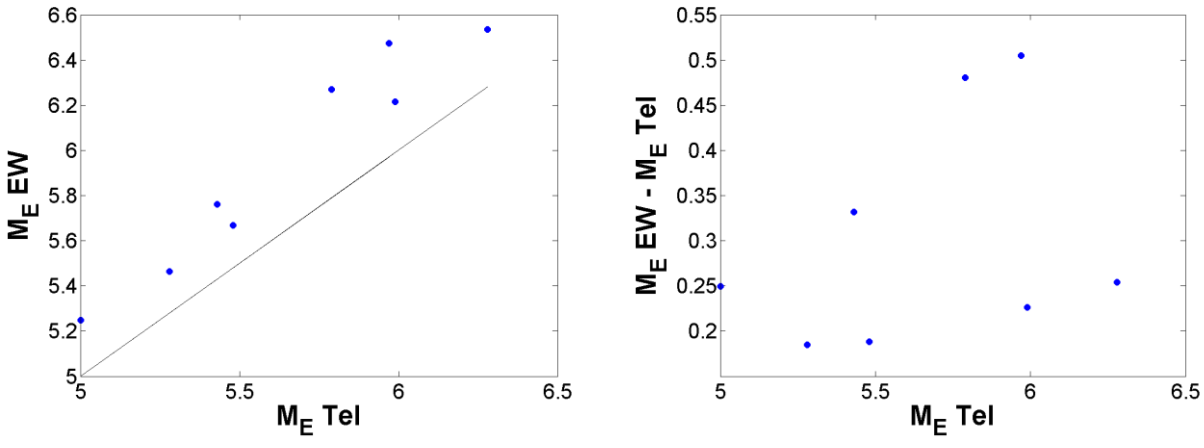

a) **b)**

Figure 3.7: Comparison between $M_{E(EW)}$ and $M_{E(TEL)}$ measurements provided by Di Giacomo et al., (2010) for 8 events of L'Aquila(2009) and Emilia (2012) seismic sequences (a). Their difference as a function of $M_{E(TEL)}$.

The magnitude range considered in this study (i.e. M_W between 4 and 6), the teleseismic measurements can underestimate of 0.2-0.3 u.m. the real energy magnitude M_E of the event. This effect is related to the frequency band used in the calculation of seismic energy E_S (equation 3.5), which is set in order to analyze the low frequency contribution that dominates in the teleseismic recordings of very large earthquakes.

Origin Time Event	**M_w**	**M_E** **(Di Giacomo et al., 2010)**	**M_E** **(EW)**	**ΔM_E**
2009/04/06 01:32:42.625	6.3	6.3	6.5	+0.2
2009/04/07 17:47:38.035	5.5	5.8	6.3	+0.5
2009/04/09 00:53:01.610	5.4	5.4	5.8	+0.4
2009/04/09 19:38:18.891	5.2	5.0	5.2	+0.2
2012/05/20 02:03:53.995	6.1	6.0	6.5	+0.5
2012/05/20 13:18:03.179	5.2	5.3	5.5	+0.2
2012/05/29 07:00:04.549	5.9	6.0	6.2	+0.2
2012/05/29 10:55:57.938	5.5	5.5	5.7	+0.2

Table 3.2: Moment magnitude, $M_{E(TEL)}$ measurements of Di Giacomo et al.(2010), $M_{E(EW)}$ estimates and their difference ΔM_E are shown for the 8 analyzed earthquakes of L'Aquila (2009) and Emilia (2012) seismic sequences.

10.3 Blind test for Japanese earthquakes

In order to verify the ability of our method to provide real-time information on the seismic energy amount for an independent data-set, we have considered two Japanese earthquakes, recorded by Kik-net and K-NET seismic networks. In particular, the analyzed events are the Miyagi-Oki (2003) and the Iwate-Miyagi (2008) earthquakes, having M_W equal to 7.0 and 6.9, respectively. Although these two seismic events have almost the same M_W and focal mechanism typology, they are characterized by a very different stress drop value. In fact, for the Miyagi-Oki (2003) earthquake, Oth et al., (2013) estimated a stress drop value about 9 times greater than the measurement correspondent to Iwate-Miyagi (2008) event. Considering the source parameters provided by Oth et al., (2013), such difference in stress drop corresponds to a consistent difference in the theoretical

E_S, which in turn corresponds to a difference of almost 1 u.m. in terms of $M_{E(THEO)}$ (Table 3.3). The goal of our analysis is verify whether our procedure, which relays on the P-wave IV2 observations is able to detect the difference between the two earthquakes. With this aim, the IV2 measurements have been calculated for the two Japanese earthquakes, as well as the theoretical M_E and E_S from the source parameters provided by Oth at al., (2013).

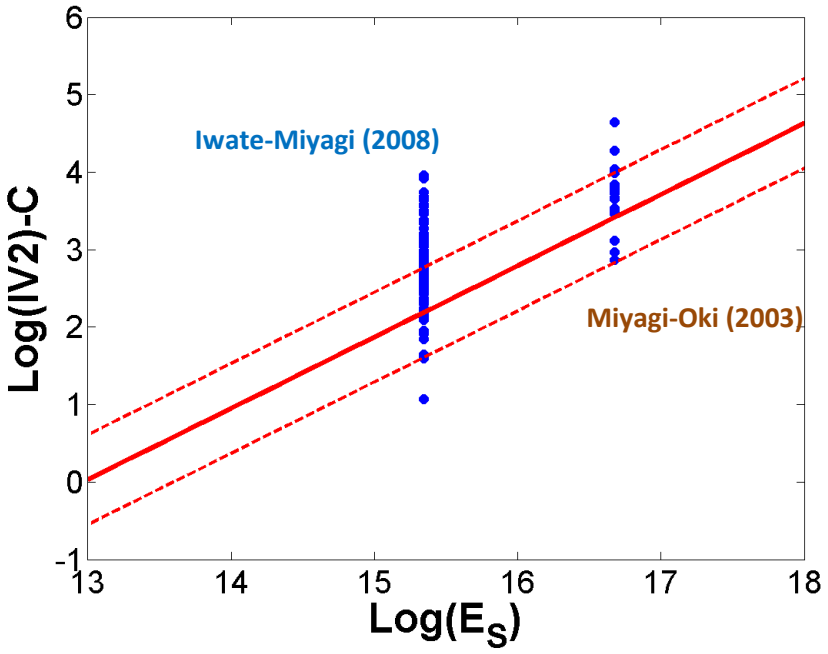

Figure 3.8: IV2 values for the Iwate-Miyagi (2008) and Miyagi-Oki (2003) earthquakes corrected for the Italian attenuation coefficients are shown as a function of theoretical seismic energy, derived by Oth et al., (2013) source parameters. In addition the regression of equation 18 (thick red line) is reported with his standard deviation (dashed red lines).

In principle, we expect that the attenuation of IV2 with hypocentral distance in Japan is different from Italy, and for this reason the equation (3.18) should be calibrated for the Japan data-base. Nevertheless, in doing this test our interest is mainly in the comparison between the $M_{E(EW)}$ estimates obtained for the two events. Therefore, we assume that any bias due to the use of an inappropriate attenuation function is now negligible, and we have used the parameterization of Eq. (3.18) obtained for the Italian database.

Figure (3.8) shows the IV2 measured from Kik-Net and K-Net recordings, considering hypocentral distance smaller than 100 km, and corrected for the Italian C_i attenuation coefficients (i.e., Table 3.1) as a function of theoretical E_S. As expected from theoretical considerations, we observe that the

difference in E_S between the Miyagi-Oki (2003) and the Iwate-Miyagi (2008) events (i.e., about a factor 10), corresponds to an average IV2 significantly higher for the former event than the one measured for the Iwate-Miyagi (2008) earthquake (figure 3.8). Interestingly, the IV2-E_S estimates for the two Japanese earthquakes are rather well in agreement with the Italian regression (i.e., Eq. 3.18). These results seem to indicate that the IV2 estimates are sensitive to the highest energetic contribution of Miyagi-Oki (2003) earthquake.

In Table (3.3) the values of Moment magnitude, theoretical energy magnitude $M_{E(THEO)}$ and the average value of $M_{E(EW)}$, provided by our method are reported for the two considered Japanese seismic events. For both earthquakes, we have found that $M_{E(THEO)}$ value is higher than $M_{W,}$ and for Miyagi-Oki (2003) event, their difference is maximum and equal to about +1 u.m. This observation, as discussed, is ascribed to the higher stress drop value measured for the Miyagi-Oki (2003) event. Despite the use of the Italian parameterization of the IV2 vs. E_S relationship might have contributed to a bias in the $M_{E(EW)}$, we consider very interesting that the $M_{E(EW)}$ estimates are in good agreement with the $M_{E(THEO)}$ for both earthquakes. These results show that, although the two analyzed Japanese events have almost the same M_W, the $M_{E(EW)}$ is able to provide real-time information on the different amount of stress-drop, and in turn E_S, associated to the events.

We believe that the further development of this regional EEW methodology could provide very important real-time indications on the seismic energy release during an occurring earthquake.

Indeed, the M_E estimates complemented with M_W, can provide useful and more complete information about the structural damage on the epicentral area, caused by the high frequency components of seismic signal. Moreover, our procedure could be of interest also for tsunami early warning systems, being in general the tsunami probability of occurrence in relation to off-shore subduction earthquakes with very high M_W and low stress drop.

Event	**M_W**	**M_E (Theoretical)**	**M_E (EW)**
Iwate-Miyagi (2008)	6.9	7.3	7.7
Miyagi-Oki (2003)	7.0	8.2	8.4

Table 3.3: Moment magnitude, theoretical energy magnitude calculated by the source parameters of Oth et al., (2013) and the average value of $M_{E(EW)}$ are shown for the 8 analyzed earthquakes of L'Aquila (2009) and Emilia (2012) seismic sequences.

10.4 Discussion and Conclusions

In this study a new regional EEW methodology, based on the IV2 parameter measured on P-waves, has been introduced with the aim to estimate the energy magnitude for events occurring in the Italian territory. In particular, this procedure is able to provide information on the seismic energy E_S amount released by an ongoing earthquake. The seismic energy and the energy magnitude are two important source parameters that, respect to moment magnitude M_W, can give more detailed indications on the dynamic of the earthquakes and the ground motion level in the high frequency range, where the civil infrastructures are most sensitive.

In the first part of this work, we have calculated a multiparameter regression in which the IV2 parameter is reported as a function of E_S and the stations hypocentral distance. This relationship has been obtained analyzing 29 Italian earthquakes with $M_W > 4$, occurred in last the 10 years, for which 900 RAN recordings and theoretical E_S measurements have been considered. In particular, for this regression, several constant attenuation coefficients have been considered in order to allow a more effective correction of IV2 measurements for the geometrical spreading effect. The accuracy of these coefficients value has been assessed by a Bootstrap approach considering 10000 random resamplings of original data set, which allow to estimate for each coefficient the relevant uncertainty.

In the second part of the study, we have derived an EEW methodology which exploits the real-time IV2 measurements and on the previous derived relationship between IV2 and E_S. Hence, the E_S predictions obtained at the recording stations are converted in energy magnitude estimations, and their average value is considered as the $M_{E(EW)}$ of the event.

In order to have a first evaluation of the method performance, this procedure has been tested on the RAN dataset used to calibrate the IV2-E_S relations. In this analysis, we have found that the difference between the theoretical $M_{E(THEO)}$ value and the average value of $M_{E(EW)}$ estimates is smaller than 0.3 u.m. for the 96,5% of the considered earthquakes.

Furthermore, we have compared the $M_{E(EW)}$ with the teleseismic M_E measurements obtained using the procedure proposed by Di Giacomo et al.(2010) for 8 Italian seismic events, correspondent to the mainshocks and the more intense aftershocks of L'Aquila (2009) and Emilia (2012) seismic sequences. For these events, the two M_E measurement are in rather good agreement. In particular, we have found that the $M_{E(EW)}$ overestimates on average of 0.3 u.m. the energy magnitude estimates obtained using the procedure proposed by Di Giacomo et al.(2010). As also indicated by Di Giacomo et al.(2010), these difference are in agreement with the low magnitude of the considered events and the limited frequency band considered in the teleseismic procedure.

Finally we performed a further test considering two Japanese earthquakes, that is to say the M_W 7.0 Miyagi-Oki (2003) and the M_W 6.9 Iwate-Miyagi (2008) earthquakes, which are characterized by a significant difference in stress drop. Interestingly, even applying the IV2 vs. E_S regression calibrated for Italy, the $M_{E(EW)}$ estimates are able to retrieve the largest stress drop of the M_W 7.0 Miyagi-Oki. We think that the new regional EEW methodology presented in this study, jointly used with the existing procedures for estimating M_W, can provide more detailed information on the damage potential of an ongoing earthquake, giving important indications on the amount of seismic energy released in the high frequency range, where the structure are more vulnerable.

Conclusions

This thesis dealt with a feasibility study for the earthquake early warning systems in Italy. The work is divided in three main parts, having as common point the aim to assess the capability of the Italian Accelerometric Network, RAN, to issue rapid and useful alerts during the occurrence of an intense earthquake considering both regional and on-site early warning approaches.

In the first part of thesis, we have considered the combination of the EEW software PRESTo and the RAN seismic network and we have evaluated the potential of a nation-wide EEWS for Italian territory, considering real and synthetic seismic data. First, considering the RAN recordings of the 40 moderate events, occurred during last 10 years in Italy, we have assessed the ability of the platform PRESTo, to provide fast and reliable earthquake location and magnitude estimates, as well as the time when this information is made available after the first P-wave arrival. The results of our analysis indicate that when only three triggered stations are used, in most of cases the obtained locations differ from the bulletin ones less than 10 kilometers. Furthermore, the magnitude estimated with three stations, available within four seconds after the first P-wave arrival, is reliable in 72.5% of cases, while it significantly overestimates and underestimates the bulletin value in 12.5% and 15% of cases, respectively. When three further seconds of signal are considered, allowing the use of more stations in the analysis, reliable estimates are provided in 87,5% of cases, while the overestimation and underestimation percentages are 2.5% and 10%.

In order to extend the feasibility analysis to the whole Italian territory and to consider the regions that did not experience earthquakes during the last ten years, we have considered a grid of virtual seismic sources covering the whole Italian surface. The analysis carried out by means of a synthetic dataset confirmed that the density of RAN stations in seismogenic zones has a crucial role for the EEWS performance, both in terms of geometrical and physical parameters of the source. In fact, we observed that, using three or six triggered stations, the RAN station distribution allows the first alert time to be on average smaller than 5 seconds in the highest hazard areas. Considering the larger earthquakes that each hazard zone is capable to generate, we have assessed that, in average, the area where the EEW might potentially provide warnings to the public is in the order of 80 kilometers, with a maximum lead time of about 25 seconds. Furthermore, our results indicates that, if an

integrated EEWS such as the RAN-PRESTo system would be operational, using the closest three stations to the epicenter most of the moderate-to-large events potentially occurring in Italy could be rapidly detected (i.e., within 5 seconds) and well characterized in terms of location and magnitude (i.e. > 95% of cases).

It is worth noting, that despite the excellent performance of the PRESTo-RAN EEWS, the geometry of the RAN constraints the blind zone radius for the highest hazard areas to be 25 and 30 km when three and six stations triggered, respectively. Such dimensions of blind zones indicate that for intense earthquakes the area most affected by damage couldn't benefit from an alert. In order to allow safety procedures also in those zones, we think that an optimal strategy would be to integrate regional and on-site EEWS.

Therefore, the second part of thesis focused on the development of a novel procedure for the on-site EEW. In particular, we have considered the IV2 parameter measured on P-waves aiming to predict the macroseismic intensity.

First, performing a regression analysis, we have shown that IV2 correlates better than PD with both PGV and I_H. In particular, considering that I_H is considered by engineers a better proxy for rapid damage assessment, we have developed a novel relationship between IV2 and I_H to predict in real time, and before the arrival of S waves, the level of structural damage that can potentially affect a target site.

We have verified that, for the most intense and damaging events (i.e. around M_w 6) recently occurred in Italy, even the availability of only 1 s of P wave signal would provide I_H estimates confined within a standard deviation of the IV2-I_H relation. Therefore, for the analyzed magnitude range, we have found that respect to regional EEW approach, the on-site EEW based on IV2 measured on 1 second time windows might lead to very small blind zones. It is worth noting that our results are representative of the magnitude range characterizing the used data set. Indeed, for larger magnitude events, as observed for PD, we expect that IV2 will be prone to saturation effects. This is an issue that will be certainly investigated in future studies by exploiting data sets with broader magnitude and distance ranges. However, we believe that the regression IV2-I_H has the potential to become a key relationship in the design of on-site EEWS.

Using the IM-I_H dataset provided by Chiauzzi et al. (2012), and exploiting the IV2-I_H regression, we derived a new relationship between IV2 and the IM and we tested it on independent data sets for EEW purposes. In particular, the IM predictions provided by our relationship have been compared to the IM values obtained by the popular PD based method. This last procedure consists in estimating PGV from PD, and in turn using the predicted PGV to predict the instrumental intensity by the Faenza and Michelini (2010) relationship. The results showed that the new IV2-IM

regression has a better performance in terms of IM prediction than the procedure based on PD. With respect to this issues, future studies will be aimed to assess our procedure on data sets covering a larger magnitudes range.

In the third part of thesis, we have focus on the estimation of the seismic radiated energy and magnitude energy in EEW through the parameter IV2. In the first part of this analysis, we have calculated a multiparameter regression in which the IV2 parameter measured on the entire P-wave signal is reported as a function of E_S and the stations hypocentral distance. This relationship has been obtained analyzing 29 Italian earthquakes with $M_W > 4$, occurred in last the 10 years, for which 900 RAN recordings and theoretical E_S measurements have been considered.

In the second part of this study, we have derived the EEW methodology, which exploits the multilinear regression IV2 vs E_S-R and IV2 measurements, to provide M_E estimations.

As first test of consistency, we have tested this procedure on the data set used to calibrate it, obtaining that our estimates differ less than 0.3 u.m. from the theoretical M_E for the 96,5% of cases.

A second test of the procedure has been the comparison of the M_E estimates obtained from our methodology and those estimates obtained using the teleseismic method proposed by Di Giacomo et al. (2010) for 8 Italian seismic events of L'Aquila (2009) and Emilia (2012) seismic sequences, for which we have obtained a very good agreement between the two kind of estimates.

Finally, we have performed test of our methodology on two Japanese earthquakes, the M_W 7.0 Miyagi-Oki (2003) and the M_W 6.9 Iwate-Miyagi (2008), which were characterized by different stress-drop (i.e. different E_S release). This test has been carried out to assess the capability of our procedure to identify under real-time conditions (i.e. having only few seconds of P-waves based IV2 estimates) the event having the largest seismic energy and stress drop values. Interestingly, even if we have applied the relationship between IV2 and E_S calibrated for Italian database, we have observed that the EEW M_E estimates are able to retrieve the largest stress drop of the M_W 7.0 Miyagi-Oki. Therefore, we think that the new regional EEW methodology for the estimation of M_E presented in this part of thesis could complement the EEW procedures for estimating M_W to obtain a more accurate prediction of the damage potential of an ongoing earthquake.

Bibliography

Abe, K. (1981). Magnitudes of large shallow earthquakes from 1904 to 1980, Phys. Earth Planet. Interiors 27, 72-92.

Aki, K. (1966). Generation and propagation of G waves from the Niigata earthquake of June 16, 1964, part 2: Estimation of earthquake moment, released energy, and stress-strain drop from the G wave spectrum, Bull. Earthq. Res. Inst. Tokyo Univ. 44, 73-88.

Aki, K., and P. Richards (1980). Quantitative Seismology. Theory and Methods, Freeman, San Francisco, CA, 932 pp.

Akkar, S., and Bommer J.J., (2007a). Empirical prediction equations for peak ground velocity derived from strong-motions records from Europe and the Middle East, Bull Seism Soc Am, 97(2):511–530, 2007.

Akkar, S.,and Bommer J. J. (2007b). Prediction of elastic displacement response spectra in Europe and the Middle East. Earthquake Engineering and Structural Dynamics, 3 6(10):1275 – 1301, 2007. doi: 10.1002/eqe.67

Allen RM. (2007). The ElarmS earthquake early warning methodology and its application across California. In: Gasparini P, Manfredi G, Zschau J, editors. Earthquake early warning systems. Berlin: Springer; 2007. p. 21–43, doi:10.1007/978-3-540-72241-0_3.

Allen RM, Gasparini P, Kamigaichi O, Böse M (2009) The status of earthquake early warning around the world: an introductory overview. Seismol Res Lett 80(5):682–693. doi:10.1785/gssrl.80.5.682.

Allen RM, Kanamori H (2003) The potential for earthquake early warning in Southern California. Science 300:786– 789. doi:10.1126/science.1080912.

Atkinson, G. M., and D. M. Boore (2006). Earthquake ground-motion prediction equations for eastern North America. Bulletin of the Seismological Society of America, 96(6):2181–2205, 2006. doi: 10.1785/0120050245

Bakun, W. H., and O. Scotti (2006) ”Regional Intensity attenuation models from France and the estimation of magnitude and location of historical earthquakes” Geophysical Journal International, Vol. 164, Issue 3, 596-610, doi: 10.1111/j.1365-246X.2005.02808.x

Barani S, Spallarossa D, Bazzurro P. (2009). Disaggregation of probabilistic ground motion hazard in Italy. Bulletin of the Seismological Society of America 2009; 99:2638–61.

Behr, Y., J. Clinton, P. Kästli, C. Cauzzi, R. Racine and M.-A. Meier (2015) “Anatomy o fan Earthquake Early Warning(EEW) alert”. Seismological Research Letters, Vol. 86, No. 3, May/June 2015, doi:10.1785/0220140179

Beresnev, I. (2009). The reality of the scaling law of earthquake-source spectra?, J. Seismology 13, 433-436, DOI 10.1007/s10950-008-9136-9.

Bernard P, Zollo A. (1989). The Irpinia (Italy) 1980 Earthquake: detailed analysis of a complex normal faulting. J. Geophys. Res. 1989; 94(B2):1631–47, doi:10.1029/ JB094iB02p01631.

Bindi, D., R.R Castro, G. Franceschina, L. Luzi and F. Pacor (2004) The 1997-1998 Umbria-Marche sequence (central Italy): Source, path, and site effects estimated from strong motion data recorded in the epicentral area. *J. Geophys. Res.* 109, B04312, doi:10.1029/2003JB002857, 2004.

Bindi, D., F. Pacor, L. Luzi, M. Massa and G. Ameri (2009) The M_W 6.3, 2009 L’Aquilaearthquake: source, path and site effects from spectral analysis of strong motion data. Geophys. J. Int. 179, 1573-1579. Doi:10.1111/j.1365-246X.2009.04392.x

Boatwright, J., and J. B. Fletcher (1984) “The partition of radiated energy between P and S waves” Seismological Society of America, Vol. 74, No.2:361-376

Boatwright, J., and G. L. Choy (1986). Teleseismic estimates of the energy radiated by shallow earthquakes, *J. Geophys. Res.* 91, 2095-2112.

Bolt, B. A. (1986). Seismic energy release over a broad frequency band, *Pageoph* 124, 919-930.

Bormann, P., M. Baumbach, M. Bock, H. Grosser, G. L. Choy, and J. Boatwright (2002). Seismic sources and source parameters, in: Bormann, P. (ed), in IASPEI New Manual Seismological Observatory Practice, GeoForschungsZentrum Potsdam, Vol. 1, Chapter 3, 94 pp.

Brune, J. N. (1970). Tectonic stress and the spectra of shear waves from earthquakes, J. Geophys. Res. 75, 4997-5009.

Campbell, K. W.(2003) Prediction of strong ground motion using the hybrid empirical method and its use in the development of ground-motion (attenuation) relations in eastern North America. Bulletin of the Seismological Society of America, 93(3):1012–1033.

Cancani, C., (1904). “Sur l’emploi d’une double echelle seismique des intesites, empirique et absolue”, Gerlands Beitrage Geophysik, 2**,** 281–283.

Castro, R.R., F. Pacor, R. Puglia, G. Ameri, J. Letort, M. Massa, and L. Luzi (2013):The 2012 May 20 and 29, Emilia earthquakes(Northern Italy) and the main aftershocks: S-wave attenuation, acceleration source functions and site effects. Geophys. J. Int 195, 597-611 doi:10.1093/gji/ggt245

Chiauzzi, L., A. Masi, M. Mucciarelli, M. Vona, F. Pacor, G. Cultrera, F. Gallov*ič* and A. Emolo (2012) “Building damage scenarios based on exploitation of Housner intensity derived from finite

faults ground motion simulations" Bull Earthquake Eng (2012) 10: 517-545 , doi:10.1007/s10518-011-9309-8

Choy, G. L., and J. Boatwright (1995). Global patterns of radiated seismic energy and apparent stress, J. Geophys. Res. 100, 18,205-18,228.

Choy, G. L., A. McGarr, S. H. Kirby, and J. Boatwirght (2006). An overview of the global variability in radiated energy and apparent stress, in Abercrombie, R., A. McGarr, and H. Kanamori (eds): Radiated energy and the physics of earthquake faulting, AGU Geophys. Monogr. Ser. 170, 43-57.

Codermartz, R., R. Nicolich and D. Slejko (2003) "Seismic risk assessments and GIS technology: applications to infrastructures in the Friuli-Venezia Giulia region (NE Italy). Earthq Eng Struct Dyn 32:1677-1690, doi:10.1002/eqe.294

Colombelli, S. et al. (2012). Test of a Threshold-Based Earthquake Early Warning Using Japanese Data. In: Bull.Seism. Soc. Am. 102, pp. 1266-1275. doi: 10.1785/0120110149.

Colombelli, S., A. Zollo, G. Festa and M. Picozzi (2014) "Evidence for a difference in rupture initiation between small and large earthquakes, Nat. Commun., 5 , 3958, doi:10.1038/ncomms4958.

Convertito, V., F. Catalli and A. Emolo (2013)"Combining stress transfer and source directivity: the case of the 2012 Emilia seismic sequence" Scientific Report Vol. 3, pp. 1-7, doi:10.1038/srep03114

CS.LL.PP. (2008). DM 14.1.2008 Norme tecniche per le Costruzioni. Gazzetta Ufficiale della Repubblica Italiana 29 (in Italian).

Cua G, Heaton T (2007) The virtual seismologist (VS) method: a Bayesian approach to earthquake early warning. In: Gasparini P, Manfredi G, Zschau J (eds) Earthquake early warning systems. Springer, Berlin. doi:10.1007/978-3- 540-72241-0_7.

Di Giacomo, Parolai S., Bormann P., Grosser H., Saul J., Wang R. and Zschau J. (2010). Suitably of rapid energy magnitude determinations for emergency response purpose. Vol 180, 1, 361-374 doi:10.1111/j.1365-246X.2009.04416.x

Doi K. (2011). The operation and performance of Earthquake Early Warnings by the Japan Meteorological Agency. Soil Dynamics and Earthquake Engineering, 31 (2011) 119–126. doi:10.1016/j.soildyn.2010.06.009.

Dolce M.(2012) "Qui DPC" Progettazione Sismica n.1, 2012, (http://www.progettazionesismica.it).

Efron, B.(1979). Bootstrap Methods: Another looks at Jackknife. The Annals of Statistics, Vol 1,(Jan., 1979), 1-26.

Faccioli E., Cauzzi C. (2006). Macroseismic intensities for seismic scenarios estimated from instrumentally based correlations. In Proceedings of the First European Conference on Earthquake Engineering and Seismology (a joint event of the 13thECEE & 30th General Assembly of the ESC)- Genève, Switzerland: paper no.569.

Faenza, L., and A. Michelini (2010) "Regression analysis of MCS intensity and ground motion parameters in Italy and its application in ShakeMap" Geophys. J. Int. (2010) 180, 1138–1152, doi: 10.1111/j.1365-246X.2009.04467.x

Faenza, L., V. Lauciani and A. Michelini (2011), "Rapid determination of the shakemaps for the L'Aquila main shock: a critical analysis" Bollettino di Geofisica Teorica ed Applicata,52(3):1-19, doi:10.4430/bgta0020

Festa, G., A. Zollo and M. Lancieri (2008) "Earhquake magnitude estimation from early radiated energy" Geophysical Research Letters, 35, doi: 10.1029/2008GL035576

Font Y, Kao H, Lallemand S, Liu CS, Chiao LY,(2004) Hypocentre determination offshore of eastern Taiwan using the Maximum Intersection method, Geophys J Int;158(2):655-75: doi: 10.1111/j.1365-246X.2004.02317.x.

Galli, P., S. Castenetto and E. Peronace. (2012) “The MCS Macroseismic survey of the Emilia 2012 earthquakes” Annals of Geophysics, 55, 4, 2012, doi: 10.4401/ag-6163

Gasparini P, Manfredi G, Zschau J. (2010). Earthquake early warning as a tool for improving society’s resilience and crisis response. Soil Dynamics and Earthquake Engineering 2010. doi:10.1016/j.soildyn.2010.09.004.

Goltz, J. D. (2002). Introducing earthquake early warning in California: A summary of social science and public policy issues, technical report, Governor’s Off. of Emergency Serv., Pasadena, Calif.

Gorini A., Nicoletti M., Marsan P., Bianconi R., De Nardis R., Filippi L., Marcucci S., Palma F., Zambonelli E. (2010). The Italian strong motion network. Bull Earthquake Eng 8:1075–1090. Doi:10.1007/s10518-009-9141-6.

Grünthal, G. (1998). European Macroseismic Scale 1998 (EMS-98). Cahiers du Centre Européen de Géodynamique et de Séismologie 15, Centre Européen de Géodynamique et de Séismologie, Luxembourg, 99 pp., 1998.

Gruppo di lavoro MPS (2004). Redazione della mappa di pericolosità sismica prevista dall’Ordinanza PCM 3274 del 20 marzo 2003. Rapporto conclusivo per il dipartimento di Protezione Civile, INGV, Milano – Roma, aprile 2004, 65 pp. + 5 appendici, Internet web site: http://zonesismiche.mi.ingv.it/elaborazioni/.

Guidoboni E., Ferrari G., Mariotti D., Comastri A., Tarabusi G. and Valensise G. (2007). CFTI4Med, Catalogue of Strong Earthquakes in Italy (461 B.C.-1997) and Mediterranean Area (760 B.C.-1500). INGV-SGA. http://storing.ingv.it/cfti4med/

Gutenberg, B. (1945a). Amplitude of surface waves and magnitude of shallow earthquakes, Bull. Seism. Soc. Am. 35, 3-12.

Gutenberg, B. (1945b). Amplitudes of P, PP, and S and magnitude of shallow earthquakes, Bull. Seism. Soc. Am. 35, 57-69.

Gutenberg, B. (1945c). Magnitude determination of deep-focus earthquakes, Bull. Seism. Soc. Am. 35, 117-130.

Gutenberg, B., and C. F. Richter (1956a). Magnitude and energy of earthquakes, Annali di Geofisica 9, 1-15.

Gutenberg, B., and C. F. Richter (1956b). Earthquake magnitude, intensity, energy and acceleration, Bull. Seism. Soc. Am. 46, 105-145.

Hanks, C., and H. Kanamori (1979). A moment magnitude scale, J. Geophys. Res. 84, 2348-2350.

Haskell, N. A. (1964). Total energy and energy spectral density of elastic wave radiation from propagating faults, Bull. Seism. Soc. Am. 54(6), 1811- 1841.

Housner, G.W. (1952) "Intensity of ground motion during strong earthquakes". Second technical report. August 1952, California Institute of Technology Pasadena, California

Iannaccone G., Zollo A., Elia L., Convertito V., Satriano C., Martino C. (2010). A prototype system for earthquake early-warning and alert management in southern Italy. Bull. Earthquake. Eng., 10.1007/s10518-009-9131-8.

Iervolino I., Chioccarelli E., Convertito V. (2011). Engineering design earthquakes from multimodal hazard disaggregation. Soil Dynamics and Earthquake Engineering 31 (2011) 1212–1231.

Kanamori, H. (1977). The energy release in great earthquakes, J. Geophys. Res. 82, 2981-2987.

Kanamori, H., and M. Kikuchi (1993). The 1992 Nicaragua earthquake: a slow tsunami earthquake associated with subducted sediments, Nature 361, 714-716.

Kanamori H. (2005). Real-time seismology and earthquake damage mitigation. Annual Review of Earth and Planetary Sciences 2005;33:195–214. doi:10.1146/ annurev.earth33.092203.122626.

Kamigaichi O., Saito M., Doi K., Matsumori T., Tsukada S., Takeda K. (2009). Earthquake early warning in Japan: warning the general public and future prospects. Seismol Res Lett 2009;80(5):717–26, doi:10.1785/gssrl.80.5.717.

Kikuchi, M. and Y. Fukao (1988). Seismic wave energy inferred from long-period body wave inversion, Bull. Seism. Soc. Am., 78, 1707-1724.

Kuyuk, H. S., R. M. Allen, H. Brown, M. Hellweg, I. Henson and D. Neuhauser (2014) "Designing a network-based early warning alghorithm for California:ElarmS-2" Bull. Seismol. Soc. Am., 104, 162-173, doi:10.1785/0120130146.

Lancieri M., Zollo A. (2008). Bayesian approach to the real-time estimation of magnitude from the early P and S wave displacement peaks. J Geophys Res 2008;113(B12), doi:10.1029/2007JB005386.

Lancieri, M., A. Fuenzalida, S. Ruiz and R. Madariaga(2011)."Magnitude Scaling of Early Warning Parameters for the M_w 7.8 Tocopilla, Chile, Earthquake and Its Aftershocks" Bulletin of Seismological Society of America, Vol. 101, No. 2, pp. 447-463, doi: 10.1785/0120100045

Li H., Michelini A., Zhu L., Bernardi F., and Spada M. (2007). Crustal Velocity Structure in Italy from Analysis of Regional Seismic Waveforms. Bulletin of the Seismological Society of America, Vol. 97, No. 6, pp. 2024–2039, December 2007, doi: 10.1785/0120070071.

Locati M., Camassi R., and Stucchi M. (2011). DBMI11, la versione 2011 del Database Macrosismico Italiano. Milano, Bologna, http://emidius.mi.ingv.it/DBMI11, DOI: 10.6092/INGV.IT-DBMI11.

Lomax, A., A. Michelini and A. Piatanesi (2007). An energy-duration procedure for rapid and accurate determination of earthquake magnitude and tsunamigenic potential, *Geophys. J. Int*. 170, 1195-1209, doi: 10.1111/j.1365-246X.2007.03469.x.

Lomax A., Satriano C., Vassallo M. (2012). Automatic picker developments and optimization: FilterPicker—a robust, broadband picker for real-time seismic monitoring and earthquake early- warning. Seism Res Lett 83(3):531–540. doi:101785/gssrl.83.3.531.

Luzi L., Hailemikael S., Bindi D., Pacor F., Mele F., Sabetta F. (2008). ITACA (ITalian ACcelerometric Archive): a web portal for the dissemination of Italian strong-motion data. Seismolog Res Lett 79(5).

Massa, M., S. Lovati, G. Franceschina, E. D'Alema, S. Marzorati, S. Mazza, M. Cattaneo, G. Selvaggi, A. Amato, A. Michelini and P. Augliera (2014). ISMD, a Web Portal for Real-Time Processing and Dissemination of INGV Strong-Motion Data Seismological Research Letters Volume 85, Number 4, doi: 10.1785/0220140024

Masi, A., M. Vona and M. Mucciarelli (2010) "Selection of natural and synthetic accelerograms for seismic vulnerability studies on RC frames" J Struct Eng., doi:10.1061/(ASCE)ST.1943-541X.209

Meletti C., Galadini F., Valensise G., Stucchi M., Basili R., Barba S. (2008). A seismic source zone model for the seismic hazard assessment of the Italian territory. Tectonophysics; 450:85–108.

Musson, R. M. W., G. Grünthal and M. Stucchi(2009) "The comparison of macroseismic intensity scales" Journal of Seismology, Springer Verlag (Germany), 2009, 14 (2) pp. 413-428, doi:10.0007/s10950-009-9172-0

Nakamura Y. (1988) On the urgent earthquake detection and alarm system (UrEDAS). In: Proceedings of ninth world conference on earthquake engineering, Tokyo–Kyoto, Japan.

Orowan, E. (1960). Mechanisms of seimic faulting in rock deformation: a symposium, *Geol. Soc. Am. Mem.* 79, 323-345.

Pacor F., Paolucci R., Ameri G., Massa M., and Puglia R. (2011). Italian strong motion records in ITACA: overview and record processing. Bull Earth. Eng. DOI 10.1007/s10518-011-9295-x.

Picozzi, M., D. Bindi, M. Pittore, K. Kieling and S. Parolai(2013) "Real-time risk assessment in seismic early warning and rapid response: a feasibility study in Bishkek (Kyrgyzstan)" Journal of Seismology 17 (2), 485-505, doi: 10.1007/s10950-012-9332-5

Picozzi, M., A. Zollo, P. Brondi, S. Colombelli, L. Elia and C. Martino (2015a) "Exploring the feasibility of a nationwide earthquake early warning system in Italy" J. Geophys. Res. Solid Earth, 120, doi:10.1002/2014JB011669

Picozzi M., Emolo A., Martino C., Zollo A., Miranda N., Verderame G., Boxberger T., and the REAKT Working Group (2015b). Earthquake Early Warning System for Schools: A Feasibility Study in Southern Italy. Seismological Research Letters, Volume 86, Number 2 March/April 2015. doi: 10.1785/0220140194.

Pinsky V., (2014). Modeling warning times for the Israel's earthquake early warning system. Journal of Seismology; DOI 10.1007/s10950-014-9454-z.

QRCMT (2012) "Quick Regional Centroid Moment Tensor" INGV Bologna: http://autorcmt.bo.ingv.it/quicks.html

Rudnicki, J. W., and L. B. Freund (1981). On energy radiation from seismic sources, *Bull. Seism. Soc. Am.* 71(3), 583-595.

Satriano, C., A. Lomax, and Zollo A. (2008). Real-Time Evolutionary Earthquake Location for Seismic Early Warning. Bulletin of the Seismological Society of America 98.3, pp. 14821494. doi:10.1785/0120060159.

Satriano C., Wu Y-M., Zollo A., Kanamori H. (2010). Earthquake early warning: Concepts, methods and physical grounds. Soil Dynamics and Earthquake Engineering. doi:10.1016/j.soildyn.2010.07.007.

Satriano C., Elia L., Martino C., Lancieri M., Zollo A., and Iannaccone G. (2011). PRESTo, the earthquake early warning system for southern Italy: concepts, capabilities and future perspectives, Soil Dyn. Earthq. Eng. doi:10.1016/j.soildyn.2010.06.008.

Savage, J. C., and M. D. Wood (1971). The relation between apparent stress and stress drop, Bull. Seism. Soc. Am. 61, 1381-1388.

SeedLink, Real-time seismological data transmission protocol (IRIS.edu page), 2009, (http;//www.iris.edu/data/dmc-seedlink.thm)

Shoja-Taheri, J. and Anderson, J.G., (1988). The 1978 Tabas, Iran earthquake: and interpretation of strong motion records. Bull. Seismol. Sot. Am., 78: 142-171

Sieberg, A. (1930) "Geologie der Erdbeben". Handbuch der Geophysik 2(4):550-555

Singh, S. K., and M. Ordaz (1994). Seismic energy release in Mexican subduction zone earthquakes, *Bull. Seism. Soc. Am.* 84(5), 1533-1550.

Thatcher, W., and T. C. Hanks, (1973) Source parameters of southern California earthquakes, J.

Geophys. Res., 78, 8547-8576.

Vassiliou, M. S., and H. Kanamori (1982). The energy release in earthquakes, *Bull. Seism. Soc. Am.* 72(2), 371-387.

Venkataraman, A., and H. Kanamori (2004a). Effect of directivity on estimates of radiated seismic energy, *J. Geophys. Res.* 109, B04301, doi:10.1029/2003JB002548.

Wu, Y. M., and H. Kanamori (2005) "Experiment of an on-site method for the Taiwan Early Warning System", Bull. Seismol. Soc. Am., 95, 347–353, doi:10.1785/0120040097.

Wu, Y.M., and H. Kanamori (2008) "Development of an Earthquake Early Warning System Using Real-Time Strong Motion Signals" Sensors (Basel); 8(1):1-9

Wu, Y.M., and L. Zhao (2006). "Magnitude estimation using the first three seconds P-wave amplitude in earthquake early warning", Geophys. Res. Letters, 33**,** L16312, doi:10.1029/2006GL026871.

Zollo, A., M. Lancieri and S. Nielsen (2006). "Earthquake magnitude estimation from peak amplitudes of very early seismic signals on strong motion" Geophys. Res. Letters, 33**,** L23312, doi:10.1029/2006GL027795.

Zollo A, Iannacone G., Lancieri M., Cantore L., Convertito V., Emolo A., Festa G., Gallovič. F., Vassallo M., Martino C., Satriano C., Gasparini P. (2009a) . Earthquake early warning system in southern Italy: methodologies and performance evaluation, *Geophys. Res. Letters,* 36**,** L00B07, doi:10.1029/2008GL036689.

Zollo, A, Iannaccone G., Convertito V. , Elia L., Iervolino I., Lancieri M., Lomax A., Martino C., Satriano C., Weber E., Gasparini P. (2009b). The earthquake early warning system in southern Italy, in *Encyclopedia of Complexity and System Science*, 5**,** 2395–2421, doi:10.1007/978-0-387-30440-3.

Zollo A., Amoroso O., Lancieri M., Wu Y.M., and Kanamori H. (2010). A threshold-based earthquake early warning using dense accelerometer networks, Geophys. J. Int., 183, pp. 963-974, doi: 10.1111/j.1365-246X.2010.04765.x

Zollo, A., G. Iannacone, V. Convertito, L. Elia, I. Iervolino, M. Lancieri, A. Lomax, C. Martino, C. Satriano, E. Weber and P. Gasparini (2011) “Earthquake Early Warning System in Southern Italy” Extreme Environmental Events, pp 175-201, doi:10.1007/978-1-4419-7695-6_13

Zollo A., Colombelli S., Elia L., Emolo A., Festa G., Iannaccone G., Martino C., and Gasparini P. (2014). An Integrated Regional and On-Site Earthquake Early Warning System for Southern Italy: Concepts, Methodologies and Performances. In: Early Warning for Geological Disasters. Ed. by Friedemann Wenzel and Jochen Zschau. Advanced Technologies in Earth Sciences. Springer Berlin Heidelberg, pp. 117, 137. isbn: 978-3-642-12232-3. doi: 10.1007/978-3-642-12233-0_7. url: http://dx.doi.org/10.1007/978-3-642-12233-0_7.